

THE EVOLUTION OF RINGS AND SATELLITES

A Dissertation

Submitted to the Faculty

of

Purdue University

by

Andrew J. Hesselbrock

In Partial Fulfillment of the

Requirements for the Degree

of

Doctor of Philosophy

December 2018

Purdue University

West Lafayette, Indiana

THE PURDUE UNIVERSITY GRADUATE SCHOOL
STATEMENT OF DISSERTATION APPROVAL

Dr. David Minton, Chair

Department of Earth, Atmospheric, and Planetary Sciences

Dr. John Finley

Department of Physics and Astronomy

Dr. Briony Horgan

Department of Earth, Atmospheric, and Planetary Sciences

Dr. H. Jay Melosh

Department of Physics and Astronomy

Approved by:

Dr. John Finley

Head of the Department of Physics and Astronomy

ACKNOWLEDGMENTS

In pursuit of this degree and completion of this work my life has gone through many stages, many challenges, and many rewards. Throughout these stages, people have come and gone, people have stayed fast, and several have had a lasting impact. First, I will thank my graduate advisor, David Minton. Both of us new to Purdue and both working hard to secure research funding, we worked through setbacks together but earned even greater rewards. His advice, guidance, and encouragement will forever be appreciated. I would also like to thank the members of my committee. I thank Jay Melosh, who served as my “substitute” advisor for some time, but who took that role seriously. I thank Briony Horgan for teaching a computational physicist that planets are not just point masses. I also thank John Finley, who provided me every opportunity I desired to develop my teaching skills while giving me perhaps too much freedom in directing his astronomy labs.

I thank my family, who may not have always understood what I do, but always understood its importance and gave me their respect. They continually reminded me that the only investment was time, and they never stopped supporting me and encouraging me.

And lastly, I thank my wife Maria. Your admiration of my pursuits was unhalting, and your unwavering patience as I worked to complete my requirements did not go unnoticed. You were my number one fan, and expressed more interest in my work than perhaps even myself at some times. I have always stopped in awe to look up at the stars, but I never expected someone to look up to me while I was looking up to them.

Thank you.

PREFACE

In each chapter and in each section of this work, I will justify my motivation for each reasoning and each hypothesis. It seems only fitting that I should justify here what brought me to this subject, this work, and this field in the first place. When I was ten years old, my parents bought me a small refractor telescope for Christmas. For months, maybe even years, my use of the telescope was purely terrestrial. Living in the expansive cornfields of the country, a telescope was the only way to see what your neighbors were up to.

One day while rummaging through my telescope case I discovered a disk to the Starry Night software suite. Loading it onto my computer I found that I could locate thousands of objects in the night sky with a few simple clicks. Dialing in my location, date, and time, I noticed one intriguing object that would be in the sky that night:

Saturn.

That evening under the deeply dark, light-pollution-free sky I set up my small, modest refractor. Within minutes I had quickly located the bright planet and wiggled it into focus. On that first attempt, with that small scope, I saw the rings of Saturn *with my own eyes*. My jaw dropped and I was transfixed. From that day I was hooked, and my fascination motivated me into studying astronomy, physics, astrophysics, and planetary science. While this dissertation may seem to most like a work on satellites, rings, numerical models, and other related topics, for me it is an apt and fitting continuance of my childhood curiosity.

TABLE OF CONTENTS

	Page
LIST OF TABLES	vii
LIST OF FIGURES	viii
SYMBOLS	xiii
ABSTRACT	xvi
1 INTRODUCTION	1
2 THREE SATELLITE-RING FORMATION REGIMES	8
2.1 The Dynamics of Coupled ring-satellite Systems	8
2.1.1 The Roche Limits	8
2.1.2 Lindblad Torques	10
2.1.3 Tidal Torques	12
2.1.4 Satellite Migration	14
2.2 Evolution of Ring Accreted Satellites	17
2.2.1 The “Boomerang” Regime: $a_{Lind} < a_{synch}$	18
2.2.2 The “Slingshot” Regime: $a_{synch} < a_{FRL}$	19
2.2.3 The “Torque-Dependent” Regime: $a_{FRL} < a_{synch} < a_{Lind}$	19
2.3 A Look at Our Solar System	21
2.4 Conclusion	23
3 DESCRIPTION OF “RING-MOONS” MODEL	27
3.1 Disk Viscosity	28
3.2 Satellite Accretion	31
3.3 Satellite Orbital Evolution	32
3.4 Disk-Satellite Torques	33
3.5 Tidal Disruption of Satellites	34
3.6 Validation of Model	34
4 THE CYCLIC NATURE OF MARTIAN SATELLITES	39
4.1 Background	39
4.2 Using RING-MOONS to Investigate the Mars Satellite System	41
4.2.1 Uncertainty in Tidal Breakup	44
4.2.2 Ring Particle Size	45
4.3 Deposition of “Astro-Sediments” onto the Martian Surface	51
4.4 Orbital Resonances with Deimos	52
4.5 Existence of a Ring Today	53

	Page
5 FORMATION OF MIRANDA FROM A MASSIVE URANIAN RING . . .	56
5.1 Motivation	59
5.2 Methods	60
5.3 Results	62
5.4 Discussion	65
6 THE TIDAL EVOLUTION OF BINARY SYSTEMS	69
6.1 Motivation	69
6.2 Methods	72
6.2.1 Tidal Evolution of Binary Systems	72
6.2.2 Mass Shedding	77
6.2.3 Formation of Contact Binaries from Collapse	80
6.3 Results	82
6.3.1 Binary Trans-Neptunian Objects	82
6.3.2 Chariklo and Chiron	83
6.4 Discussion	90
7 CONCLUSION	93
7.1 Boomerangs	93
7.2 RING-MOONS	95
7.3 Mars	96
7.4 Miranda	99
7.5 Small Bodies	100
7.6 Denouement	101
REFERENCES	103
A TABLES	110
VITA	114

LIST OF TABLES

Table	Page
A.1 Masses and Timescales for Mars Ring/Satellite Cycles	111
A.2 Global and Equatorial Depths of Estimated Ring Deposits Onto Mars . .	112
A.3 Maximum Semi-Major Axis of Satellites	113

LIST OF FIGURES

Figure	Page	
2.1	Diagram showing the relationships that define the three evolution regimes for coupled ring-satellites. The large grey circle represents a primary body of radius R_p orbited by a ring (shaded region), and a small satellite (small circle) that has formed at the ring edge. The rigid Roche limit (RRL), fluid Roche limit (FRL), the maximum orbit Lindblad torques may migrate a satellite (a_{Lind}), and the synchronous orbit (a_{synch}) are all marked with vertical lines. Distances are shown in units of primary radii. The primary and satellite are assumed to have the same density. (a) Boomerang regime: For a slowly rotating primary, a_{synch} lies beyond a_{Lind} . (b) Torque-Dependent regime: For a moderate rotation period, a_{synch} lies between the FRL and a_{Lind} . (c) Slingshot regime: For rapidly rotating primaries a_{synch} lies inside the FRL.	16
2.2	The boundaries of the three ring-satellite evolution regimes defined by Equation 2.13 (assuming $M_s/M_p \ll 1$). The dark gray regime marks the Boomerang regime (systems where $a_{synch} > a_{Lind}$), while the light gray regime marks the Slingshot regime (systems where $a_{synch} < a_{FRL}$). The middle zone in white marks the Torque-Dependent regime (systems where $a_{FRL} < a_{synch} < a_{Lind}$). Additionally, I display the expected regime for Roche-interior rings orbiting various bodies in the solar system given their rotation rates today and estimated satellite densities. In this figure, $M_s/M_p \ll 1$. Fast rotating primaries with low satellite densities fall within the Slingshot regime (e.g. Jupiter, Saturn), while slowly rotating primaries with high density satellites exist within the boomerang regime (e.g. Mars). The evolution of satellites accreting from a Roche-interior ring orbiting Uranus and Neptune is dependent upon the magnitude of the Lindblad and tidal torques.	26
3.1	Here I compare the results from the model, RING-MOONS (black line) for a sharply peaked ring viscously spreading in the Saturn system to others in the literature. To solve the viscous spreading of the rings, I follow the viscous spreading model described in Salmon et al. [2010a]. Despite my implementation of a different integration scheme, my results convincingly match the results displayed in Figure 3 of Salmon et al. [2010a] (red line).	35

Figure	Page	
3.2	Here I display the results of the model, RING-MOONS (black dots) for the accretion of satellites from Saturns rings, and their orbital evolution over ~ 4 Gy, assuming no tidal dissipation in the satellites and the tidal quality factor of Saturn $Q = 1680$. I perform this simulation to benchmark my model against the actual Saturn system (blue squares) and other models in the literature (red diamonds). RING-MOONS is similar in many ways to the HYDRORINGS model described in Charnoz et al. [2011], and presents similar results.	36
4.1	a. The ring, shaded corresponding to its surface mass density, has viscously spread to Mars (orange) and to the fluid Roche limit (FRL). b. Ring material has accreted into a satellite (blue, size exaggerated) that is perturbed outwards via Lindblad torques. c. Being inside the synchronous orbit (Synch.), the ring has depleted and tidal torques evolve the satellite inwards. d. The satellite has reached the rigid Roche limit (RRL), disrupting into a new ring. e.,f. The cycle repeats, producing Phobos.	43
4.2	Here I compare the final satellite mass to the initial ring mass for a Martian satellite-ring cycle. I plot the ratio of the final satellite mass to the initial ring mass for each cycle while varying the location of total satellite breakup. Satellite breakup may occur anywhere within $1.2 - 1.7R_M$ (Black and Mittal [2015]). I find that if a satellite disrupts at a location closer to Mars, the resulting ring will produce a final satellite with a mass smaller than if the breakup was to occur farther away from the planet.	46
4.3	Here I show snapshots of satellites produced in my nominal case with time estimated for a ring composed of 0.18 m radius particles. Satellites are represented as dots with radius scaled to the satellites mass. Each cycle begins by spreading ring material to the FRL to accrete into satellites that evolve away from the ring via Lindblad torques. Tidal torques eventually move the satellites inwards until they disrupt at the RRL, and the cycle repeats. Satellites in Cycle 6 approach the 2:1 mean motion resonance with Deimos (2:1 MMR).	49
4.4	Results for the mass evolution for Martian satellites over time, assuming all particles in the ring have a radius of 1 km (red circles), or a radius of 100 m (black diamonds). The y-axis represents the mass of the satellites. The x-axis displays the time each satellite crossed the Rigid Roche Limit, save for the final Phobos analogs (bottom right). Time is represented as a fraction of the total time (t_{Tot}) from the initial conditions to placing a Phobos analog in the current orbit of Phobos. In rings with 1 km radius particles, each cycle produces one massive satellite. In rings with 100 m radius particles, early cycles may create several satellites which reach the RRL at different times.	50

Figure	Page
4.5 Here I display the surface mass density (Σ) of the ring during Cycle 1, the ring that produces Phobos, for the “nominal case” at different times during the cycle. Although a ring still exists at the completion of the simulation, there is likely not a ring visible today. My results indicate the ring at the completion of Cycle 1 is optically thin, with $\tau \leq 0.03$. I hypothesize that this low mass remnant ring may be depleted due to solar radiation effects, which I do not model currently.	55
5.1 Orbital architecture of the Ice Giant systems. The dark circles show the present-day orbits of known satellites (abbreviated names adjacent) while the gray lines mark the locations of known rings. The location of the Rigid Roche Limits (RRL), Fluid Roche Limits (FRL), synchronous orbits (a_{synch}), and maximum orbits (a_{max}) for satellites perturbed by Lindblad Torques are also shown. Uranus (panel a) has 13 satellites with orbits within a_{max} , indicating they may have accreted from an ancient Uranian ring. The satellite Miranda, orbiting just beyond a_{synch} may have also accreted from this ring. Neptune (panel b) has 5 satellites with orbits within a_{max} , indicating they may have accreted from an ancient Neptunian ring, however the Triton capture event complicates the ability to test this hypothesis. It is possible the satellites S/2004 N 1 and Proteus, orbiting beyond a_{Lind} may also have accreted from such a ring.	58

Figure	Page	
5.2	<p>Evolution of the surface mass density of a Uranian ring with an initial mass of 3.0×10^{23} g. The horizontal axis marks the distance from Uranus, the left vertical axis marks the surface-mass density of the ring (black line), and the right vertical axis marks the mass of the satellites. Solid black circles represent RING-MOONS satellites while the current satellite population is shown as gray squares. The locations of the RRL, FRL, and the synchronous orbit are marked with vertical lines. The open circle marks the required surface-mass density at the $\mathcal{M} = 2$ mode for Equation 2.15 to be true for a satellite at a_{synch}, ignoring all other modes. (a) Initial conditions. (b) Two satellites have evolved beyond a_{synch} and the surface-mass density is above the threshold value. (c) The surface-mass density of the ring has fallen such that Equation 2.15 is no longer true. (d) The surface-mass density of the ring has declined. The two satellites orbiting beyond a_{synch} have merged into a Miranda-mass satellite. The 18 satellites interior to a_{synch} have merged into one massive satellite that has migrated to the RRL. (e) The massive satellite has been disrupted at the RRL, generating a new ring which has begun to viscously spread. (f) The ring generated by the destruction of the massive satellite has accreted a new generation of 14 satellites. However, the surface-mass density of the ring has fallen below the threshold value. Overtime these satellites may gravitationally scatter to produce a system similar to the one observed today.</p>	63
6.1	<p>If the RRL is located at the point of contact between two objects, the satellite will begin to shed mass at its equator during contact. Given the ratio between the satellite and primary bulk densities, I show the required mass ratio for this to occur. The solid line marks the mass ratio where $a_{RRL} = a_C$ and the dashed line represents the semi-major axis of the contact point/RRL. If the mass ratio of the system is greater than q_{shed}, the system will not shed mass during contact. For systems with $q \leq q_{shed}$ the satellite will shed material from its equator during contact.</p>	78
6.2	<p>Here I plot the current population of observed known and likely Binary Trans-Neptunian Objects (BTNOs) as a function of their mass ratio (q), and the semi-major axis of their mutual orbit (a). The grey line marks the location of the critical orbit. BTNOs below the curve in fully synchronous orbits will likely experience a complete tidal collapse of their mutual orbit if they are disturbed. The nearly horizontal lines mark the evolution timescale, τ_{tide}, in years as a function of q and a for a system with $R_p = 50$ km and $\rho_p = 1$ g/cm³.</p>	84

Figure	Page	
6.3	Here I display the total momentum of a Chariklo system as a function of the mass ratio q with $\rho_p = \rho_s$. Blue lines designate the momentum of the Chariklo system today (J_t) assuming it is two spheres in contact. Red lines designate the momentum of a fully synchronous system with semi-major axis a_{crit} (J_{crit}). The critical mass ratio q_c is the mass ratio at the intersection of the two curves. The line type corresponds to varying the density of the bodies from $0.9 - 1.5 \text{ g/cm}^3$. As the density of the bodies increases, the value of q_c decreases.	86
6.4	Here I display the total momentum of a binary system as a function of the mass ratio q . Blue lines designate the momentum of the Chiron system today (J_t) assuming it is two spheres in contact. Red lines designate the momentum of a fully synchronous system with semi-major axis a_{crit} (J_{crit}). The critical mass ratio q_c is the mass ratio at the intersection of the two curves. The line type corresponds to varying the density of the bodies from $1.3 - 1.6 \text{ g/cm}^3$	87
6.5	Here I display the collapse of the mutual orbit of a Chariklo analog binary system. The system has a critical mass ratio $q_c \sim 0.25$ and the initial semi-major axis is the critical orbit (a_{crit}) with a period of ~ 10 hours. $\rho_p = 1.4 \text{ g/cm}^3$ and $\rho_s = 0.5\rho_p$. In black I display the mutual orbit, in purple the location of the synchronous orbit, green the location of the FRL, blue the location of the RRL, orange the location of the maximum orbit allowed by the system's angular momentum, and in red the contact point. In $< 10^3$ years the mutual tidal interaction has caused the orbit to collapse until the bodies have come into contact. Assuming no slippage at contact, the final rotation period matches the currently observed 7 hours.	89
6.6	Here I display the collapse of the mutual orbit of a Chiron analog binary system. The system has a critical mass ratio $q_c \sim 0.25$ and the initial semi-major axis is the critical orbit (a_{crit}) with a period of ~ 8.5 hours. $\rho_p = 2 \text{ g/cm}^3$ and $\rho_s = 0.5\rho_p$. In black I display the mutual orbit, in purple the location of the synchronous orbit, green the location of the FRL, blue the location of the RRL, orange the location of the maximum orbit allowed by the system's angular momentum, and in red the contact point. In $< 10^3$ years the mutual tidal interaction has caused the orbit to collapse until the bodies have come into contact. Assuming no slippage at contact, the final rotation period matches the currently observed 5.9 hours.	90

SYMBOLS

G	Newton's Constant of Gravitation
M_p	Mass of primary body
R_p	Radius of primary body
ρ_p	Density of primary body
M_s	Mass of satellite
R_s	Radius of satellite
ρ_s	Density of satellite
a	Semi-major axis
a_{RRL}	Semi-major axis of rigid Roche limit
a_{FRL}	Semi-major axis of fluid Roche limit
\mathcal{M}	Order of Lindblad resonance
$r_{\mathcal{M}}$	Semi-major axis of Lindblad resonance, order \mathcal{M}
$\Gamma_{\mathcal{M}}$	Torque exerted by material at $r_{\mathcal{M}}$
$\Sigma(r)$	Surface mass density of ring at location r
Γ	Total Lindblad torque exerted on satellite
$T(r)$	Torque exerted on disk by satellites
a_{Lind}	Maximum orbit Lindblad torques may perturb a satellite
a_{synch}	Semi-major axis of the synchronous orbit
T_p	Rotational period of primary body
n	Mean motion
ω	Orbital speed
e	Eccentricity
k_2	Tidal Love number
Q	Tidal dissipation factor
f	Satellite-Ring evolution regime function

i	Bin identification number
r_i	Midpoint location of bin i
Δr	Bin width
r_{Init}	Interior limit of the disk
r_{Fin}	Exterior limit of the disk
N	Number of bins in the disk
ΔA_i	Cross-sectional area of bin i
m_i	Mass of bin i
I_i	Moment of Inertia of bin i
R_i^*	Moment of Inertia factor
ν	Ring Viscosity
Q_i	Toomre's Stability Parameter for bin i
σ_r	Velocity dispersion
ν_i^{trans}	Translational viscosity of bin i
ν_i^{coll}	Collisional viscosity of bin i
ν_i^{grav}	Gravitational viscosity of bin i
r_{Hill}	Hill Sphere radius
$\kappa(y)$	Transition function (0 to 1)
$\eta(y)$	Transition function (1 to 0)
m_{pdisk}	Mass of individual ring particle
r_{pdisk}	Radius of individual ring particle
τ_i	Opacity of bin i
Δa_j	Spacing between satellites
m_{min}	Minimum satellite mass
Δm_L	Mass loss to ring at r_M
Δt	Stable timestep
ΔR	Depth of "Astro-Sediment" deposit
M	Mars Mass
ρ_M	Mars bulk density

R_M	Mars radii
R_U	Uranus radii
R_N	Neptune radii
a_I	Initial semi-major axis
a_F	Final semi-major axis
L	Orbital angular momentum
S	Spin angular momentum
J	Total angular momentum
α	Moment of inertia coefficient
q	Mass ratio of binary system
\mathcal{R}	Density ratio of binary system
q_{shed}	Mass ratio for collapsing binary system to shed mass
a_{crit}	Semi-major axis of the critical orbit
a_C	Semi-major axis of binary system contact point
τ_{tide}	Binary system timescale of tidal migration

ABSTRACT

Hesselbrock, Andrew J. PhD, Purdue University, December 2018. The Evolution of Rings and Satellites. Major Professor: David Minton.

Planetary rings are, and have been, a common feature throughout the solar system. Rings have been observed orbiting each of the giant planets, several Trans-Neptunian Objects, and debris rings are thought to have orbited both Earth and Mars. The bright, massive planetary rings orbiting Saturn have been observed for centuries, and the Cassini Mission has given researchers a recent and extensive closeup view of these rings. The Saturn ring system has served as a natural laboratory for scientists to understand the dynamics of planetary ring systems, as well as their influence on satellites orbiting nearby. Researchers have shown that planetary ring systems and nearby satellites can be tightly-coupled systems.

In this work, I discuss the physics which dominate the dynamical evolution of planetary ring systems, as well as the interactions with any nearby satellites. Many of these dynamics have been incorporated into a one-dimensional mixed Eulerian-Lagrangian numerical model that I call “RING-MOONS,” to simulate the long-term evolution of tightly coupled satellite-ring systems. In developing RING-MOONS, I have discovered that there are three evolution regimes for tightly-coupled satellite-ring systems which I designate as the “Boomerang,” “Torque-Dependent,” and “Slingshot” regimes. Each regime may be defined using the rotation period of the primary body and the bulk density of the ring material.

The slow rotation period of Mars places it in the Boomerang regime. I hypothesize that a giant impact with Mars ejected material into orbit, forming a debris ring around the planet. Using RING-MOONS, I demonstrate how Lindblad torques cause satellites which form at the edge of the ring to initially migrate away from the ring, but

over time as the mass of the ring decreases, tidal torques always cause the satellites to migrate inwards. Assuming the satellites rapidly tidally disrupt upon migrating to the rigid Roche limit, a new ring is formed. I show that debris material cycles between orbiting Mars as a planetary ring, or as discrete satellites, and that Phobos may be a product of a repeated satellite-ring cycle. Uranus, which has a faster rotation rate falls within the Torque-Dependent regime. Hypothesizing that a massive ring once orbited Uranus, I use RING-MOONS to demonstrate how the satellite Miranda may have formed from such a ring, and migrated outwards to its current orbit, but that any other satellites would have migrated inwards overtime.

Lastly, I examine Trans-Neptunian Objects (TNOs) in binary systems. Tidal torques exerted on each body can decrease the mutual semi-major axis of the system. I outline the conditions for which a fully synchronous system may experience a complete decay of the mutual orbit due to tidal torques. As the semi-major axis decreases, it is possible for the smaller of the two bodies to shed mass before coming into contact with the more massive to form a contact binary. I hypothesize that Chariklo and Chiron are contact binaries that formed via the tidal collapse of a binary TNOs system, and demonstrate how mass shedding may have occurred to form the rings observed today.

1. INTRODUCTION

Portions of this chapter have been accepted into The Astronomical Journal as A. J. Hesselbrock and D. A. Minton, “Three Dynamical Evolution Regimes for Coupled Ring-Satellite Systems and Implications for the Formation of the Uranian Satellite Miranda,” The Astronomical Journal, 2018.

Planetary rings are disks of solid particles in orbit around a primary body, and are common throughout our solar system today. While Saturn was the first object in the solar system known to have rings [Huygens, 1659], later observations of Jupiter [Smith et al., 1979], Uranus [Elliot et al., 1977], and Neptune [Hubbard et al., 1986] revealed that all of the giant planets are orbited by planetary rings. The giant planets were long thought to be the only objects in the solar system to have rings, however recent discoveries have shown that rings orbit small bodies as well. Stellar occultation observations suggest that there are rings in orbit around the centaurs 10199 Chariklo and 2060 Chiron [Braga-Ribas et al., 2014, Ortiz et al., 2015], as well as the dwarf planet Haumea [Ortiz et al., 2017]. These discoveries indicate that rings may be a common feature of many bodies in the solar system.

Satellite surface processes, giant impacts, tidal disruptions, and impact-generated dust and fragments are a few of the processes that create rings around solar system bodies. While rings take many forms, I will distinguish between “ephemeral” and “massive” rings. Ephemeral rings are optically thin and are strongly influenced by non-gravitational forces. For instance, ice crystals ejected from active geysers on Saturn’s ice satellite Enceladus have collected to form Saturn’s E ring [Hamilton and Burns, 1994]. Heliocentric impacts may catastrophically disrupt satellites [Colwell and Esposito, 1992], or create dust and fragments that subsequently form rings [Miner et al., 2007].

In contrast, massive rings are optically thick and their dynamics are dominated by gravitational, collisional, and tidal processes, such as Saturn’s main rings. Massive rings can potentially be generated by a variety of processes. Close encounters between scattered Kuiper belt objects with the giant planets may have tidally disrupted passing objects into forming rings [Hyodo et al., 2017]. Material ejected from a primary’s surface during a giant impact may be placed into orbit, forming a ring [Cameron and Ward, 1976]. Satellites orbiting close to their primary may also be tidally disrupted to form a ring of material [Black and Mittal, 2015, Canup, 2010, Hesselbrock and Minton, 2017, Leinhardt et al., 2012]. Massive rings are the focus of this work.

In addition to the rings known to exist today, massive rings may have once orbited both the Earth and Mars. A giant impact has been implicated for the formation of Earth’s satellite [Cameron and Ward, 1976]. This impact may have ejected a large amount of material into orbit around Earth, forming a ring around the planet. Before the ring collapsed onto the Earth, some of its material would have accreted to form our Moon.

Recent work has hypothesized that Mars may have had a ring system in the past as well. Large impacts, such as that proposed to have formed the Borealis Basin, could have ejected material into orbit to form a ring [Citron et al., 2015, Marinova et al., 2008]. As this ring evolved over time, it may have produced the satellites Phobos and Deimos [Canup and Salmon, 2018, Hesselbrock and Minton, 2017, Hyodo et al., 2017, Rosenblatt and Charnoz, 2012, Rosenblatt et al., 2016].

The massive main ring system of Saturn provides a natural laboratory to study the dynamics of planetary rings and how they evolve over time. Analysis of Saturn’s rings has demonstrated that although planetary rings are composed of solid particles, collectively the ring particles behave similar to a fluid. As the ring particles orbit the primary they continuously collide with other nearby particles. Inelastic collisions between ring particles deplete the orbital energy of the ring system. The intra-ring collisions causes the ring material to “flow” from one location to another through a process known as “viscous spreading” [Goldreich and Tremaine, 1978, Lynden-Bell

and Pringle, 1974]. Intra-ring interactions also cause some particles to clump together, however for massive rings in orbit close to the primary, tidal forces disrupt these clumps before they can accrete into satellites.

The farther the ring particles orbit the primary, the less likely they are to be disrupted by tidal forces. Ring particles far enough from the primary are able to accrete into satellites [Chandrasekhar, 1969]. Once accreted, these “ring satellites” gravitationally interact with the material in the ring, perturbing the orbits of the ring particles. Observations of Saturn’s rings reveal that ring satellite perturbations create a wide variety of ring structures [Miner et al., 2007]. Ring satellites may exchange angular momentum with the ring particles, which can influence the orbits of the ring particles [Goldreich and Tremaine, 1979]. Perturbations between the ring particles and ring satellites are particularly strong for locations within the ring that are in resonance with the orbiting satellite [Goldreich and Tremaine, 1979]. Resonance interactions between ring particles and ring satellites create density waves in the ring which in turn give rise to torques on the satellite’s orbit. For satellites in orbits exterior to the ring, these resonant “Lindblad” torques cause the satellite to migrate away from the ring [Goldreich and Tremaine, 1982].

In addition to interacting with ring particles, ring satellites gravitationally interact with both other ring satellites and with the primary body. Close encounters between satellites result in gravitational scattering, and collisions can result in a variety of outcomes, including hit-and-run collisions, merging, or fragmentation [Charnoz et al., 2010, 2011, Crida and Charnoz, 2012, Leinhardt and Stewart, 2012]. A variety of resonant interactions may occur as well, including resonant capture [Murray and Dermott, 1999, Salmon and Canup, 2017]. Tidal interactions between ring satellites and the primary body give rise to additional torques [Murray and Dermott, 1999].

While inner Lindblad torques always cause outward satellite migration, the direction of the tidal torques depends on the relationship between the satellites’ semi-major axes and the synchronous (or corotation) orbit, which is the location where the orbital period of the satellite is the same as the rotation period of the primary. If a satellite

orbits beyond the synchronous orbit, tides will increase the satellite’s semi-major axis, causing it to migrate away from the primary and the ring. Tides cause the orbits of satellites that orbit within the synchronous orbit to decay, causing the satellite to migrate inward, towards the primary [Murray and Dermott, 1999].

The formation of ring satellites from planetary rings, and the subsequent interactions within the ring-satellite environment indicate that these are strongly coupled systems. Numerical simulations modeling the dynamics of ring-satellite systems demonstrate how coupled ring-satellite systems evolve over time. Models of the spreading of a viscous ring that forms satellites which exchange angular momentum with the ring and the primary body have been applied to the formation of the inner satellites of the giant planets [Charnoz et al., 2010, 2011, Crida and Charnoz, 2012, Salmon and Canup, 2017]. Numerical models have also explored the long-term evolution of a ring-satellite system in orbit around Mars and revealed it is strikingly different than for a similar system in orbit around Saturn [Charnoz et al., 2010, 2011, Hesselbrock and Minton, 2017, Rosenblatt and Charnoz, 2012, Rosenblatt et al., 2016]. While Saturn’s ring satellites always migrate away from the rings, ring satellites generated by a Martian ring can migrate inward where they can be tidally disrupted to form new rings.

In this work I investigate the major factors that control the long term evolution of coupled ring-satellite systems, including the location of the synchronous orbit relative to the location where ring satellites form. In Chapter 2 I analyze the physics and dynamics of coupled ring-satellite systems and discuss how various parameters affect the evolution of these systems. I show that the dynamics of coupled ring-satellite systems gives rise to three regimes of dynamical evolution, which I term “Boomerang,” “Slingshot,” and “Torque-Dependent.” The long-term evolution of ring-satellites is markedly different across each regime. For example, left undisturbed, satellites in the Slingshot regime exist in perpetuity, while satellites in the Boomerang regime never survive. Identifying in which regime a satellite-ring system exists provides an understanding of the likely history of a particular ring-satellite system. I will

explain how the rotation period and density of the primary body, and the density of the satellites constrain the formation regime of a satellite-ring system. I will then identify what regime several of our solar system’s observed and hypothetical ring systems belong. The satellite-ring evolution regimes of Mars, Uranus, Chariklo, and Chiron will prove to be particularly interesting cases of study.

In Chapter 3 I describe a numerical model I developed to analyze the evolution of ring-satellite systems. My model, which I’ve named “RING-MOONS,” incorporates all of the physics reviewed in Chapter 2. RING-MOONS is a 1-D mixed Eulerian-Lagrangian numerical code. A planetary ring is modeled as a series of Eulerian bins, with each bin representing an annulus of the ring. At the ring edge, ring material is able to form discrete Lagrangian satellites that interact with the ring, and with each other. I will describe how RING-MOONS was designed, the detailed numerical approaches I took to analyze the dynamics of ring-satellite systems, and tests performed against “HYDRORINGS,” a similar model in the literature [Charnoz et al., 2011].

In Chapter 4, I review my motivation for studying the Martian system. For many years the Martian moons, Phobos and Deimos, were thought to be asteroids captured by Mars’s gravity. While this hypothesis may explain the physical characteristics of the satellites, it fails to explain the satellite’s orbits. Both satellites have close, circular orbits aligned with the Martian equator, and are very similar to the orbits expected for ring-satellites. Marinova et al. [2008] argued that Mars likely experienced a giant impact roughly ~ 4.4 By ago that would have ejected a significant mass of material into orbit. Following this hypothesis, many scientists have analyzed the possible dynamics and evolution of a ring in orbit around Mars, and whether it may be possible to form the satellites Phobos and Deimos. Using my analysis in Chapter 2, I realize that an impact-generated ring in orbit around Mars may exist in the Boomerang regime. The dynamics of satellites in the Boomerang regime are unique, motivating me to investigate the formation of Phobos and Deimos. I then implement

RING-MOONS to model the evolution of an impact-generated ring in orbit around Mars and posit a new formation hypothesis for Phobos.

In Chapter 2 I realize that the ring-satellite system of Uranus likely lies in the Torque-Dependent regime. In Chapter 5 I describe the Uranian system as it is understood today. I then investigate a formation hypothesis for the Uranian satellite Miranda. I hypothesize that a giant impact, sufficient to cause Uranus's large obliquity may have produced a massive debris ring around the planet [Morbidelli et al., 2012, Slattery, 1992]. Using RING-MOONS, I model the evolution of an impact generated Uranian ring. I will demonstrate how the dynamics of the Torque-Dependent regime may have caused the ring-satellite system of Uranus to transition from a Slingshot-type evolution, producing Miranda, to a Boomerang-type evolution, producing the inner satellite system observed today.

My final project is described in Chapter 6. Many of the dynamics described in Chapter 2 have been specifically applied to problems where the primary's mass is orders of magnitude larger than the satellites'. In Chapter 6 I analyze how systems with more similar masses evolve over time. I focus on binary systems in the population of Trans-Neptunian Objects (BTNOs). For binary systems, the tidal interaction between the two bodies can result in large-scale changes to the mutual semi-major axis of the system, as well as the rotation rates of both bodies. For some systems, tides can cause the semi-major axis to decrease rapidly. I will outline conditions in which tidal interactions would cause the orbit of a nearly synchronous binary system to completely decay, and show how this could cause mass to shed from the satellite's surface before the two bodies collide to form a contact binary. I compare these conditions to the currently observed population of BTNOs. I focus on TNOs as there is expected be both a significant number of binary and contact binary systems (in which two bodies are attached together) within the population.

The ability of a tidal collapse to cause mass shedding could serve as a source of material for producing rings. Indeed, rings have been observed around the TNOs Chariklo, Chiron, and Haumea, providing additional motivation for my focus on

studying BTNOs. Observations of Chariklo and Chiron have provided rough estimates to their overall body size, revealed their rotation rates, and indicated the existence of planetary rings. I hypothesize that Chariklo and Chiron are actually contact binaries that formed after a nearly synchronous binary system experienced a tidal collapse. With this hypothesis I determine characteristics of the near synchronous binary systems that could have formed Chariklo and Chiron. I then provide results showing the evolution of the tidal collapse, during which the satellite sheds mass. The end result is the formation of a contact binary orbited by a ring. The tidal collapse of BTNOs systems provides a mechanism for TNO rings to form, and the comparison of collapse conditions against the known population of BTNOs indicates how common TNO ring systems may be.

2. THREE SATELLITE-RING FORMATION REGIMES

A version of this chapter has been accepted into The Astronomical Journal as A. J. Hesselbrock and D. A. Minton, "Three Dynamical Evolution Regimes for Coupled Ring-Satellite Systems and Implications for the Formation of the Uranian Satellite Miranda," The Astronomical Journal, 2018.

2.1 The Dynamics of Coupled ring-satellite Systems

In this section I describe the various dynamical processes that affect the evolution of ring-satellite systems over time. My goal is to identify parameters which strongly affect the long-term evolution of coupled ring-satellite systems. The major processes in my model that affect the formation and orbital migration of rings and satellites includes the locations of the Roche limits, Lindblad torques, and tidal torques. I define the Roche limits in Section 2.1.1, the effect of Lindblad torques in Section 2.1.2, and the effect of tidal torques in Section 2.1.3. I define three regimes for the evolution of coupled ring-satellite systems that depend on the rotational period of the primary and the bulk densities of the satellites and the primary. The implications of these regimes on the dynamical evolution of satellites produced by the ring are discussed in Section 2.2.

2.1.1 The Roche Limits

The Roche Limit is the semi-major axis at which the tensional forces acting on a cohesionless satellite due to tides are greater than the compressional forces from self-gravity [Murray and Dermott, 1999]. It can be calculated by solving for the semi-major axis at which a particle on the equator of a synchronously rotating satellite has

zero acceleration. For orbits outside the Roche limit, the self-gravity of the satellite dominates and the particle remains on the body’s surface. Conversely, for orbits interior to the Roche limit, the gravitational attraction of the primary dominates and the particle is accelerated away from the satellite’s surface.

The shape of the satellite plays a role in the definition of the Roche limit. Two common definitions for the Roche limit are the “rigid Roche limit” (RRL) and the “fluid Roche limit” (FRL). The assumption that the satellite can maintain a rigid spherical shape gives rise to the RRL. The semi-major axis of the RRL is [Murray and Dermott, 1999]:

$$a_{RRL} = R_p \left(\frac{3\rho_p}{\rho_s} \right)^{1/3} \approx 1.442R_p \left(\frac{\rho_p}{\rho_s} \right)^{1/3}. \quad (2.1)$$

Here R_p and ρ_p are the radius and bulk density of the primary, while ρ_s is the bulk density of the satellite.

Most satellites are not rigid spheres, and therefore the RRL is a lower limit for a “cohesionless” satellite. At the opposite extreme, the satellite behaves as a fluid that can flow into a hydrostatic equilibrium shape. The resulting ellipsoidal figure of equilibrium for a fluid satellite is a prolate spheroid [Chandrasekhar, 1969]. Because the particles on the equator of a prolate body are located a greater distance from the body center as compared to a spherical body, the self-gravity component of the acceleration is reduced when calculating the “fluid Roche limit” (FRL) [Chandrasekhar, 1969]. Thus, the FRL is farther from the primary than the RRL. The semi-major axis of the FRL is [Murray and Dermott, 1999]:

$$a_{FRL} \approx 2.456R_p \left(\frac{\rho_p}{\rho_s} \right)^{1/3}. \quad (2.2)$$

Although the material in planetary rings is solid, the interactions between ring particles can be approximated as a fluid. This means that ring material orbiting inside the FRL is continually tidally disrupted, and is unable to accrete into satellites. If ring material is transported beyond the FRL, where tidal forces are weaker, it can accrete into satellites. Thus, the FRL marks the approximate outside boundary of a massive ring.

Once formed, interparticle forces within the satellite may prevent it from attaining a hydrostatic equilibrium shape. Internal friction can allow even strengthless aggregates of particles to maintain non-hydrostatic shapes. Therefore, the location where a fully formed satellite can be disrupted into a ring may be inward of where it formed. The RRL is approximately the innermost boundary where such a strengthless satellite could hold together [Hesselbrock and Minton, 2017].

For a given primary body, calculating the Roche limits allows us to estimate where rings and satellites may orbit the body. Ring material is confined to orbit inside the FRL. While satellites may only accrete outside the FRL, if they have internal cohesion they may exist anywhere outside the RRL. Assuming the satellites have no strength, but only cohesion sufficient to hold themselves together, no satellites should orbit inside the RRL, as they would be tidally disrupted [Black and Mittal, 2015]

As the particles within rings collide and exchange energy and angular momentum, any ring in orbit around a primary will spread out overtime due to a process called “viscous spreading” [Goldreich and Tremaine, 1982, Lynden-Bell and Pringle, 1974]. This spreading process causes material to be transported both inwards, towards the primary, and outwards toward the FRL. Thus, as the ring spreads out, some material is transported beyond the FRL where it may accrete into satellites [Charnoz et al., 2010, Crida and Charnoz, 2012, Hesselbrock and Minton, 2017, Rosenblatt and Charnoz, 2012, Salmon and Canup, 2017].

2.1.2 Lindblad Torques

Once a satellite has formed, it begins to gravitationally interact with material in the ring. The orbital speed of the interior ring material is greater than that of the exterior orbiting satellite. Ring material is gravitationally attracted to the perturbing satellite, causing a density perturbation that is carried ahead of the satellite. The interactions between the ring material and the satellite are strongest for material in a first order resonance with the satellite. The resonant perturbations cause the ring

material and the exterior satellite to exchange angular momentum through a series of torques called “Lindblad torques” [Goldreich and Tremaine, 1979, Lynden-Bell and Pringle, 1974]. Lindblad torques concentrate the ring material into spiral density waves [Goldreich and Tremaine, 1979] which in turn perturb the orbit of the exterior satellite. The resonant interaction transfers angular momentum from the ring to the exterior satellite, increasing the satellite’s semi-major axis. While the satellite and the ring are gravitationally attracted, Lindblad torques work to repel the satellite from the ring [Esposito, 2006].

I may determine the locations within a ring that are in resonance with a satellite. For a satellite in a first order resonance of order $\mathcal{M}(> 1)$, the Lindblad resonance locations in a Keplerian ring interior to the satellite $r_{\mathcal{M}}$ can be found as [Takeuchi et al., 1996]:

$$r_{\mathcal{M}} = \left(1 - \frac{1}{\mathcal{M}}\right)^{2/3} a, \quad (2.3)$$

where a is the semi-major axis of the exterior satellite.

The magnitude of the Lindblad torques are a function of the distance to the satellite and the surface-mass density of the ring near the resonance. The Lindblad torque exerted by the ring material at a specific resonance of order \mathcal{M} onto the satellite can be calculated as [Esposito, 2006]:

$$\Gamma_{\mathcal{M}} = \pm \sigma(r_{\mathcal{M}}) \left(\frac{GaM_s^2}{M_p}\right) [\mathcal{M}^2 (\mathcal{M} - 1)]^{2/3}, \quad (2.4)$$

where G is Newton’s gravitational constant, M_p and M_s are the mass of the primary and the satellite, and $\sigma(r_{\mathcal{M}})$ is the surface-mass density of the ring at the location of the Lindblad resonance. For a satellite exterior to a ring the sign of the torque is positive, while for a satellite interior to a ring the sign of the torque is negative. I will only consider the case of satellites exterior to rings here. The total torque Γ exerted onto the satellite by the ring is the sum of the individual resonant torques, or:

$$\Gamma = \sum_{\mathcal{M}=2}^{\infty} \Gamma_{\mathcal{M}}. \quad (2.5)$$

Lindblad torques transfer angular momentum from the ring particles to the satellite’s orbital angular momentum, which causes the satellite to migrate away from the ring.

The change in an exterior satellite's semi-major axis due to an inner Lindblad torque is [Takeuchi et al., 1996]:

$$\frac{da}{dt} = \frac{2\Gamma}{M_s} \left(\frac{a}{GM_p} \right)^{1/2}. \quad (2.6)$$

The ring can exert a Lindblad torque on the satellite as long as some ring material is in a first-order resonance with the satellite. Therefore, there is a maximum distance a satellite can be perturbed to via Lindblad torques, as eventually the satellite will orbit too far away to be in resonance with any material in the ring. The farthest the satellite may be perturbed to via Lindblad torques is when the satellite is in resonance with the material at the edge of the ring, at the FRL. To find the satellite semi-major axes that may be in resonance with the ring edge, I substitute a_{FRL} for $r_{\mathcal{M}}$ and rearrange Equation 2.3 to yield:

$$a_{\mathcal{M}} = a_{FRL} \left(1 - \frac{1}{\mathcal{M}} \right)^{-2/3}. \quad (2.7)$$

The greatest satellite semi-major axis that the ring edge may be in resonance with occurs when $\mathcal{M} = 2$, which corresponds to the 2 : 1 mean motion resonance. Therefore, I find that the maximum orbit a satellite may migrate to via Lindblad torques is:

$$a_{Lind} = 4^{1/3} a_{FRL} \approx 2.456 R_p \left(\frac{4\rho_p}{\rho_s} \right)^{1/3}. \quad (2.8)$$

2.1.3 Tidal Torques

In addition to accelerating the material in the ring, the satellite also exerts an acceleration on the surface of the primary [Murray and Dermott, 1999]. The acceleration from the orbiting satellite varies in magnitude across the primary's surface and is greatest for the surface closest to the satellite. The gradient tidal potential across the primary's surface distorts the primary's shape, creating a tidal bulge. The internal structure of the primary determines the response of the surface to the tidal potential. Internal friction dissipates the tidal acceleration and results in a lag between the tidal disturbance and the tidal response. The effect of tidal dissipation can lead to dramatic physical and orbital consequences for the primary and the satellite.

Although the satellite creates the tidal bulge on the primary, the acceleration of the bulge on the satellite exerts a torque on the satellite. The consequence of the tidal torque is dependent upon the semi-major axis of the satellite relative to the synchronous orbit. For a satellite in a Keplerian orbit, the synchronous orbit can be calculated as:

$$a_{synch} = \left[\frac{G(M_p + M_s)T_p^2}{4\pi^2} \right]^{1/3}, \quad (2.9)$$

where T_p is the rotational period of the primary. If the satellite is in a synchronous orbit with the primary, it completes one orbit for every full revolution of the primary, and therefore is always aligned with the tidal bulge. The gravitational attraction between the tidal bulge and the satellite is perpendicular to the satellite's motion, and no torque results.

However, if the satellite orbits interior to the synchronous orbit, its orbital period is shorter than the rotational period of the primary. As the satellite orbits, it passes over the surface of the primary. Due to the lag in the formation of the tidal bulge, the satellite is always “ahead” of the tidal bulge on the primary surface. The gravitational attraction between the tidal bulge and the satellite is no longer strictly perpendicular to the satellite's motion, and the tidal bulge exerts a torque on the satellite. For satellites orbiting interior to the synchronous orbit this torque transfers angular momentum from the satellite's orbit to the spin angular momentum of the primary, causing the satellite to migrate towards the primary.

Alternatively, if the satellite orbits exterior to the synchronous orbit, its orbital period is longer than the rotational period of the primary. As the satellite orbits, the surface of the primary rotates past the satellite. Due to the lag in the formation of the tidal bulge, the satellite is always “behind” the tidal bulge on the primary surface. The bulge again exerts a torque on the satellite. However, for satellites orbiting exterior to the synchronous orbit the tidal torque transfers spin angular momentum from the primary to the satellite's orbital angular momentum, causing the satellite to migrate away from the primary. Thus, satellites which lie interior to the synchronous orbit migrate inwards by tides, whereas satellites which orbit exterior migrate outwards.

For satellites that are not located at a_{synch} , the transfer between the satellite's orbital angular momentum and the spin angular momentum of the primary causes the satellite to migrate in its orbit. The torque exerted by the tidal bulge changes the semi-major axis of the satellite. The change in the satellite's semi-major axis due to the tidal interaction is calculated as [Murray and Dermott, 1999]:

$$\frac{da}{dt} = \text{sign}(\omega_p - n) \frac{3nM_s R_p^5}{a^4 M_p} \left(\frac{k_2}{Q} \right) \left[1 + \frac{51e^2}{4} \right]. \quad (2.10)$$

Here the mean motion $n = [G(M_p + M_s)/a^3]^{1/2}$, e is the eccentricity of the satellite, while ω_p , k_2 and Q are the rotation rate, tidal potential love number, and tidal quality factor of the primary. In general, $\text{sign}(\omega_p - n) > 0$ for a satellite with $a > a_{synch}$, and $\text{sign}(\omega_p - n) < 0$ for a satellite with $a < a_{synch}$.

2.1.4 Satellite Migration

The tidal interaction with the primary, as well as the Lindblad torques combine to drive the orbital migration of the satellite. To determine the change in the semi-major axis of a satellite orbiting exterior to a ring I may combine Equations 2.6 and 2.10. The total change in the semi-major axis of a satellite in time due to Lindblad and tidal torques is given as [Rosenblatt and Charnoz, 2012]:

$$\frac{da}{dt} = \text{sign}(\omega_p - n) \frac{3nM_s R_p^5}{a^4 M_p} \left(\frac{k_2}{Q} \right) \left[1 + \frac{51e^2}{4} \right] + \frac{2\Gamma}{M_s} \left(\frac{a}{GM_p} \right)^{1/2}. \quad (2.11)$$

As shown in Equation 2.11, if $a > a_{synch}$ for a satellite exterior to the ring, both terms are positive, da/dt is positive, and the semi-major axis of the satellite increases. However, if $a < a_{synch}$, the two terms are opposite in sign, and a competition exists: the tidal torques work to evolve the satellite inwards while the Lindblad torques work to drive the satellite away. da/dt is no longer strictly positive because the relative magnitude of these two torques determines the sign of Equation 2.11. The location of the synchronous orbit relative to the FRL determines whether tidal torques cause newly formed ring satellites to migrate towards or away from the ring, thus playing a key role in understanding the migration of satellites accreting at the ring edge.

The locations of the RRL, FRL, and a_{Lind} are all functions of the bulk density of the primary body and the satellites. Independently, the synchronous orbit is only a function of the rotational period of the primary. From Equation 2.9 we see that the rotation period of the primary and the location of the synchronous orbit are directly related. In Figure 2.1 I display three identical ring-satellite systems, however in each panel the rotation period of the primary has been varied. In each panel, $\rho_s/\rho_p = 1$. Using Equations 2.1, 2.2, and 2.8 we may determine the locations of the RRL, FRL, and a_{Lind} in terms of primary radii. For a given primary rotation period, we may determine the location of a_{synch} . In Figure 2.1a I have marked the location of a_{synch} for a primary with T_p such that $a_{synch} > a_{Lind}$. In Figure 2.1b I have displayed a similar system, however the primary rotates with a shorter T_p such that $a_{FRL} < a_{synch} < a_{Lind}$. Finally, in Figure 2.1c, I display an identical system, but with a rapidly rotating primary such that $a_{synch} < a_{FRL}$.

I define a function f , which I use to determine the location of a_{synch} relative to a_{FRL} and a_{Lind} . The value of f for a coupled ring-satellite system determines the regimes shown in Figure 2.1. To define f , I derive the conditions for $a_{synch} = a_{Lind}$. I set $a_{synch} = a_{Lind}$ using Equations 2.9 and 2.8:

$$\frac{1}{2.456^3} \frac{G\rho_s T_p^2}{3\pi} \left(1 + \frac{M_s}{M_p}\right) = 4. \quad (2.12)$$

I define the left hand side of Equation 2.12 to be the function f , such that:

$$f(T_p, \rho_s) = \frac{1}{2.456^3} \frac{G\rho_s T_p^2}{3\pi} \left(1 + \frac{M_s}{M_p}\right). \quad (2.13)$$

Thus, the right hand side of Equation 2.12 yields the condition when $a_{synch} = a_{Lind}$. In this scenario $f(T_p, \rho_s) = 4$. Therefore, for ring-satellite systems where $f(T_p, \rho_s) > 4$, the synchronous orbit lies beyond the maximum orbit to which a ring-accreted satellite could migrate via Lindblad torques.

In order to determine the location of a_{synch} relative to a_{FRL} I may derive the conditions for when $a_{synch} = a_{FRL}$. Using Equations 2.9 and 2.2:

$$\frac{1}{2.456^3} \frac{G\rho_s T_p^2}{3\pi} \left(1 + \frac{M_s}{M_p}\right) = 1. \quad (2.14)$$

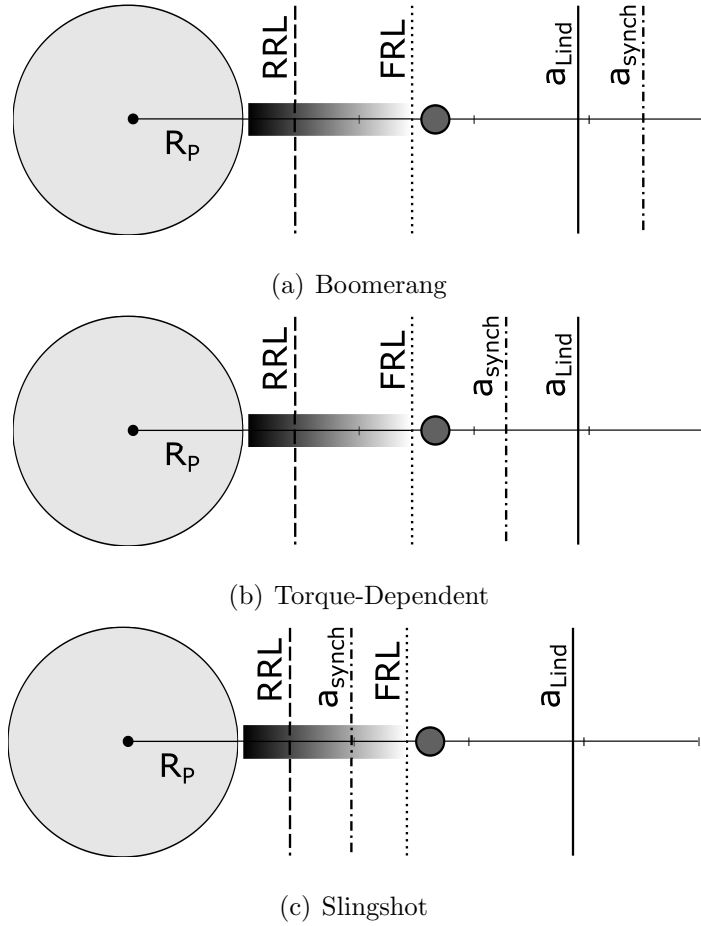


Figure 2.1. Diagram showing the relationships that define the three evolution regimes for coupled ring-satellites. The large grey circle represents a primary body of radius R_p orbited by a ring (shaded region), and a small satellite (small circle) that has formed at the ring edge. The rigid Roche limit (RRL), fluid Roche limit (FRL), the maximum orbit Lindblad torques may migrate a satellite (a_{Lind}), and the synchronous orbit (a_{synch}) are all marked with vertical lines. Distances are shown in units of primary radii. The primary and satellite are assumed to have the same density. (a) Boomerang regime: For a slowly rotating primary, a_{synch} lies beyond a_{Lind} . (b) Torque-Dependent regime: For a moderate rotation period, a_{synch} lies between the FRL and a_{Lind} . (c) Slingshot regime: For rapidly rotating primaries a_{synch} lies inside the FRL.

During this derivation I recover the function f and the conditions for when $a_{synch} = a_{FRL}$. In this scenario $f(T_p, \rho_s) = 1$.

The function $f(T_p, \rho_s)$ may be applied to any planetary ring system to determine in which formation regime the system exists. In ring systems where $f(T_p, \rho_s) > 4$, the synchronous orbit lies beyond the maximum orbit a satellite could migrate via Lindblad torques (i.e. Figure 2.1a). For ring systems where $1 < f(T_p, \rho_s) < 4$, the synchronous orbit lies between the FRL and a_{Lind} (i.e. Figure 2.1b). Finally, in ring systems where $f(T_p, \rho_s) < 1$, the synchronous orbit lies inside the FRL (i.e. Figure 2.1c). In each scenario depicted in Figure 2.1, and further defined by Equation 2.13, the orbital migration of the satellite that has accreted at the ring edge, as determined by Equation 2.11, is different. In Section 2.2, I explore the long-term evolution of ring-satellite systems in each of the three formation regimes.

2.2 Evolution of Ring Accreted Satellites

The scenarios depicted in Figure 2.1 represent three distinct formation regimes for satellites accreting from planetary rings. In the “Boomerang” regime the synchronous orbit lies beyond the maximum orbit a satellite may be perturbed via Lindblad torques, as shown for the system in Figure 2.1a. In the “Slingshot” regime the synchronous orbit lies inside the ring edge, as displayed in Figure 2.1c. And finally, in the “Torque-Dependent” regime the synchronous orbit lies between the edge of the ring and a_{Lind} , as in Figure 2.1b, creating a competition between the tidal and Lindblad torques exerted on a newly formed satellite. Depending upon the magnitudes of the ring and tidal torques satellites in this regime either migrate away from the primary and survive, similar to satellites in a Slingshot regime, or migrate towards the RRL, similar to satellites in a Boomerang regime.

In Section 2.1 I defined the function $f(T_p, \rho_s)$, which I use to determine the location of a_{synch} relative to a_{Lind} and the FRL. This relation can be applied to any known or hypothesized planetary ring system in order to predict the long term evolution of

satellites that may accrete at the FRL. In the following section I will use this relation to characterize and analyze each of the regimes for satellite evolution.

2.2.1 The “Boomerang” Regime: $a_{Lind} < a_{synch}$

For slowly rotating primaries, the synchronous orbit lies far from the primary’s surface. For planetary ring systems where $f(T_p, \rho_s) > 4$, a_{synch} lies beyond a_{Lind} , as in Figure 2.1a. I may examine Equation 2.11 to determine the orbital migration of a satellite that accretes from a planetary ring in the Boomerang regime. In the Boomerang regime da/dt for a newly accreted satellite at the FRL is not necessarily positive. The ring may have sufficient mass for Lindblad torques to temporarily drive a satellite away from the primary. However, planetary tides always work to migrate the satellite inwards.

As the satellite is driven away from the ring, eventually an equilibrium between the Lindblad and tidal torques is reached, and $da/dt = 0$. Over time the ring is depleted of material as mass is deposited onto the primary through the ring’s inner edge, and mass is lost to satellite formation at the ring’s outer edge [Hesselbrock and Minton, 2017, Rosenblatt and Charnoz, 2012, Rosenblatt et al., 2016]. As the ring loses mass, the effect of Lindblad torques on the satellites’ evolution is diminished until tidal torques with the primary dominate. Similar to a boomerang, satellites in this regime may initially be driven away from the ring, but eventually are driven inwards as Equation 2.11 becomes negative. Regardless of how massive the ring is, the orbit of a satellite accreting at the FRL in this “boomerang” regime will eventually decay. Therefore, I define the Boomerang regime as any planetary ring system with $f(T_p, \rho_s) > 4$.

Furthermore, as the satellite approaches the RRL, the magnitude of the tidal stress increases and material begins to leave the surface of the satellite. This removed material creates a collisional cascade that quickly disrupts the body. The disrupted satellite material then forms a new ring of material that would begin to deposit its

material onto the primary’s surface [Black and Mittal, 2015]. As the new ring begins to spread out through viscous spreading, it may transport material beyond the FRL to form a new generation of satellites [Hesselbrock and Minton, 2017]. However, as these satellites accrete in the Boomerang regime they will follow a similar migration path. I recently showed that the innermost satellite of Mars, Phobos, may have formed in the Boomerang regime [Hesselbrock and Minton, 2017]. Therefore, slowly rotating primaries where a_{synch} lies beyond a_{Lind} serve as desirable candidates for ring-satellite cycles, as proposed in HM17.

2.2.2 The “Slingshot” Regime: $a_{synch} < a_{FRL}$

As shown in Section 2.1, for ring systems where $f(T_p, \rho_s) < 1$ the edge of the ring lies beyond the synchronous orbit. For a satellite accreting at the edge of the ring in Figure 2.1c, both the tidal torques and the Lindblad torques work to increase the semi-major axis of the satellite. da/dt in Equation 2.11 is strictly positive and any satellites that form at the ring edge are driven away from the primary. Similar to a projectile fired from a slingshot, in these systems satellites that form at the FRL are forever driven away from the primary. I define the “Slingshot” regime as any planetary ring system where $f(T_p, \rho_s) < 1$.

2.2.3 The “Torque-Dependent” Regime: $a_{FRL} < a_{synch} < a_{Lind}$

Similar to the Boomerang regime, for a ring-satellite system where a_{synch} lies between the FRL and a_{Lind} , satellites that accrete at the FRL experience a competition between Lindblad and tidal torques. As the satellites are pulled inwards by planetary tides, da/dt in Equation 2.11 is not strictly positive. However, if the magnitude of the total Lindblad torque is greater than the inward tidal torque, it may be possible for Equation 2.11 to remain positive for a sufficient amount of time for a satellite to migrate beyond a_{synch} . At this point in the satellite’s migration Equation 2.11 becomes strictly positive, regardless of the magnitude of the Lindblad torque, and

the satellite survives to migrate away from the primary, similar to the evolution of a satellite in the Slingshot regime.

Alternatively, if the magnitude of the tidal torque is greater than the total Lindblad torque for a satellite orbiting inside a_{synch} , Equation 2.11 is negative and the satellite would be unable to migrate beyond a_{synch} . As $da/dt < 0$, the satellite's orbit migrates inwards towards the RRL. Depending on the magnitude of the Lindblad torques, satellites that accrete in this regime may undergo an identical evolution to satellites that accrete in the Boomerang regime. As the outcome of the satellites' orbital migration is dependent upon the competition between the tidal and Lindblad torques, I refer to this regime as the "Torque-Dependent" regime and define the regime as any ring system where $1 < f(T_p, \rho_s) < 4$.

In order to predict the migration of satellites accreting in the Torque-Dependent regime we must closely examine the contribution of the Lindblad and tidal torques to the satellite's migration. The magnitude of the total Lindblad torque in Equation 2.5 compared to the tidal torque with the primary is a determining factor to the migration of a satellite interior to a_{synch} . Examining Equations 2.11 and 2.5, we see that depending on the tidal parameters of the bodies and the surface-mass density of the ring, it is possible for the total Lindblad torque exerted on the satellite to be greater in magnitude than the tidal torque. In this case, da/dt in Equation 2.11 is positive and the satellite is driven away from the ring edge. I define this as a scenario in which the Lindblad torques are able to overcome the tidal interactions that work to drive the satellite inwards.

We may also examine when the magnitude of the total Lindblad torque is less than that of the tidal torque for a satellite interior to a_{synch} . In these cases, da/dt in Equation 2.11 is negative, and the Lindblad torques are unable to overcome the tidal interactions. Thus, if the surface-mass density of the ring is small, and/or the satellite is strongly affected by tidal interactions with the primary, the satellite will migrate inwards.

It is possible to determine whether the Lindblad torques dominate over tides or not by setting Equation 2.11 equal to zero. This allows me to determine the conditions for which the Lindblad and tidal torques are equal in magnitude. If the magnitude of the tidal term in Equation 2.11 is less than the magnitude of the Lindblad term, the satellite will be driven outwards. By substituting the total Lindblad torque in Equation 2.5 into the Lindblad term in Equation 2.11, I find that the satellite will be driven away from the ring so long as the following statement is true:

$$\sum_{\mathcal{M}=2}^{\infty} \sigma(r_L) [\mathcal{M}^2 (\mathcal{M} - 1)]^{2/3} > \frac{3k_2 M_p R_p^5}{2Qa^7}. \quad (2.15)$$

Here I have assumed that the satellite eccentricity is zero. Equation 2.15 is similar to Equation A.2 in Rosenblatt and Charnoz [2012].

If Equation 2.15 is true for the entirety of the satellite's evolution to the synchronous orbit, the satellite will be driven away from the primary until it reaches an orbit beyond a_{synch} . At this point da/dt becomes strictly positive and the satellite will be forever driven away from the primary. If the ring is sufficiently massive the satellite will follow an evolution similar to satellites in a Slingshot regime. However, as discussed in Section 2.2.1, material is constantly removed from the ring over time, diminishing the magnitude of the Lindblad torques. If Equation 2.15 becomes false before the satellite has evolved to a_{synch} , the satellite will be pulled inwards towards the primary. Similar to satellites in the Boomerang regime, the satellite's orbit will decay until either the satellite is tidally disrupted, forming a new ring, or the satellite is deposited onto the primary.

2.3 A Look at Our Solar System

In Section 2.2, I identified three regimes for the evolution of coupled ring-satellite systems. I defined these regimes with the function f in Equation 2.13, which is dependent upon the bulk density of the satellite and the rotation period of the primary. Figure 2.2 plots the boundaries of the three regimes defined by Equation 2.13 assuming the satellite mass is small relative to the primary ($M_s/M_p \ll 1$).

The dark gray region in Figure 2.2 corresponds to the Boomerang regime (see Figure 2.1). For slowly rotating primaries ($T_p \sim 25$ hrs) I find that the synchronous orbit lies beyond the maximum orbit for a wide-range of satellite densities. The light gray region in Figure 2.2 corresponds to the Slingshot regime. For rapidly rotating primaries ($T_p \sim 10$ hrs) I find that the synchronous orbit lies inside the ring edge for a wide range of satellite densities. Lastly, the white region in Figure 2.2 corresponds to the Torque-Dependent regime. For primaries with moderate rotation rates ($T_p \sim 15$ hrs), satellites with a wide range of densities accreting at the ring edge will undergo a competition between Lindblad and tidal torques. If the magnitude of the Lindblad torque is greater than the tidal torques, the system will evolve similar to a Slingshot system. Otherwise, the system will exhibit an evolution similar to a Boomerang system.

In Figure 2.2 I use the current rotation period of primary bodies in the Solar System with estimates for the density of their secondaries to determine the evolution regime for real and hypothetical ring systems in the Solar System. We see that the hypothetical Mars system, modeled in HM17, with its slow rotation rate and satellites with relatively high bulk densities is located within the Boomerang regime. Additionally, we see that the Saturn system, with its rapid rotation rate and low-density satellites is located within the Slingshot regime. This is in agreement with observations of the architecture of the inner ring satellites of Saturn and recent simulation results [Charnoz et al., 2010, 2011, Salmon and Canup, 2017].

Recently stellar occultations have revealed rings in orbit around small bodies. These observations have shown that the centaurs 10199 Chariklo and 2060 Chiron are both orbited by ring systems [Braga-Ribas et al., 2014, Ortiz et al., 2015]. Furthermore, Ortiz et al. [2017] also reports that a planetary ring orbits Haumea, a dwarf planet in the Kuiper belt with two known satellites. All of these bodies are rapid rotators, with Haumea approaching a Jacobi ellipsoid in hydrostatic equilibrium. As shown in Figure 2.2, the short spin period of these three bodies place them in the Slingshot regime for a wide range of satellite densities. Satellites generated from these

rings would migrate away from the primary body. Therefore, it is unlikely the tidal disruption of an inwardly migrating satellite would have produced the ring systems observed today.

Uranus and Neptune both fall into the Torque-Dependent regime, as shown in Figure 2.2. Both of these giant planets have rings and inner satellites that orbit near the rings' edges and may be products of tidal disruption [Leinhardt et al., 2012]. Furthermore, both Uranus and Neptune are orbited by satellites on either side of the synchronous orbit. It may be possible that these planets had primordial rings that were sufficiently massive to cause satellites to migrate far from the FRL and beyond a_{synch} , similar to a system in the Slingshot regime.

2.4 Conclusion

In this chapter I have developed a framework to investigate the evolution of coupled ring-satellite systems. Satellites in orbits near massive planetary rings may exchange angular momentum with both the ring and the primary body. The dynamics of how angular momentum is exchanged with the satellite creates three distinct evolution regimes for satellites accreting from massive planetary rings. I term these the Boomerang, Slingshot, and Torque-Dependent regimes. The three formation regimes, outlined in Section 2.2, provide a method to analyze the dominant dynamics of massive ring systems interacting with nearby satellites. Identifying in which regime a ring-satellite system exists enables us to hypothesize the past and future evolution of the system. Furthermore, my model makes predictions of the behavior of many systems and motivates future searches for potential rings and/or satellites.

In the Slingshot regime, the synchronous orbit lies inside the location of the FRL. If a ring in the Slingshot regime is able to viscously spread material to the FRL, the system should produce at least one satellite that would likely be observable today as both the ring and tidal torques would cause the satellite to migrate away from the primary. In the Boomerang regime the synchronous orbit lies outside the maximum

orbit Lindblad torques could perturb a satellite. Satellites that form out of massive rings in the Boomerang regime may migrate away from the primary via Lindblad torques, however over time tidal torques cause the satellite to migrate inwards. As a satellite's semi-major axis decreases, tidal stresses across the body increase and may disrupt the satellite into forming a new ring. As shown in HM17, it is possible for a planetary body in the Boomerang regime to have a cycle of ring formation and satellite accretion that persists for billions of years. The dynamics of the coupled ring-satellite systems in the Boomerang regime provide a mechanism to repeatedly generate satellites, and rings, provided satellites disrupt interior to the FRL [Black and Mittal, 2015, Hesselbrock and Minton, 2017]. An observation of a system that is in the Boomerang regime with a satellite inside a_{synch} is an indication that a ring may have existed, or currently exists, at the system. Satellites in Boomerang regime systems (such as at Eris, see Figure 2.2) could motivate a search for rings.

In the Torque-Dependent regime the synchronous orbit lies between the FRL and the maximum orbit Lindblad torques could perturb a satellite. Planetary systems with rings in the Torque-Dependent regime may exhibit characteristics of both Boomerang and Slingshot systems. Much like satellites that accrete from a ring in the Boomerang regime, satellites in the Torque-Dependent regime experience a competition between Lindblad and tidal torques. As Torque-Dependent systems evolve over time, they may transition from having rings that are sufficiently massive to cause satellites to migrate beyond the synchronous orbit (Slingshot), to systems in which tidal interactions dominate the migration of ring-accreted satellites (Boomerang). Rings in the Torque-Dependent regime may initially be massive enough to cause a satellite that accretes at the FRL to migrate beyond the synchronous orbit, however over time the mass of the ring may deplete such that tidal torques dominate a satellite's migration.

Torque-Dependent regime systems like Uranus and Neptune may repeatedly generate satellites and rings, similar to systems in the Boomerang regime. As the mass of a ring is depleted, any satellites interior to the synchronous orbit could migrate back

toward the primary, possibly going through complex phases of scattering, disruption, and reaccretion. Thus, satellites identified in Torque-Dependent regime systems (such as at Quaoar, see Figure 2.2) would also motivate a search for potential rings or interior satellites.

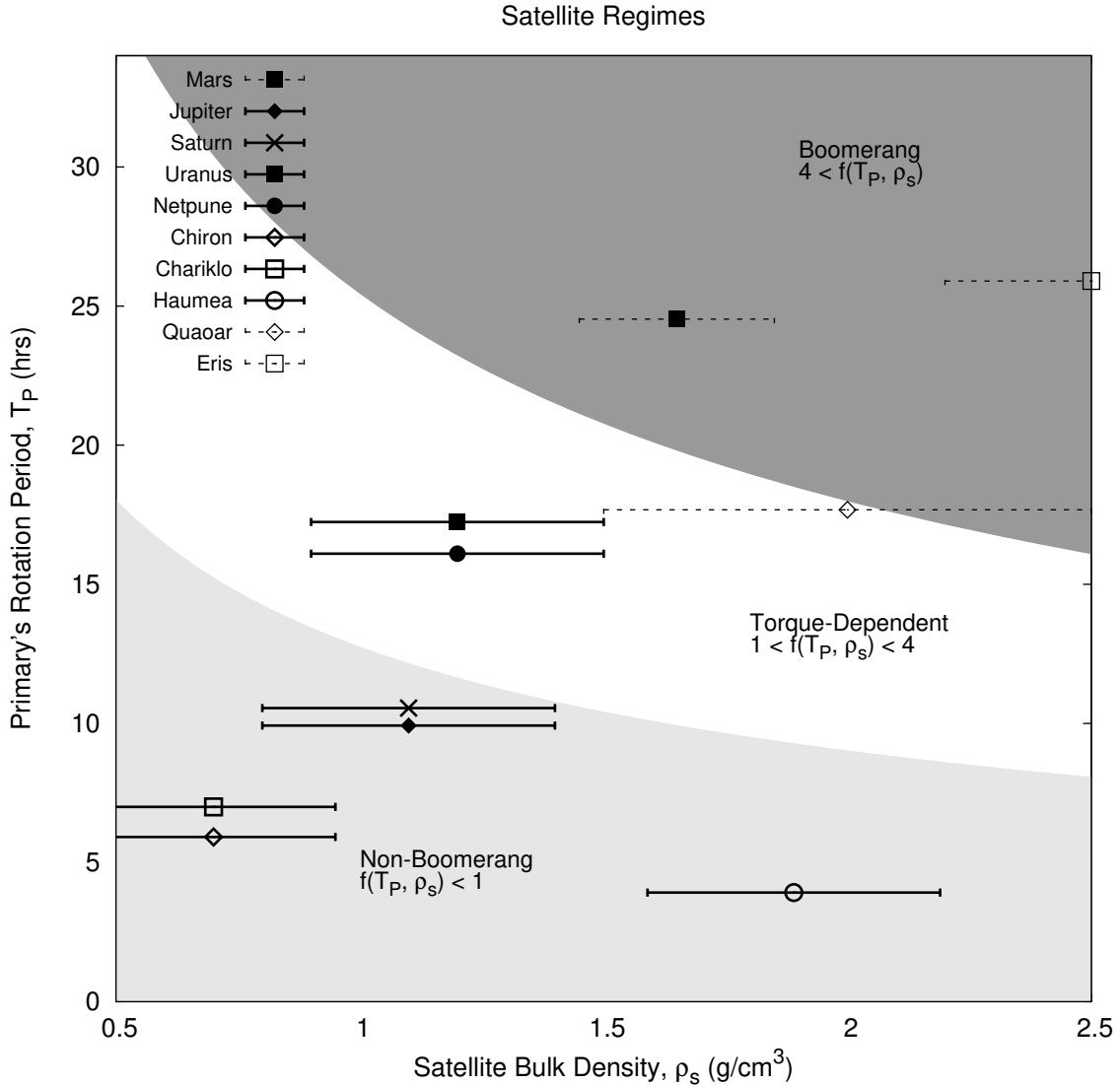


Figure 2.2. The boundaries of the three ring-satellite evolution regimes defined by Equation 2.13 (assuming $M_s/M_p \ll 1$). The dark gray regime marks the Boomerang regime (systems where $a_{synch} > a_{Lind}$), while the light gray regime marks the Slingshot regime (systems where $a_{synch} < a_{FRL}$). The middle zone in white marks the Torque-Dependent regime (systems where $a_{FRL} < a_{synch} < a_{Lind}$). Additionally, I display the expected regime for Roche-interior rings orbiting various bodies in the solar system given their rotation rates today and estimated satellite densities. In this figure, $M_s/M_p \ll 1$. Fast rotating primaries with low satellite densities fall within the Slingshot regime (e.g. Jupiter, Saturn), while slowly rotating primaries with high density satellites exist within the boomerang regime (e.g. Mars). The evolution of satellites accreting from a Roche-interior ring orbiting Uranus and Neptune is dependent upon the magnitude of the Lindblad and tidal torques.

3. DESCRIPTION OF “RING-MOONS” MODEL

A version of this chapter has been published in A. J. Hesselbrock and D. A. Minton, “An ongoing satellite-ring cycle of Mars and the origins of Phobos and Deimos,” Nature Geoscience, 10:266269, Mar. 2017. doi:10.1038/ngeo2916.

I have developed a model to study the evolution of debris disk and satellite systems. My model contains a 1-D Eulerian treatment for the disk and a simple Lagrangian treatment for the satellites. The disk is represented as a finite series of bins that extend radially from the planet. Each bin in my Eulerian disk model represents an annulus of the disk with a given surface mass density. Each bin is identified via the identifying location, i . The midpoint location of each bin is $r_i = r_{Init} + \Delta r(i + 1/2)$ where $\Delta r = \frac{r_{Fin} - r_{Init}}{N}$, and N is the number of bins. The quantities r_{Init} and r_{Fin} are the interior and exterior limits of the disk. The horizontal area of each bin can then be calculated: $\Delta A_i = \pi \left[\left(r_i + \frac{\Delta r}{2} \right)^2 - \left(r_i - \frac{\Delta r}{2} \right)^2 \right] = 2\Delta r \left[r_{Init} + \Delta r \left(i + \frac{1}{2} \right) \right] \pi$.

From that the surface mass density of each bin is assigned with a power law, $\Sigma_i = c \left(\frac{r_i}{r_{Init}} \right)^{-p}$, with c and p variables to set the mass of the disk. Then the mass for each bin is solved by integrating:

$$m_i = \int_0^{2\pi} \int_{r_i - \Delta r/2}^{r_i + \Delta r/2} \Sigma(r) r dr d\theta. \quad (3.1)$$

The moment of inertia of each ring annulus, which, in my coordinate system, is defined as:

$$I_i = m_i \left(r_i^2 + \frac{\Delta r^2}{4} \right) = m_i R_i^*, \quad (3.2)$$

where $R_i^* \equiv r_i^2 + \frac{\Delta r^2}{4}$. Additionally, ω_i is the orbital speed of bin i , which is simply the orbital speed for an object in a circular orbit with semi-major axis r_i :

$$\omega_i = \sqrt{\frac{GM_p}{r_i^3}}. \quad (3.3)$$

In many ways my disk model is very similar to those described in both Rosenblatt and Charnoz [2012] and Salmon et al. [2010b]. The results published in those studies serve as useful calibrations of my disk model. With the framework of a disk in place I am able to implement relevant disk and satellite dynamics.

3.1 Disk Viscosity

The disk is composed of particles which collide, transferring energy and momentum to each other. As these particles collide, their momentum is conserved but their energy is not. This loss of energy causes some particles to fall inwards toward the central region of the disk and lose angular momentum. Thus, to conserve the momentum of the system, their angular momentum is transferred outwards away from the central region of the disk by moving some material outwards. The net effect is to flatten the disk and to cause it to spread. Some material flows inwards, and some flows outwards (see Figure 3.1). Disks are typically described in terms of their surface mass density. Therefore, by combining mass conservation with angular momentum conservation, the change in surface mass density over time for a region of the disk may be calculated. The change to the surface mass density of a location depends upon its current surface mass density, semi-major axis, and viscosity.

The evolution of the surface mass density of the disk at location r can be found by solving the following equation (Bath and Pringle [1981b]):

$$\frac{\partial \Sigma}{\partial t} = \frac{3}{r} \frac{\partial}{\partial r} \left[\sqrt{r} \frac{\partial}{\partial r} (\nu \Sigma \sqrt{r}) \right], \quad (3.4)$$

where ν is the viscosity at r . As shown in Bath and Pringle [1981a], this equation can be solved after performing the following variable change: $X_i = 2\sqrt{r_i}$, $S_i = X_i\Sigma_i = 2\Sigma_i\sqrt{r_i}$. Then the above equation can be recast as:

$$\frac{\partial S}{\partial t} = \frac{12}{X_i^2} \left[\frac{\partial^2}{\partial X^2} (S_i\nu_i) \right] \quad (3.5)$$

Finite difference solutions of this equation may go unstable. Therefore, a stability analysis shows that the necessary timestep for a solution is found as (Anderson [1995]):

$$\begin{aligned} \Delta t &\leq \frac{1}{2} \left[\frac{X_i^2(\Delta r)^2}{12\nu_i} \right], \\ &\leq \frac{(\Delta r)^2}{6} \left(\frac{r_i}{\nu_i} \right). \end{aligned} \quad (3.6)$$

Δt is calculated for all bins, then the minimum one is chosen to be the next timestep. The surface mass density is then solved using a second order central difference method for a second derivative.

$$S_i^{n+1} = S_i^n + \frac{12\Delta t}{X_i^2(\Delta r)^2} (S_{i-1}^n\nu_{i-1}^n + S_{i+1}^n\nu_{i+1}^n - 2S_i^n\nu_i^n) \quad (3.7)$$

Here n refers to the current state of the system, with $n + 1$ the value at the next timestep. Thus, $\Sigma_i^{n+1} = S_i^{n+1}/X_i$, and $m_i = \Sigma_i\Delta A_i$.

I follow the viscosity prescription described in Salmon et al. [2010a] where the total viscosity is calculated as the sum of three separate components. First is the “translational viscosity” which is related to the transport of angular momentum due to the random motion of the disk particles. Second is the “collisional viscosity” describing the transport of angular momentum via sound waves passing between the centers of colliding particles. The final component, which Salmon et al. [2010a] refer to as the “gravitational component” describes how angular momentum is transported due to the scattering of particles from gravitational wakes.

If a disk is gravitationally unstable, which can be found by calculating the Toomre Parameter (Toomre [1964]), it will produce gravitational wakes which affect the transport of angular momentum. Particles move randomly outside of a wake, but within a

wake they move coherently. This effectively increases the viscosity of the disk in the region of the wake. If the disk is gravitationally stable, the gravitational component to the viscosity is zero (Salmon et al. [2010a]). The Toomre Q parameter (Salmon et al. [2010a], Toomre [1964]), adapted to my model can be calculated for each bin as:

$$Q_i = \frac{\omega_i \sigma_r}{3.36 G \Sigma_i} \quad (3.8)$$

σ_r is the velocity dispersion.

Salmon et al. [2010a] thus defines the kinematic viscosity as the sum of the translational, collisional, and gravitational viscosities. Therefore, $\nu_i = \nu_i^{trans} + \nu_i^{coll} + \nu_i^{grav}$. These viscosities, applied in accordance with Salmon et al. [2010a], are shown below:

$$\nu_i^{trans} = \begin{cases} \frac{\sigma_r^2}{2\omega_i} \left(\frac{0.46\tau_i}{1+\tau_i^2} \right) & \text{if } Q_i > 2, \\ 13r_h^* \left(\frac{G^2 \Sigma_i^2}{\omega_i^3} \right) & \text{if } Q_i < 2, \end{cases} \quad (3.9a)$$

$$\nu_i^{coll} = r_{pdisk}^2 \omega_i \tau_i, \quad (3.9b)$$

$$\nu_i^{grav} = \begin{cases} 0 & \text{if } Q_i > 2, \\ \nu_i^{trans} & \text{if } Q_i < 2. \end{cases} \quad (3.9c)$$

Here $r_h^* \equiv \frac{r_{Hill}}{2r_{pdisk}} = \frac{r_i}{2r_{pdisk}} \sqrt[3]{\frac{m_{pdisk}}{M_p}}$ where r_{Hill} is the radius of the Hill Sphere (Carroll and Ostlie [2007]), and m_{pdisk} and r_{pdisk} are the mass and radius of the disk particles. τ_i is the optical depth of the ring and is calculated as:

$$\tau_i = \frac{\pi r_{pdisk}^2 \Sigma_i}{m_{pdisk}} \quad (3.10)$$

Following Salmon et al. [2010a], the velocity dispersion is set by r_h^* .

$$\sigma_r = \begin{cases} 2r_{pdisk} \omega_i & \text{if } r_h^* \leq 0.5, \\ \sqrt{\frac{G m_{pdisk}}{r_{pdisk}}} & \text{if } r_h^* > 0.5, \end{cases} \quad (3.11)$$

The stability of the disk is set by the Toomre Parameter, and in the model described by Salmon et al. [2010a], the value of Q marks the switch between a gravitationally stable disk, and one that is not. This is most obviously seen in the treatment of ν_i^{grav} which is either zero if $Q_i > 0$, or non-zero if $Q_i < 2$. In an effort to avoid any stability issues solving these equations, I have included a function to model the viscosity of the disk as a gradual transition, rather than a step function, for regions where $Q_i \approx 2$. $\kappa(y)$ is the function I use to transition a value from zero to one, while $\eta(y)$ transitions a value from one to zero:

$$\kappa(y) = \frac{1}{2} \left[1 + \tanh \left(\frac{2y - 1}{y(1 - y)} \right) \right] \quad (3.12a)$$

$$\eta(y) = \frac{1}{2} \left[1 - \tanh \left(\frac{2y - 1}{y(1 - y)} \right) \right] \quad (3.12b)$$

This essentially allows me to gradually “turn off” the viscosity treatment for one case, while simultaneously “turning on” the other. Here y marks the location the transition occurs, which for a transition between values of 0 and 1 would be 0.5. Therefore, I model the viscosity of the disk as:

$$\nu_i^{trans} = \nu_i^{trans}(Q > 2) \times \kappa(y) + \nu_i^{trans}(Q < 2) \times \eta(y) \quad (3.13a)$$

$$\nu_i^{grav} = \nu_i^{trans} \times \eta(y) \quad (3.13b)$$

Setting $y = Q/4$ centers this transition to occur at $Q = 2$. (The ν_i^{coll} term is not dependent on the value of Q_i and is thus unaffected.) A similar treatment is applied to the velocity dispersion of the disk (Equation 3.11).

3.2 Satellite Accretion

Overlapping the region of the disk is a separate series of bins to track any accreting satellites. Given a minimum satellite mass, these satellite bins extend radially and are spaced one hill radius apart: $\Delta a_j = R_{Hill} = a_j \left(\frac{m_{min}}{3M} \right)^{\frac{1}{3}}$, where Δa_j is the satellite bin spacing, a_j is the semi-major axis of the satellite bin, and m_{min} is the minimum satellite mass. As disk material viscously spreads across the FRL a satellite is created

at any locations that have a mass greater than or equal to the minimum satellite mass. Once a satellite exists it may begin to accrete material from the disk.

Canup and Esposito [1995] and Kokubo et al. [2000] have studied satellite formation out of a debris disk using N-body models. These models predict a fast accretion rate of material, where satellites would accrete in < 500 orbits. However, these studies were examining a scenario for the formation of the Earth's moon which has a greater planet to disk mass ratio than considered here. Additionally, due to computational constraints, these models included disk particle sizes that were much larger than is considered in my work. I conducted N-body simulations using the SyMBA integrator [Duncan et al., 1998] for a martian system with disks of various mass and surface mass density. While preliminary, the results from these simulations indicate that satellite accretion for such a system would follow a mass growth law similar to $\frac{dm_j}{dt} \propto m_j^{3/2}$, producing a Phobos-mass satellite on the order of 10^3 years. Therefore, once a satellite has been created, I use a Runge-Kutta integrator to solve the satellite's mass in time following this power law, provided there is disk material within its hill sphere available for the satellite to accrete.

3.3 Satellite Orbital Evolution

Once formed, satellites will begin to exchange angular momentum with the primary via tidal interactions. As discussed in Section 2.1.3, this angular momentum exchange either increases or decreases the semi-major axis of the satellite, depending on whether it is located inside or outside the synchronous limit. The change to the satellite semi-major axis due to the tidal interaction is given by Equation 2.10

In addition to exchanging angular momentum with the planet, satellites will also exchange angular momentum with material in the disk located at the Lindblad resonance locations. As discussed in Section 2.1.2, the Lindblad resonance locations can be found via Equation 2.3. To find the total torque exerted on a satellite I implement Equation 2.4 to calculate the torque exerted by each mode and sum over all modes via

Equation 2.5. As \mathcal{M} increases, the distance between successive resonance locations decreases. I carry the sum out until the distance between successive resonances for satellite j is smaller than the bin width:

$$r_{\mathcal{M}}(j, \mathcal{M} + 1) - r_{\mathcal{M}}(j, \mathcal{M}) \leq \Delta r. \quad (3.14)$$

The complete orbital evolution of a satellite depends upon both the planet-tidal torques and the satellite-disk torques. In Section 2.1.4 I sum Equations 2.10 and 2.6 to yield Equation 2.11. Thus, the satellite orbits are evolved by solving Equation 2.11 at each timestep.

It is possible for one satellite to catch up with another. When satellite j is within $2 R_{Hill}$ of satellite k , the two are merged with the location being weighted between the two to conserve angular momentum via:

$$a_j = \sqrt{\frac{m_j a_j^2 + m_k a_k^2}{m_j m_k}}. \quad (3.15)$$

Currently, this is handled instantaneously.

3.4 Disk-Satellite Torques

While the ring material exerts a torque on the satellite, the satellite exerts an equal and opposite torque on the ring material. This torque acts on material very near the resonance, causing it to move inwards, away from the resonance location. Therefore, at the resonance location, the ring loses angular momentum by transporting material towards the primary. I approximate the effect of this torque by calculating the mass loss of the ring at a resonance location as:

$$\Delta m_L = \Delta t \left(\frac{\Gamma_j}{\omega_L R_L^*} \right), \quad (3.16)$$

where Δt is the simulation timestep. For a resonance at bin i , this mass is deposited into bin $i - 1$.

3.5 Tidal Disruption of Satellites

Planetary tides are capable of causing the orbit of a satellite to decay. Furthermore, these tides can tidally disrupt the satellite. As explained in Chapter 1, the RRL marks the location where planetary tides are strong enough to remove a particle from the satellite's equator. As particles are loosed from the satellite, they enter orbit around primary and a collisional cascade quickly results. These particles rapidly collide with the satellite, eroding its surface. Within a few orbits the satellite rapidly disrupts and forms a new ring. I typically set the location of tidal breakup at the RRL. If a satellite evolves to this orbit, its mass is distributed to the ring bins in the immediate vicinity of the RRL following $m_i = 0.4m_j$, $m_{i\pm 1} = 0.2m_j$, and $m_{i\pm 2} = 0.1m_j$.

3.6 Validation of Model

Here I demonstrate the validity of my model by comparing it to others published in the literature, as well as with systems we may observe today.

My treatment of the Lindblad Torques and the effect of the satellites torque onto the ring is not explicitly rigorous, however as the torque exerted on the ring by the satellites has no long-term effect on the ring [Charnoz et al., 2010], I feel this treatment is sufficient for the scenarios I wish to study. A thorough treatment of this angular momentum exchange would most likely affect the rate at which material is deposited onto the primary. Lindblad Torques between the satellites and the ring may open up gaps within the ring, which would be reflected in the deposits onto the primary. Additionally, very massive rings are capable of producing satellites that may be massive enough to depart from the linear treatment I have implemented here. A departure from this linearity would result in material at the outer edge of the ring becoming confined to an extremely narrow region of space, but the orbital migration of the satellites should remain accurate.

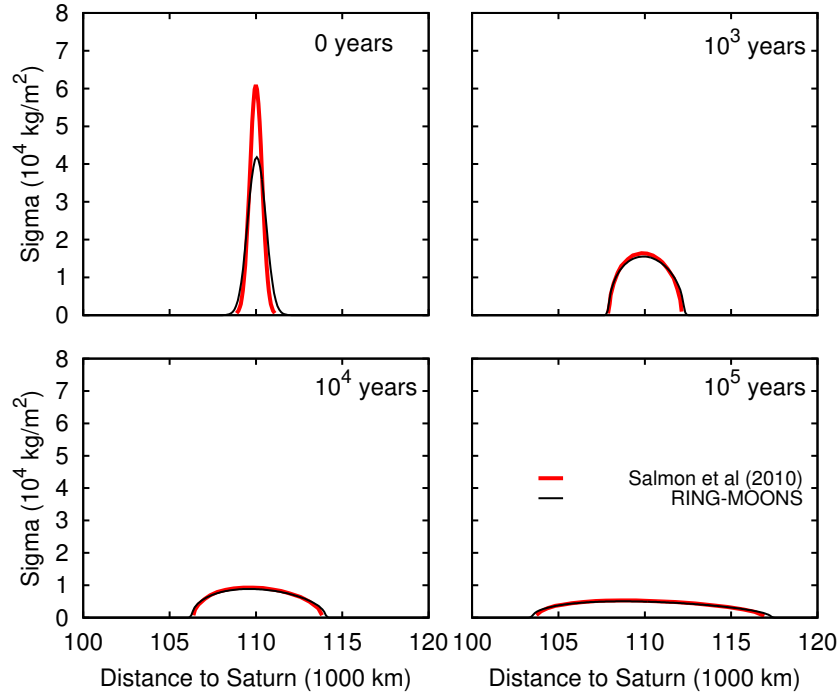


Figure 3.1. Here I compare the results from the model, RING-MOONS (black line) for a sharply peaked ring viscously spreading in the Saturn system to others in the literature. To solve the viscous spreading of the rings, I follow the viscous spreading model described in Salmon et al. [2010a]. Despite my implementation of a different integration scheme, my results convincingly match the results displayed in Figure 3 of Salmon et al. [2010a] (red line).

As described in Section 3.1, I use the work of Salmon et al. [2010a] to describe the physics of how the ring viscously spreads. In order to test my solution of Equation 3.4, I replicated their results for the spreading of a variably viscous ring orbiting Saturn. I chose initial conditions that were nearly identical to those of Salmon et al. [2010a]. The initial surface mass density of the ring is a steeply peaked Gaussian function, centered at a semi-major axis of 110,000 km. The mass of the ring is equal

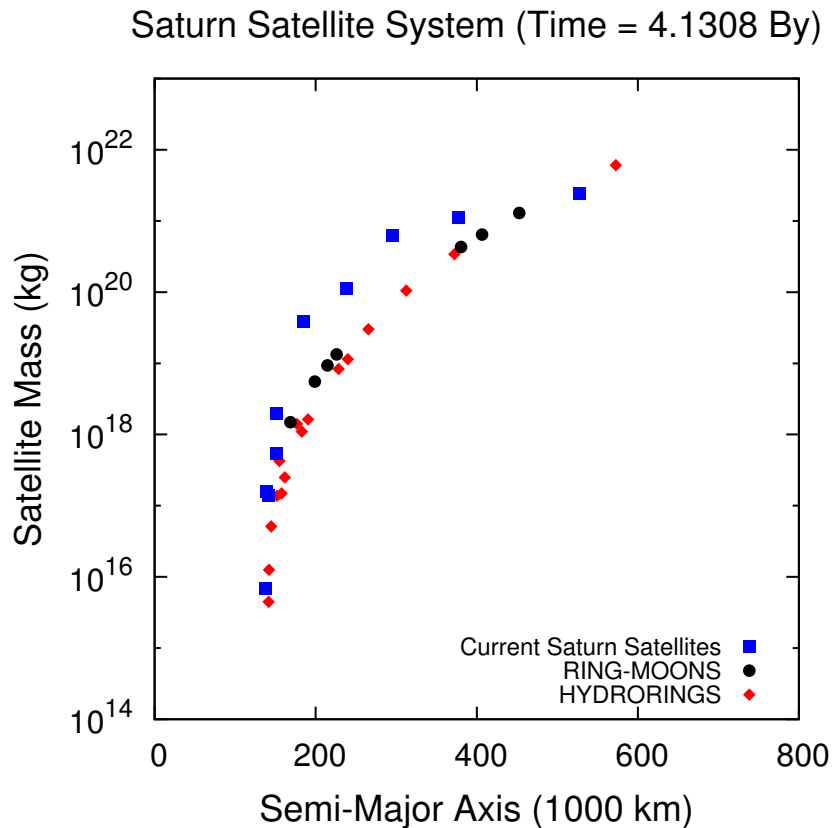


Figure 3.2. Here I display the results of the model, RING-MOONS (black dots) for the accretion of satellites from Saturn's rings, and their orbital evolution over ~ 4 Gy, assuming no tidal dissipation in the satellites and the tidal quality factor of Saturn $Q = 1680$. I perform this simulation to benchmark my model against the actual Saturn system (blue squares) and other models in the literature (red diamonds). RING-MOONS is similar in many ways to the HYDRORINGS model described in Charnoz et al. [2011], and presents similar results.

to a Mimas mass, and the particles in the ring have a radius of 1 m and a density of 1000 kg/m^3 . In Figure 3.1 I display these results at various points in time for 10^5 years of evolution, achieving good agreement with the results of Salmon et al. [2010a].

In addition to validating my description of the spreading of the ring, I also compare my RING-MOONS code to HYDRORINGS, a code used in Charnoz et al. [2011]

to model the accretion of satellites out of Saturn's rings. The viscous spreading of Saturn's rings and the accretion of small satellites is directly analogous to my model for the evolution of ring/satellite systems. Fig. 3 of Charnoz et al. [2011] displays results for a viscously spreading ring accreting material into satellites over 4 Gy, assuming various tidal parameters between the satellites and Saturn. Panel d of this figure includes HYDRORINGS results for a system in which satellites undergo tidal interactions with the planet, but not other satellites. This scenario is very similar to cases I wish to investigate. Because of the observational evidence for small satellite accretion from the saturnian rings and the observed mass-distance relationship of the accreted satellites, the results of Charnoz et al. [2011] are an ideal test case to check the validity of my model against reality and other models established in the literature.

The HYDRORINGS code is not publicly available, however the results displayed in Charnoz et al. [2011] are fairly well described, and should be reproducible by my model. In Fig. 3, panel d of that work are displayed the results of satellites accreting out of a ring after ~ 4 Gy, given no tidal dissipation between the satellites. In these results the mass of the initial ring is set at 4 Rhea masses ($\sim 9.2 \times 10^{21}$ kg) and the density of particles within the ring is set at 900 kg/m^3 . The tidal dissipation factors for Saturn are set to be $k_2 = 0.341$ and $Q = 1680$. I use these same conditions to test whether the output of my model matches the results of HYDRORINGS, 4.1308 Gy after the simulation has progressed, and the current satellite mass-distance relationship of Saturn's satellites.

The results of Charnoz et al. [2011] do not include a description of the initial profile of the surface mass density of the ring, the size of the ring particles, nor the radial extent of the ring. In comparing my model to this work, I model the surface mass density profile of the ring as $\Sigma(r) \propto r^{-3}$, and the ring extends from the surface of Saturn to 90% of Saturn's FRL. For computational efficiency I set the particles in the ring to have a radius of 1 km. In Figure 3.2 I compare the results of my model, RING-MOONS against the results of HYDRORINGS (Charnoz et al. [2011]), and the current Saturn system. In the described scenario, after 4 Gy HYDRORINGS

produces at least 16 satellites, while RING-MOONS produces 7. As displayed in Charnoz et al. [2011], the current Saturn system contains 10 satellites that may have accreted from Saturn's rings. Additionally, I find the general trend of Saturn satellites to have greater masses at greater semi-major axis as reproduced by HYDRORINGS is also reproduced with my model. The initial conditions selected here may differ than those selected in Charnoz et al. [2011], and may explain discrepancies between the results of the two models. However, dependent upon further work, both models may be able to reproduce the actual Saturn system.

RING-MOONS and HYDRORINGS model much of the same physics, but differ in the manner in which these dynamics are solved. Thus, Figures 3.1 3.2 give me confidence that my model is solving the dynamics of satellites and rings at an appropriate level. The fact that RING-MOONS does not perfectly reproduce the Saturn ring-satellite system indicates that further improvements could continue to be made, as with all models.

4. THE CYCLIC NATURE OF MARTIAN SATELLITES

A version of this chapter has been published in A. J. Hesselbrock and D. A. Minton. An ongoing satellite-ring cycle of Mars and the origins of Phobos and Deimos. Nature Geoscience, 10:266269, Mar. 2017. doi:10.1038/ngeo2916.

4.1 Background

The origin of the martian satellites, Phobos and Deimos, is not well understood. The spectra of the two satellites closely resemble carbonaceous asteroids [Burns, 1992, Rivkin et al., 2002], indicating that they could be captured. However, Phobos and Deimos have orbits that are circular (with eccentricities ≤ 0.015), aligned to Mars's equator (with inclinations $\leq 1.8^\circ$), prograde, and deep inside the Hill Sphere of Mars. These orbits are indicative of satellites that have accreted from a debris ring [Cameron and Ward, 1976, Charnoz et al., 2010, Crida and Charnoz, 2012], leading many researchers to favor a giant impact origin for Phobos and Deimos over capture [Canup and Salmon, 2016, Citron et al., 2015, Craddock, 2011, Rosenblatt and Charnoz, 2012].

A giant impact by a ~ 2000 km diameter body > 4.3 Gy ago has been implicated for the formation of the hemispherical dichotomy seen on Mars [Andrews-Hanna et al., 2008, Leone et al., 2014, Marinova et al., 2008, Nimmo et al., 2008]. Numerical models of giant impacts that could form the dichotomy show that the collision could have ejected as much as 10^{23} g of debris into martian orbit [Citron et al., 2015, Marinova et al., 2011], of which some portion should form a debris ring of mixed composition orbiting the planet. A debris ring composed of a mixture of impactor and martian material that proceeds to accrete satellites may explain both the physical and orbital

characteristics of the martian satellites [Craddock, 2011]. However, a number of unresolved difficulties remain.

As shown in Figure 2.2, a debris ring in orbit around Mars exists within the Boomerang regime. It is therefore unlikely that Deimos formed from an FRL-interior debris ring and subsequently migrated to its current orbit beyond the synchronous orbit of Mars, located at ~ 6 Mars radii. Phobos, lying inside the synchronous orbit is gradually evolving inwards, towards Mars [Murray and Dermott, 1999], and may have formed from an FRL-interior ring. In fact, Black and Mittal [2015] suggest that in less than 70 My, the orbit of Phobos will have decayed such that the satellite will either collide with Mars, or be tidally torn apart. The orbital migration of the satellites has remained a major challenge, resulting in many studies which attempt to form both satellites far from Mars [Canup and Salmon, 2016, Rosenblatt and Charnoz, 2012, Rosenblatt et al., 2016], near the synchronous orbit. Tidal evolution of Phobos from such an orbit would place the satellite in its current location after ~ 4 Gy, however would likely result in resonance interactions with Deimos that would raise the outer satellite’s eccentricity to a value too great to be satisfactorily explained [Murray and Dermott, 1999, Yoder, 1979].

Previous studies have succeeded at forming Phobos analogs from a giant impact, but either result in the satellite’s orbit decaying completely [Rosenblatt and Charnoz, 2012], result in an eccentricity for the outer moon Deimos that is too large [Yoder, 1979], or requires different tidal dissipation rates between the two satellites [Rosenblatt et al., 2016]. Recent work suggests that a giant-impact debris ring accreted a very massive satellite which subsequently prompted the accretion of Phobos and Deimos before crashing onto the planet [Rosenblatt et al., 2016]. While Deimos may have formed in this manner, I argue that any primordial massive satellites would exist in the Boomerang Regime and would have been tidally disrupted into a ring upon reaching the Rigid Roche Limit (RRL) [Black and Mittal, 2015, Murray and Dermott, 1999]. This ring could evolve to accrete new satellites. I propose that a ring-satellite-tering cycle is a natural consequence of satellite formation in the Boomerang Regime

and is a compelling alternate formation hypothesis that overcomes the timing, orbital constraint, and tidal dissipation difficulties faced by Rosenblatt and Charnoz [2012] and Rosenblatt et al. [2016].

4.2 Using RING-MOONS to Investigate the Mars Satellite System

I have used “RING-MOONS,” a satellite-ring dynamical model to simulate the evolution of a massive Martian debris ring and accreting satellites formed after a giant impact. The gridspace of the ring extends from the surface of Mars to beyond the FRL at ~ 3.2 Mars radii (R_M). Ring material viscously spreading beyond the FRL accretes into Lagrangian satellites. These satellites accrete mass and undergo orbital evolution via torques exerted by Mars and the ring (Equation 2.11). Any satellites that evolve to the RRL at $\sim 1.6R_M$ are disrupted and their mass is redistributed to the ring at the RRL. Computational constraints require me to model the ring material as relatively large, single-sized particles. However, I have developed a method that uses my studies to calculate how the system will behave with any realistic particle size.

For a preliminary investigation I confined the initial ring to exist inside the FRL. While testing the model I conducted numerous simulations modeling the initial surface mass density of the ring as a steeply peaked gaussian centered at the RRL. During these tests I varied the initial mass of the ring, as well as the radius of the ring particles. During these initial investigations I found that $\sim 80\%$ of the initial mass of the ring (M_{Init}^{Disk}) viscously spread through the inner boundary and was deposited onto Mars, while the remaining $\sim 20\%$ spread beyond the FRL, and accreted into satellites. Therefore the total mass of all satellites produced from an FRL-interior ring, M_{Fin}^{Sat} , could be found via:

$$M_{Fin}^{Sat} \approx 0.2M_{Init}^{Disk}. \quad (4.1)$$

This relation remained true independent of the initial ring mass or radius of the ring particles.

Once satellites formed, resonant ring interactions (Lindblad torques) perturbed the satellites outwards from the ring while the ring was still sufficiently massive. After the ring had depleted, with the bulk of its mass deposited onto Mars, tidal torques eventually always overcame the Lindblad torques and the satellites evolved inwards. During this process, these satellites typically accreted into one single satellite before evolving to the RRL to create a new ring.

Therefore, given a satellite mass I may use Equation 4.1 to estimate the mass of the ring that must have produced it. Furthermore, assuming that a ring was produced by the disruption of an ancient satellite, I may determine the mass of the ring that formed the ancient satellite as well. Knowing the mass of a satellite (e.g. Phobos) I may calculate the mass of the ring that produced it. This result is a consequence of selecting tidal breakup to occur at the RRL. For instance, the satellite/ring system that preceded Phobos was $\sim 5\times$ as massive as Phobos, and the satellite/ring system that preceded it was $\sim 5\times$ larger still (see Figure 4.1).

The dichotomy-forming impact event sets two constraints: the upper limit to the mass of the initial ring created by the impact, and the starting time for the ring/satellite cycle. From a study of the formation of the martian hemispherical dichotomy from an impact using a large suite of smoothed particle hydrodynamics (SPH) simulations, the maximum mass of a ring created by the best case scenario is $\sim 3 \times 10^{23}$ g [Marinova et al., 2011]. My preliminary results indicate that a satellite that is disrupted at the RRL will eventually accrete a new satellite with a mass $\sim 20\%$ of the primordial satellite’s mass (see Equation 4.1). Based upon this result, I calculate the mass of the ring that must have formed Phobos and call this “Cycle 1.” Assuming this ring formed as a result of the tidal breakup of a primordial satellite that also evolved to the RRL, I calculate the mass in the previous cycle and call this “Cycle 2,” and so on. Beginning with Phobos, in Table A.1 I use Equation 4.1 to calculate the system mass for each previous cycle until I reach an initial ring mass that is greater than what would be expected to form out of the dichotomy forming

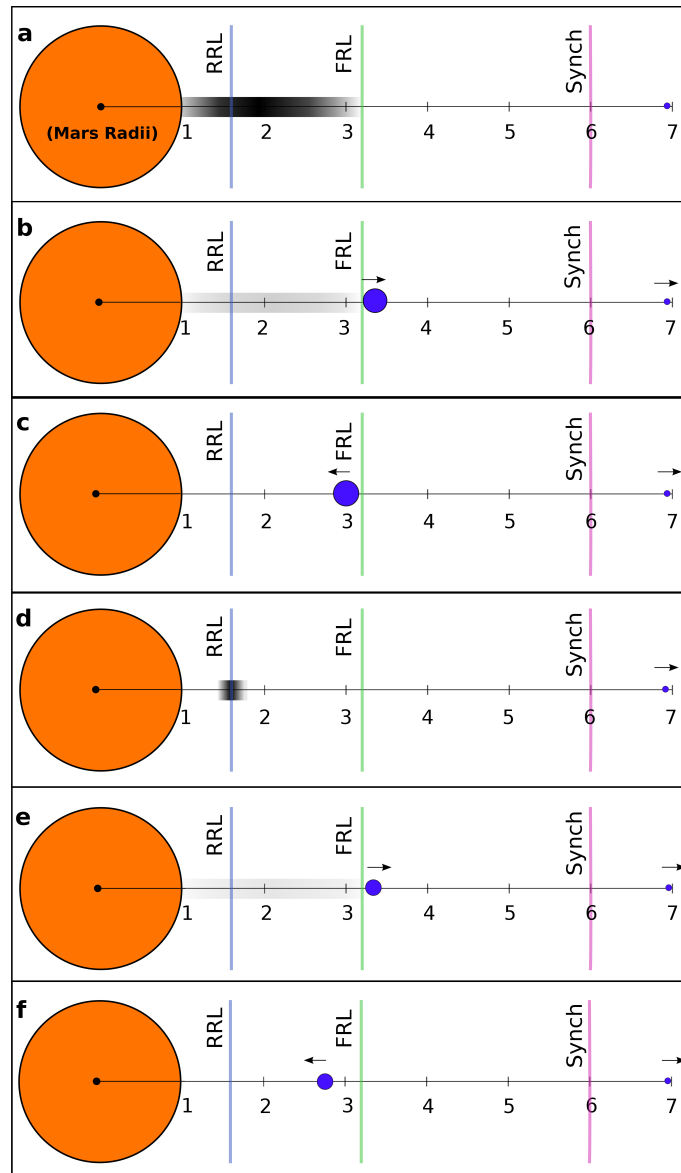


Figure 4.1. **a.** The ring, shaded corresponding to its surface mass density, has viscously spread to Mars (orange) and to the fluid Roche limit (FRL). **b.** Ring material has accreted into a satellite (blue, size exaggerated) that is perturbed outwards via Lindblad torques. **c.** Being inside the synchronous orbit (Synch.), the ring has depleted and tidal torques evolve the satellite inwards. **d.** The satellite has reached the rigid Roche limit (RRL), disrupting into a new ring. **e.,f.** The cycle repeats, producing Phobos.

impact ejecta. I find that a ring with any of the initial masses listed in Table A.1 will eventually form Phobos.

For the initial conditions I modeled the ring following a surface mass density of a narrow Gaussian centered at the RRL, with a total mass of 1.2×10^{23} g. Although the exact conditions of the martian system immediately after the dichotomy forming impact are not strictly known, my choice of initial conditions is unlikely to be realistic. It is more likely that the dichotomy forming impact would disperse material from the planet, with a mass distribution that would decrease as some function of distance. This would result in a ring contained within the FRL with a surface mass density $\Sigma(r) \propto r^{-p}$, and a population of satellites extending beyond the FRL. Deimos likely marks the very outside edge of this initial impact debris system. However, as the mass distribution of the initial ring is erased after the first cycle, my choice of initial conditions does not strongly affect my results, and thus how I observe the martian system today. If the dichotomy forming impact is able to produce a satellite with a mass of 2.6×10^{22} g interior to the synchronous orbit, this satellite will likely scatter any exterior satellites, possibly leaving the lone survivor Deimos. Assuming tidal breakup of satellites occurs at the RRL, I find that if the dichotomy-forming impact produced a satellite with a mass of $\sim 2.6 \times 10^{22}$ g, this system would eventually evolve over 5 cycles to produce a single satellite with the mass of Phobos.

4.2.1 Uncertainty in Tidal Breakup

The above mass estimates are determined by the location where satellite breakup occurs, which I took to be at the RRL, located at $\sim 1.6R_M$. The greatest uncertainty in my estimation of the total number of cycles is the location where tidal breakup of each satellite occurs. Severe tidal deformation of a satellite may occur when the satellite is only a few Mars radii away, yet Phobos orbits Mars at $\sim 2.76R_M$ as a coherent body and is not believed to be losing material due to tidal torques. Therefore, I know tidal breakup should only occur when the satellite's semi-major axis is less

than that of Phobos, which is currently orbiting inside the FRL. The Rigid Roche Limit (RRL) is defined as the orbital location where a particle on the equator of a spherical satellite is no longer bound to the surface of the satellite. Assuming the satellite is a gravitational aggregate with no cohesion forces between particles, this occurs when the outward centrifugal forces of the satellite’s rotation and tidal shear are stronger than the attractive gravitational forces of the satellite [Murray and Dermott, 1999].

However, real satellites may have some internal cohesive strength, and it has been found that for a satellites with a plausible range of internal strength tidal breakup should occur somewhere within $1.2 - 1.7R_M$ [Black and Mittal, 2015]. In Figure 4.2 I ran simulations for a ring composed of particles with a 1 km radius and with a total ring mass of $\sim 1.2 \times 10^{23}$ g until the cycle mechanism resulted in a satellite with a mass less than or equal to Phobos. However, in these simulations I varied the location where tidal breakup of the satellite occurred. I then compared the mass of the ring at the beginning of a cycle to the final satellite mass produced by the cycle.

These results show that if tidal breakup of the satellites occurs at $1.2R_M$, each cycle will produce a satellite with $\sim 6\%$ the mass of the ring at the beginning of the cycle. On the other hand, if satellite breakup were to occur at $1.7R_M$, I find that if the dichotomy forming impact produced either a ring or a satellite with a mass of $\sim 1.7 \times 10^{23}$ g, Phobos would form after 7 cycles. Because this breakup location is the largest source of uncertainty in the per-cycle mass loss estimates in my model, I define the “nominal case” as the one where breakup occurs at the RRL at $\sim 1.6R_M$, and use the estimated limits of the satellite breakup location to determine the uncertainty in my results.

4.2.2 Ring Particle Size

As the impact event that formed the dichotomy likely occurred 4.3 – 4.5 Gy ago, the entire process, from the initial impact debris ring which cycles to produce a Phobos

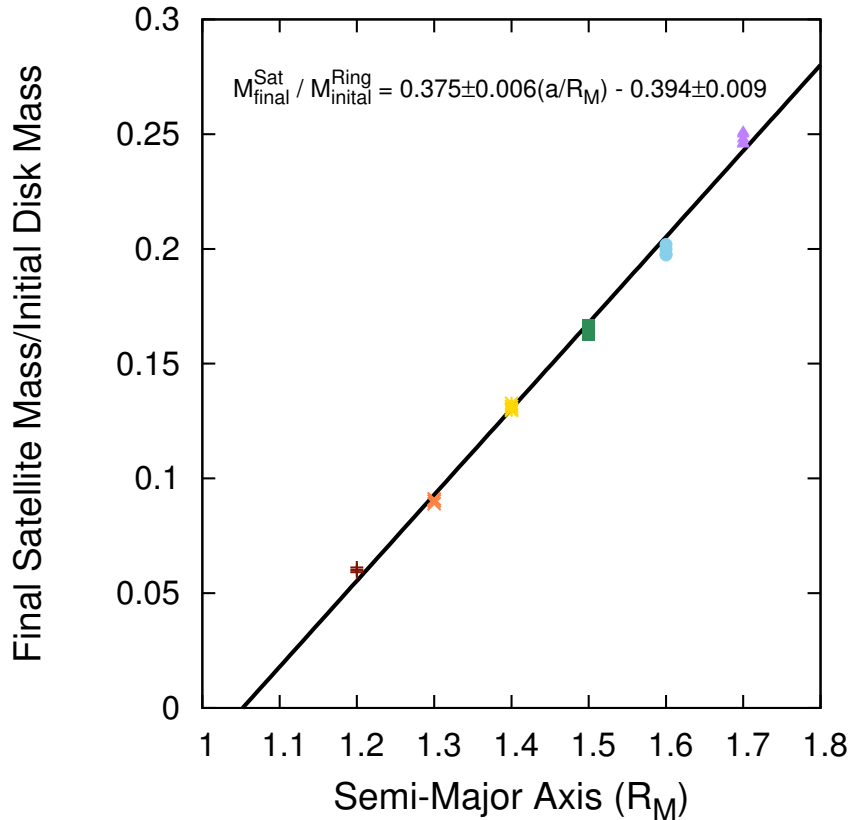


Figure 4.2. Here I compare the final satellite mass to the initial ring mass for a Martian satellite-ring cycle. I plot the ratio of the final satellite mass to the initial ring mass for each cycle while varying the location of total satellite breakup. Satellite breakup may occur anywhere within $1.2 - 1.7R_M$ (Black and Mittal [2015]). I find that if a satellite disrupts at a location closer to Mars, the resulting ring will produce a final satellite with a mass smaller than if the breakup was to occur farther away from the planet.

sized satellite that evolves into the orbit I observe today, *must* take at least ~ 4.3 Gy. There are several factors that affect the timescale of an individual cycle including: the mass of the ring, the tidal parameters chosen for Mars and the satellites, and the size of the particles within the ring. The mass of the ring is determined via Equation 4.1, and I find it unlikely that the tidal parameters of the satellites are much different than previously found [Black and Mittal, 2015, Rosenblatt and Charnoz, 2012].

Because the ring particle size is unconstrained, I use this as a free parameter in the model and choose a value that allows the complete evolution to occur over the time since the dichotomy-forming impact 4.3 Gy ago. Between my results for different size ring particles I compare four timescales: the time for the ring to evolve from the RRL to the FRL, the time for satellites to accrete from the ring and evolve outwards due to ring torques, the time for the ring to deplete such that Lindblad torques no longer dominate the orbital evolution of the satellites, and the time for satellites to evolve inwards to the RRL due to planetary tides.

The time for the ring to evolve from the RRL to the FRL scales directly with particle radius, and is confirmed by my results for all cycles and all particle sizes. The time for the particles to accrete and evolve outwards has some dependency on particle size. This is confirmed by my results for rings composed of particles with a radius of 1 km and 100 m for all cycles, and for my results for rings composed of particles with a radius of 10 m for cycles 6, 5, and 4. The time for the ring to deplete has a strong dependence on particle size being largely set by the spreading timescale of the ring, similar to the evolution of ring material from the RRL to the FRL. The time for the satellites to evolve to the RRL after the ring has depleted is largely independent from the radius of the ring particles, as it is mainly driven by the orbital evolution of the satellite due to planetary tides.

To determine the necessary ring particle size needed to fit the giant impact age constraint I compare the timescales in my results for rings composed of different sized particles. For the early cycles, the time required for the ring to spread to the FRL is short compared to the time required to eventually evolve accreted satellites to the RRL. Thus, the mass of the ring, and not the particle size, is the primary factor determining the time it takes for the early cycles to complete. However, in the later cycles the mass of the ring is never sufficient for Lindblad torques to greatly perturb the satellites' orbits [Rosenblatt and Charnoz, 2012], and the satellites orbit near the edge of the ring. In these later cycles the time it takes for the ring to spread to the FRL, where it may begin to accrete into satellites, is much longer than the satellites'

orbital evolution. Therefore, the time it takes for later cycles to complete is driven by the dynamics of the ring and shows a much greater dependency on particle size.

Because the evolution of the ring scales with the size of the ring particles, for cycles 3, 2, and 1 I assume that the ratio between these timescales for rings composed of particles which differ by an order of magnitude in radius remains constant. I am then able to extrapolate the amount of time a ring composed of any size particle will take to complete a given cycle. With this methodology, I estimate that modeling the ring particles as 0.18 m bodies would take the system roughly ~ 4.3 Gy to form Phobos and place it in its current orbit. This result is in agreement with Saturn’s rings today, which are estimated to be composed of particles with a radius between few centimeters to several meters [Salmon et al., 2010a].

I used the most massive cycle in Table A.1 to set the initial conditions for RING-MOONS. I assume that the dichotomy-forming impact formed both Deimos and a ring with a mass of $1.2_{-0.7}^{+0.5} \times 10^{23}$ g. Although I find that rings composed of smaller particles take longer to complete a cycle than rings composed of larger particles, the mass ratio between the initial ring mass and the total mass of the satellites produced remained constant, independent of ring particle size. I conducted multiple simulations of all cycles, varying the radius of the particles in the ring to determine the duration of each cycle. I then estimate the necessary particle size for the entire process to complete in 4.3 Gy, which is the latest that the dichotomy-forming impact is expected to have occurred [Marinova et al., 2008].

For each cycle I compare the time it takes for the ring to spread material from the RRL to the FRL, the time to accrete satellites, the time for the ring to deplete, and the time to evolve satellites to the RRL. I then analyze how these timescales vary between rings composed of different sized particles, and different locations of satellite breakup. In my “nominal case” I find a ring with an initial mass of 1.2×10^{23} g that is composed of particles with a radius of 0.18 m will evolve over 6 cycles to produce Phobos. If satellite breakup occurs at $1.2R_M$ the initial ring is less massive, fewer cycles occur, and the required particle radius is smaller. If satellite breakup occurs at

$1.7R_M$, the initial ring is more massive, more cycles occur, and the required particle radius is larger. Therefore, I find that an initial ring with a mass of $1.2_{-0.7}^{+0.5} \times 10^{23}$ g that is composed of particles with a radius of $0.18_{-0.03}^{+0.14}$ m would complete 6_{-3}^{+1} cycles to place Phobos in its current orbit after ~ 4.3 Gy.

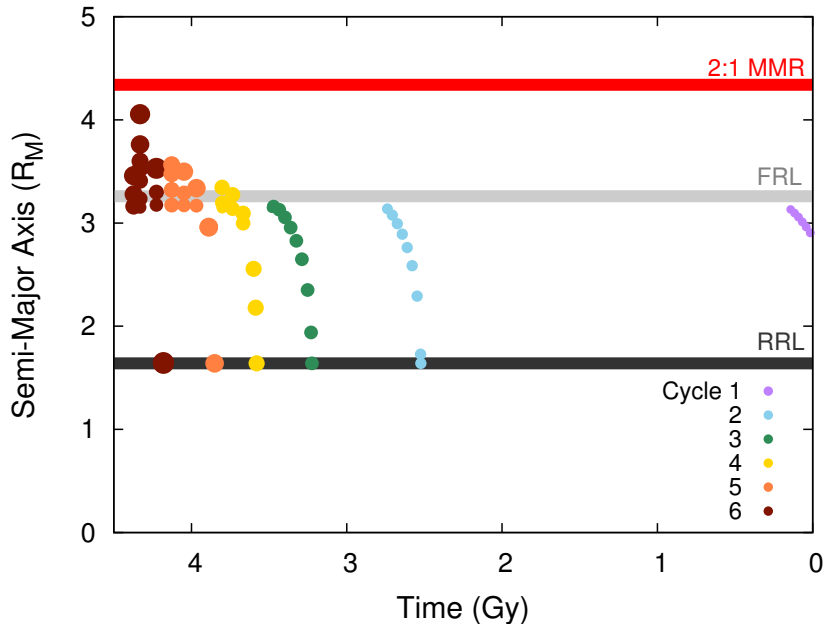


Figure 4.3. Here I show snapshots of satellites produced in my nominal case with time estimated for a ring composed of 0.18 m radius particles. Satellites are represented as dots with radius scaled to the satellites mass. Each cycle begins by spreading ring material to the FRL to accrete into satellites that evolve away from the ring via Lindblad torques. Tidal torques eventually move the satellites inwards until they disrupt at the RRL, and the cycle repeats. Satellites in Cycle 6 approach the 2:1 mean motion resonance with Deimos (2:1 MMR).

Beginning with Cycle 6, in Figure 4.3 I display a history of satellites produced via the martian ring-satellite cycles through 4.3 Gy of evolution, as modeled by RING-MOONS. In Cycles 6, 5, and 4, ring torques are sufficient to evolve satellites away from the ring, producing multiple satellites with the most exterior being the most massive. After the ring depletes, tidal torques overcome the Lindblad torques and

perturb these satellites inwards. The most exterior satellite rapidly evolves inwards and accretes any inner satellites. For Cycles 3, 2, and 1, the ring is not sufficiently massive to perturb satellites away from the ring and only one satellite is produced.

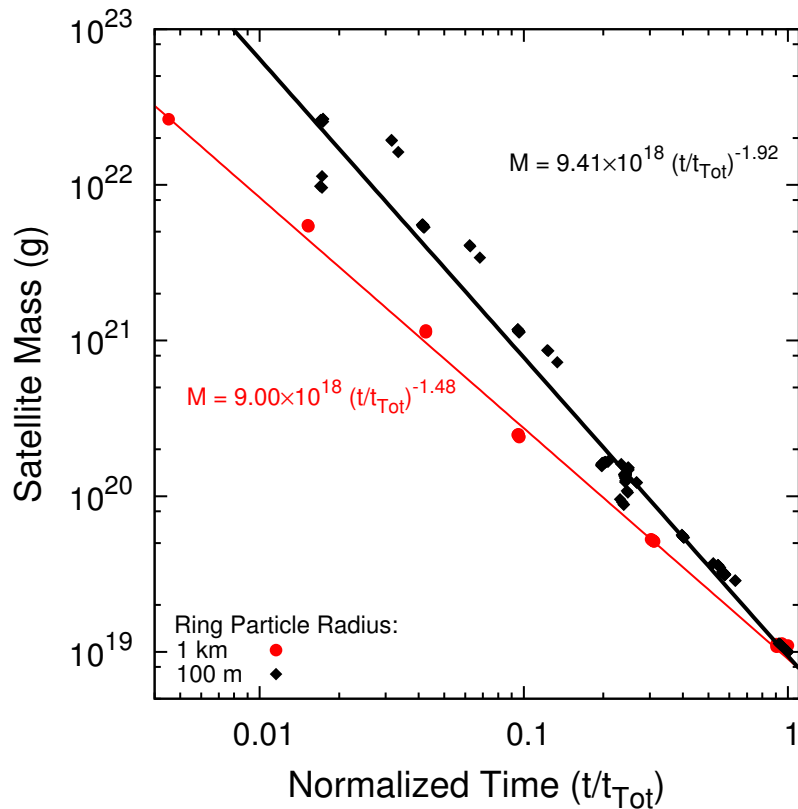


Figure 4.4. Results for the mass evolution for Martian satellites over time, assuming all particles in the ring have a radius of 1 km (red circles), or a radius of 100 m (black diamonds). The y-axis represents the mass of the satellites. The x-axis displays the time each satellite crossed the Rigid Roche Limit, save for the final Phobos analogs (bottom right). Time is represented as a fraction of the total time (t_{Tot}) from the initial conditions to placing a Phobos analog in the current orbit of Phobos. In rings with 1 km radius particles, each cycle produces one massive satellite. In rings with 100 m radius particles, early cycles may create several satellites which reach the RRL at different times.

4.3 Deposition of “Astro-Sediments” onto the Martian Surface

In the “nominal” case, roughly 80% of the ring mass is deposited onto Mars. Initially the ring evolves very rapidly, depositing the bulk of this material in a fraction of the total cycle time. As the mass of the ring decreases, so does the rate of its evolution. Using my estimates of the timescales for a ring composed of 0.18 m particles (our “best case” scenario), in Table A.2 I estimate the amount of time it would take for the ring to deposit $\sim 80\%$ of the total cycle’s deposit, as well as at what time the deposit would have occurred in Mars geologic history. I may also estimate the total volume and possible depths of these deposits onto the Martian surface.

For each cycle I am able to calculate the total amount of material that passes through the interior ring boundary and falls onto the planet. I estimate the depth of each deposit by approximating Mars as a perfect sphere and performing a simple volume integral. Given the mass and density of the deposited material, m and ρ , and the maximum latitude at which the deposit is expected to fall in degrees, x , performing a volume integral yields the depth of the deposit, ΔR , via:

$$\Delta R = \left[R_M^3 - \frac{3m}{4\pi\rho \cos\left(\frac{\pi}{2} + \frac{x\pi}{180^\circ}\right)} \right]^{1/3} - R_M \quad (4.2)$$

The values in Table 2 were calculated setting $\rho = 1.876 \text{ g/cm}^3$, the bulk density of Phobos, $x = 90^\circ$ to find the depth of a global deposit, and $x = 10^\circ$ to find the depth of a 20° band across the equator.

The mass of the ring in the early cycles is sufficient for Lindblad torques to efficiently evolve multiple massive satellites far from the ring [Rosenblatt et al., 2016]. After the ring has been depleted, it is possible that inner satellites could quickly evolve to the RRL before they could be accreted by distant exterior satellites. Therefore, the simple progression of discrete cycles may be more complicated in reality (see Figure 4.4). Deposits would still occur throughout Martian history, but if satellites reach the RRL at different times, a single cycle would yield multiple smaller deposits than the individual deposits displayed in Table A.2.

As these “astro-sediment” deposits would occur during different geologic epochs and would thus be subject to different types of weathering and cementation processes making speculation of their composition or exact contribution to the martian geologic record difficult. In addition to not knowing the interior and bulk composition of Phobos, there are a multitude of factors affecting the composition of the astro-sediments including their interaction as they enter the atmosphere, the Martian geologic period at which the deposit occurs, and any weathering that would occur on the planet after the deposit, among others. However, there is evidence for numerous equatorial “enigmatic sedimentary deposits” on Mars whose origins are not currently understood, including the Medusa Fossae Formation Kite et al. [2013] Thus, the deposition of these astro-sediments during the ring cycle process may be an additional hypothesis for the origin of these sedimentary packages.

4.4 Orbital Resonances with Deimos

Deimos’s orbit is very nearly circular, with an eccentricity less than 3×10^{-4} , and as of yet no model has been able to form the Martian satellite system with the eccentricity of Deimos observed today. Furthermore, all models that evolve Phobos from a location near the synchronous orbit face the greater difficulty of Phobos entering into a resonance Deimos, which should excite the eccentricity of Deimos to an order of magnitude greater than its current value [Murray and Dermott, 1999, Yoder, 1979]. While it is possible for the satellites to relax from these excited orbits into their orbits observed today, this would require the satellites to have different tidal dissipation rates [Rosenblatt et al., 2016]. In my model Phobos does not evolve from the synchronous orbit to its current location, but rather near the ring’s edge located at the FRL, avoiding the Deimos eccentricity boosting 2:1 resonance. Furthermore, my model results in a different age between the two satellites and permits each of the gravitational aggregate bodies to dissipate tides at the same rate.

The orbital evolution of the satellites is very sensitive to the competition between the Lindblad and tidal torques. Using tidal dissipation parameters for Mars today, I find that cycle 6 could possibly evolve massive satellites beyond the 2:1 resonance (see Table A.3). Primordial massive satellites orbiting beyond the 2:1 resonance would cause Deimos, accreting from an outer disk of debris, to have either a semi-major axis or eccentricity that is too great. This may constrain Cycle 5 to be the first cycle to occur, rather than Cycle 6. Cycle 5 has low enough mass that Lindblad torques will not evolve massive satellites beyond the 2:1 resonance with Deimos.

These results do seem to reconcile the mystery of why I have the convenient opportunity to observe Phobos only a few tens of millions of years before its demise, as the system I observe today is only a snapshot of a process that has likely been repeating for billions of years. Phobos may be in the last stage of a given cycle, finally completing its accretion phase in perhaps only the last ~ 200 My. I hypothesize that while the body was accreting, impacts with ring material and smaller ring-generated satellites would have saturated the surface of Phobos with craters. This more recent estimate of the satellite's age makes our observation of it slightly less fortuitous. Further analysis allows me to conclude that as Phobos enters the RRL in less than 70 My, it too will be ripped apart and turned into a ring [Hurford et al., 2015]. This ring would take ~ 8 Gy to spread material beyond the FRL, and would accrete a satellite with a final mass of $\sim 2.3 \times 10^{18}$ g, roughly the same mass as present day Deimos.

4.5 Existence of a Ring Today

At the completion of Cycle 1, the simulation results in a Phobos-mass satellite orbiting Mars at its current semi-major axis. However, my simulations also result in the existence of a low-mass ring orbiting Mars. As there is no evidence that a ring exists today, this remains as a caveat to my work. The surface mass density of the remnant ring is on the order of ~ 1 g/cm² (see Figure 4.5). I estimate that the

radius of the ring particles would be $0.18_{-0.03}^{+0.14}$ m and therefore this ring would have an optical depth $\tau \ll 1$ (see Equation 3.10). Although I have modeled the ring to have particles of identical size, a more realistic ring may have a distribution of particle sizes. For an optically thin ring, the effects of solar radiation may work to deplete the material, with the smallest particles experiencing Poynting-Robertson drag and the larger particles affected by the Yarkovsky Effect. Both these processes may work to remove material from the low mass remnant ring, explaining why I do not see it in the present day. Modeling of the effects of solar radiation on the remnant ring is beyond the scope of the present work.

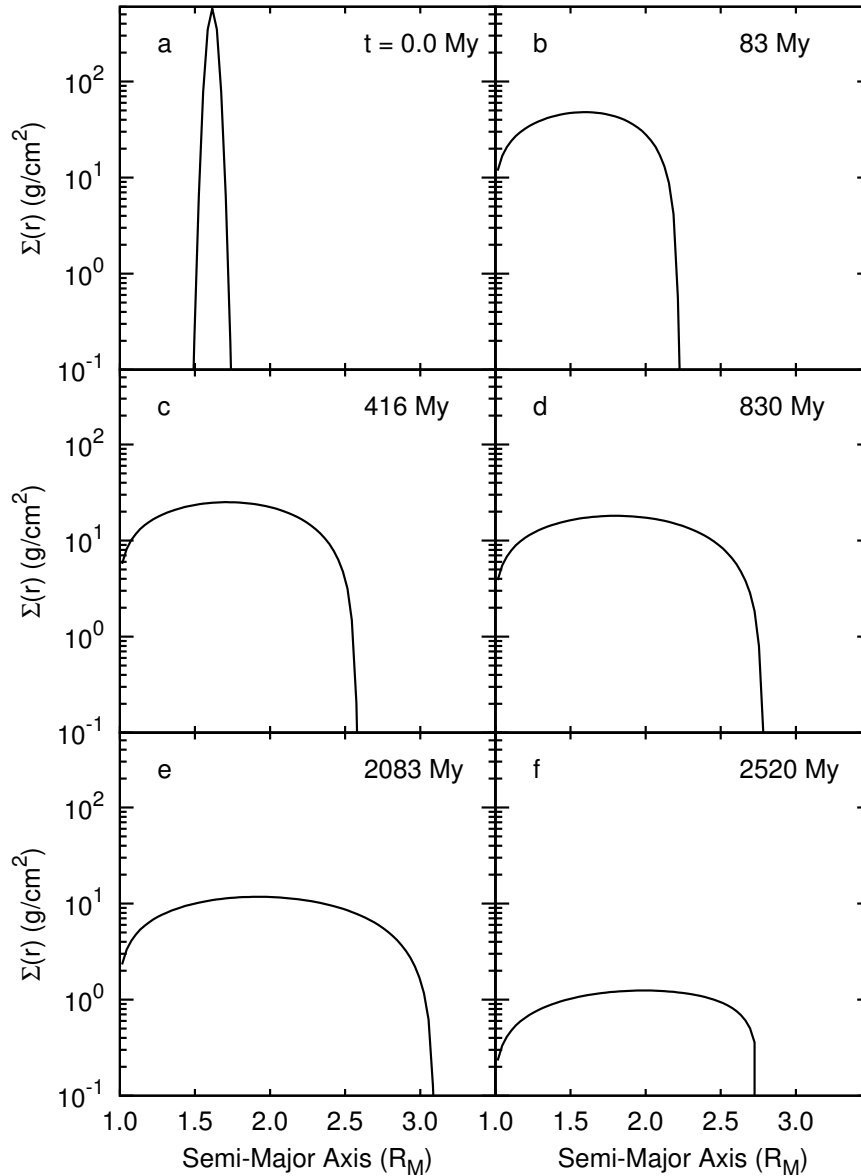


Figure 4.5. Here I display the surface mass density (Σ) of the ring during Cycle 1, the ring that produces Phobos, for the “nominal case” at different times during the cycle. Although a ring still exists at the completion of the simulation, there is likely not a ring visible today. My results indicate the ring at the completion of Cycle 1 is optically thin, with $\tau \leq 0.03$. I hypothesize that this low mass remnant ring may be depleted due to solar radiation effects, which I do not model currently.

5. FORMATION OF MIRANDA FROM A MASSIVE URANIAN RING

Before I begin, in Chapter 2 I described an approximation of the Lindblad torque exerted onto satellites via gravitational interactions as given in Esposito [2006]. The satellite-ring system of Uranus, the focus of this chapter, is very tightly coupled. In order to hypothesize the type of rings that may have produced the satellites observed today, in this chapter any Lindblad torques exerted onto satellites are explicitly calculated, not approximated. This includes corrections to Equations 2.4 and 2.15.

To first-order, the Lindblad torque exerted onto a satellite with semi-major axis a by the ring at resonance location $r_{\mathcal{M}}$ is given as [Tajeddine et al., 2017]:

$$\Gamma_{\mathcal{M}} = \mp \frac{4\pi^2}{3} \left(\frac{\mathcal{M}}{\mathcal{M}-1} \right) \sigma(r_{\mathcal{M}}) \left(r_{\mathcal{M}}^2 \beta n \frac{M_s}{M_p} A_{\mathcal{M}} \right)^2. \quad (5.1)$$

$\beta = r_{\mathcal{M}}/a$ and $A_{\mathcal{M}}$ is a dimensionless quantity that depends upon Laplace coefficients and their derivatives. The latter is calculated as:

$$A_{\mathcal{M}} = \frac{1}{2} [2\mathcal{M}b_{1/2}^{\mathcal{M}}(\beta) + \beta Db_{1/2}^{\mathcal{M}}(\beta)]. \quad (5.2)$$

$b_{1/2}^{\mathcal{M}}(\beta)$ is the Laplace coefficient and D is its derivative. Murray and Dermott [1999] provides an algorithm to calculate the Laplace coefficients and their derivatives. The derivative, D is simply a function of Laplace coefficients.

$$Db_{1/2}^{\mathcal{M}}(\beta) = \frac{1}{2} [b_{3/2}^{\mathcal{M}-1}(\beta) - 2\beta b_{3/2}^{\mathcal{M}}(\beta) + b_{3/2}^{\mathcal{M}+1}(\beta)]. \quad (5.3)$$

Equation 2.15 may now be corrected to include the explicit calculation of Lindblad torques:

$$\sum_{\mathcal{M}=2}^{\infty} \left(\frac{\mathcal{M}}{\mathcal{M}-1} \right) \sigma(r_{\mathcal{M}}) r_{\mathcal{M}}^3 A_{\mathcal{M}}^2 > \frac{9}{8\pi^2} \left(\frac{k_2}{Q} \right) \frac{M_p R_p^5}{a^4}. \quad (5.4)$$

Motivation for this correction was a result of the peer review process in publishing this work. While a direct calculation of the Lindblad torque is of clear benefit, the

difference between the approximated torque given in Equation 2.4 and the direct calculation in Equation 5.1 is not major. Both results agree within the same order of magnitude. While I proceed with the direct calculation in this Chapter, the impact to the results of Chapter 4 are likely to be minimal.

A version of this chapter has been accepted into The Astronomical Journal as A. J. Hesselbrock and D. A. Minton, “Three Dynamical Evolution Regimes for Coupled Ring-Satellite Systems and Implications for the Formation of the Uranian Satellite Miranda,” The Astronomical Journal, 2018.

Perhaps the most interesting feature of Figure 2.2 is the location of the satellite-ring systems of Uranus and Neptune. Both of these giant planets have rings and inner satellites that orbit near the rings’ edges. Leinhardt et al. [2012] proposed a tidal disruption origin of the inner satellites of Uranus and Neptune. Furthermore, some of these satellites lie within the synchronous orbit, but some lie beyond. It may be possible that these planets had primordial rings that were sufficiently massive to cause satellites to migrate far from the FRL and beyond a_{synch} , similar to a system in the Slingshot regime. However, as the primordial ring decayed over time the evolution of satellites may have transitioned to follow an orbital migration similar to a system in the Boomerang regime [Charnoz et al., 2018].

Unfortunately, the dynamics of the Neptune-Triton capture event makes it difficult to compare the locations of the satellites today to a primordial ring system. Such a dynamic capture event is not thought to have occurred at Uranus, making a comparison between its present day satellite system to a primordial ring more straightforward. As the ring-satellite system at Uranus lies within the Torque-Dependent regime, it serves as a candidate for special scrutiny [Charnoz et al., 2018]. By examining Equation 2.15, I may hypothesize the type of massive primordial ring that may have produced the Uranian satellites and migrated them to their current orbits. In the following sections I will further examine the dynamics of the Uranian ring-satellite system in order to examine whether a massive primordial ring may have produced the system we observe today.

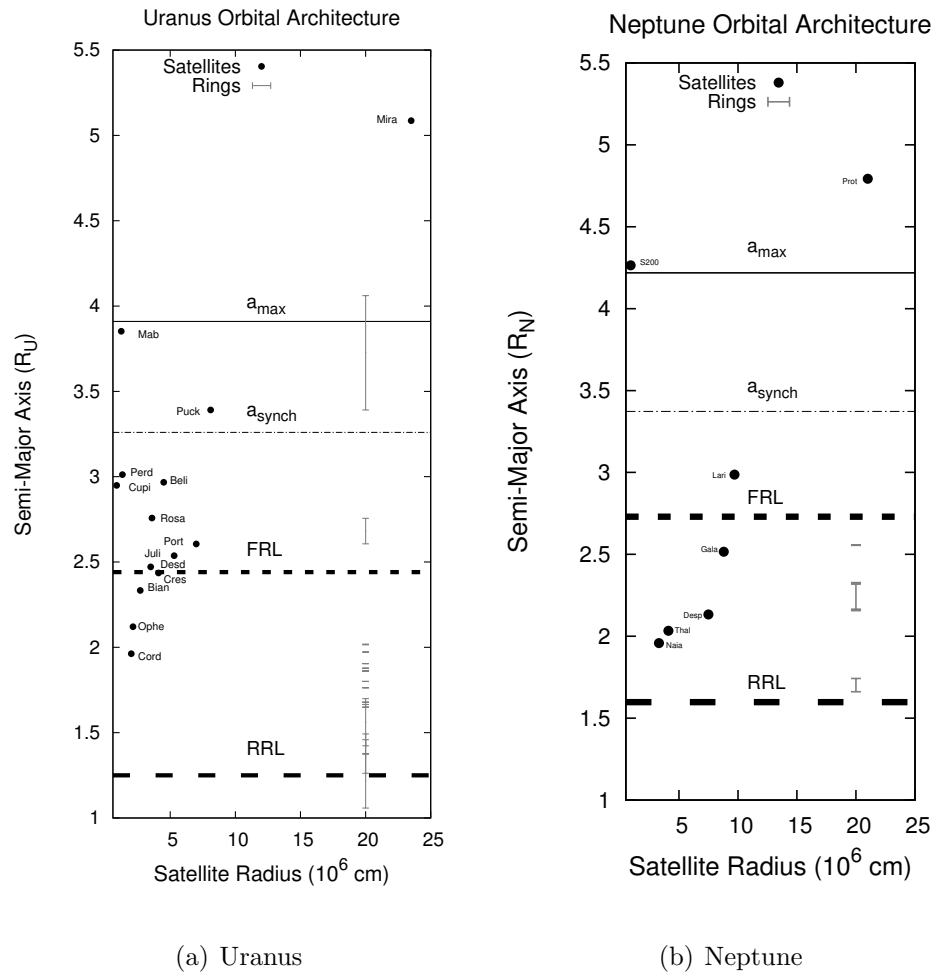


Figure 5.1. Orbital architecture of the Ice Giant systems. The dark circles show the present-day orbits of known satellites (abbreviated names adjacent) while the gray lines mark the locations of known rings. The location of the Rigid Roche Limits (RRL), Fluid Roche Limits (FRL), synchronous orbits (a_{synch}), and maximum orbits (a_{max}) for satellites perturbed by Lindblad Torques are also shown. Uranus (panel a) has 13 satellites with orbits within a_{max} , indicating they may have accreted from an ancient Uranian ring. The satellite Miranda, orbiting just beyond a_{synch} may have also accreted from this ring. Neptune (panel b) has 5 satellites with orbits within a_{max} , indicating they may have accreted from an ancient Neptunian ring, however the Triton capture event complicates the ability to test this hypothesis. It is possible the satellites S/2004 N 1 and Proteus, orbiting beyond a_{Lind} may also have accreted from such a ring.

5.1 Motivation

Examination of Figure 2.2 reveals that Uranus falls within the Torque-Dependent regime for a wide range of satellite densities. The planet is orbited by several rings and has multiple satellites, with 13 known to orbit within a_{Lind} (see Figure 5.1). The masses and densities of 11 of these inner satellites are not well constrained. Each of these satellites are assumed to have a bulk density of $\sim 1.3 \text{ g cm}^{-3}$. However, Jacobson et al. [1992] used Voyager radar and image observations to determine the bulk density of Miranda to be $\sim 1.2 \text{ g cm}^{-3}$. Additionally, Chancia et al. [2017] used perturbations in Uranus’s η ring to determine the bulk density of Cressida to be $\sim 0.86 \text{ g cm}^{-3}$. Therefore, the other 11 inner satellites of Uranus may have a bulk density less than typically assumed.

In this chapter I implement RING-MOONS to examine whether Miranda may have formed from an ancient primordial ring in orbit around Uranus. Uranus has a mass of $8.68 \times 10^{28} \text{ g}$, an average radius $R_U \sim 2.54 \times 10^9 \text{ cm}$, a bulk density of 1.27 g cm^{-3} , and an obliquity of 97.8° . A giant impact has been proposed to explain the large tilt of Uranus’s rotation axis [Slattery, 1992]. Such an impact may have occurred soon after the planet formed and may have placed a large amount of material into orbit. This material would have collapsed into a Roche-interior ring around Uranus [Morbidelli et al., 2012]. The current inner satellite system may have accreted from this Roche-interior ring [Charnoz et al., 2018]. Furthermore, such an impact event may have produced Uranus’s current rotation period of 17.24 hours [Slattery, 1992].

Miranda is a massive satellite that currently orbits Uranus beyond a_{Lind} . It has a radius of $2.36 \times 10^7 \text{ cm}$, an estimated mass of $6.6 \times 10^{22} \text{ g}$, and a bulk density of 1.2 g cm^{-3} [Jacobson et al., 1992]. Miranda has a semi-major axis of $1.30 \times 10^{10} \text{ cm} \sim 5.13R_U$, and an eccentricity of 0.0013. The low eccentricity of Miranda’s orbit is indicative of formation from a planetary ring [Charnoz et al., 2010]. Yet, Miranda orbits Uranus with an inclination of 4.3° , which is unexpected for satellites accreting from a planetary ring. Miranda does not exhibit any mean motion resonances today,

and the relatively high inclination of its orbit (as compared to the satellites which orbit interior to Miranda) is not currently understood. However, it may be possible that after accreting from a planetary ring, Miranda at some point crossed the 3 : 1 MMR with Umbriel [Moons and Henrard, 1994].

Tiscareno et al. [2013] determined that the location of transition from ring material to satellites at Uranus implies a critical Roche density of 1.2 g cm^{-3} . Satellites with a bulk density of $\sim 1.2 \text{ g cm}^{-3}$ accreting from a Roche-interior ring in orbit around Uranus fall within the Torque-Dependent regime (see Figure 2.2). Examination of Equation 2.11 shows that the evolution of a satellite depends upon the tidal love number k_2 , and the tidal dissipation factor Q . However these values are not well constrained for the Uranian satellites. For Uranus, k_2 is thought to be ~ 0.104 [Murray and Dermott, 1999], while Q could be as small as 500 or as large as 10,000 [Lainey, 2016].

5.2 Methods

I hypothesize that Miranda accreted from an ancient ring orbiting Uranus 4 Gy ago that was sufficiently massive for Lindblad torques to migrate the satellite from the FRL to an orbit beyond a_{synch} . I further hypothesize that after migrating to an orbit beyond a_{synch} , tidal torques caused the satellite to migrate to its current orbit. With this hypothesis in mind, I use the current semi-major axis of Miranda as a constraint in calculating the tidal ratio k_2/Q . If I assume Miranda evolved to its current orbit from a_{synch} over 4 Gy from tidal torques alone, I may place a lower bound on the value of k_2/Q . With these constraints I may integrate Equation 2.11 to determine k_2/Q .

Ignoring Lindblad torques, integration of Equation 2.11 for a satellite in a circular orbit yields:

$$a_F^{13/2} - a_I^{13/2} = \frac{39M_s R_p^5}{2} \sqrt{\frac{G}{M_p}} \left(\frac{k_2}{Q} \right) \Delta t. \quad (5.5)$$

Here Δt is the amount of time tidal torques will cause a satellite to migrate from an initial semi-major axis a_I to a final semi-major axis a_F . If I assume that tidal torques caused Miranda to migrate from a_{synch} to its current orbit in 4 Gy, I may determine the required tidal ratio k_2/Q for this to occur by rearranging Equation 5.5 to yield:

$$\frac{k_2}{Q} = \frac{2}{39M_s R_p^5 \Delta t} \sqrt{\frac{M_p}{G}} \left[a_F^{13/2} - a_I^{13/2} \right]. \quad (5.6)$$

I set a_F equal to Miranda’s current semi-major axis, $a_I = a_{synch} \sim 3.26R_p$, and $\Delta t = 4 \times 10^9$ years. By substituting the mass and radius of Uranus into Equation 5.6, as well as the current mass of Miranda, I find $k_2/Q \approx 3.3 \times 10^{-5}$. If $k_2 = 0.104$ [Murray and Dermott, 1999], this corresponds to a tidal dissipation factor of ~ 3150 , and is well within the expected range for Q [Laine, 2016].

By definition, a satellite that accretes within the “Torque-Dependent” regime would be in a 2:1 resonance ($\mathcal{M} = 2$) with a location interior to the FRL when the satellite is located at the synchronous orbit. Examining Equation 5.4, I calculate the necessary surface-mass density of the ring for Lindblad torques to overcome the tidal torques. I find that a Uranian ring with a surface-mass density of $\geq 18 \text{ g cm}^{-2}$ in a 2:1 resonance with a satellite located at a_{synch} would be able to perturb the satellite to beyond a_{synch} . At this point tidal torques would continue to migrate the satellite away from the planet. This surface-mass density is on the order of the estimated surface-mass density of the Uranian rings today [Esposito, 2006].

In order to simulate the Uranian system in “RING-MOONS” I need to define the initial conditions of the system [Hesselbrock and Minton, 2017]. The physical characteristics of the particles in the ring and the accreted satellites, as well as the surface mass density profile of the ring all affect the outcome of the system. As I am testing a hypothesis on the formation of Miranda, I assume the bulk density of the ring material, and any accreting satellites, to be identical to the bulk density of Miranda, $\rho_s = 1.2 \text{ g cm}^{-3}$ [Tiscareno et al., 2013]. Furthermore, I set the initial surface-mass density of the ring to follow a power law, such that $\sigma(r) = \sigma_0 r^{-3}$, where σ_0 is a constant determined by the initial mass of the ring. The ring extends from the upper

atmosphere of Uranus to the FRL. Lastly, I assume $k_2 = 0.104$ [Murray and Dermott, 1999] and set $Q = 3000$. This corresponds to a tidal ratio of $k_2/Q = 3.5 \times 10^{-5}$, which is slightly more than the calculated lower bound of $k_2/Q = 3.3 \times 10^{-5}$.

5.3 Results

In Figure 5.2 I display the results from a RING-MOONS simulation. The initial surface-mass density of a ring with a total mass of 3.0×10^{23} g, as well as the current mass and location of the inner Uranian satellites is shown in Figure 5.2a. Additionally, I have marked the semi-major axes of the RRL, FRL, and a_{synch} . For a satellite to migrate beyond a_{synch} , the locations in the ring that are in resonance with the satellite must have a sufficient surface mass density to satisfy Equation 5.4. A satellite orbiting Uranus at a_{synch} could be in resonance with both the $\mathcal{M} = 2$ and $\mathcal{M} = 3$ modes in the ring. This permits multiple surface-mass density profiles for Equation 5.4 to remain true. However, in Figure 5.2a I have marked the surface-mass density for the $\mathcal{M} = 2$ resonance mode to alone satisfy Equation 5.4 for a satellite at a_{synch} .

I find that the ring quickly transports ring material beyond the FRL where it is able to accrete into satellites [Crida and Charnoz, 2012, Hesselbrock and Minton, 2017]. Additionally, the surface mass density of the ring is initially sufficient for Lindblad torques to overcome the tidal torques, migrating the satellites away from the ring edge. As displayed in Figure 5.2b, we see that after 17 My the surface-mass density of the ring has decreased, yet remains sufficient to satisfy Equation 5.4. In 17 My the ring has produced a collection of 25 satellites, including two satellites which have migrated beyond a_{synch} . Furthermore, Figure 5.2b shows that the surface mass density of the ring at the $\mathcal{M} = 2$ resonance location is sufficient for Lindblad torques to migrate the Miranda-mass satellite beyond a_{synch} .

The results of the simulation after 183 My are displayed in Figure 5.2c. At this point we see that the two exterior satellites have migrated beyond a_{synch} . Once beyond the synchronous orbit, Equation 2.11 is positive as the tidal torques cause

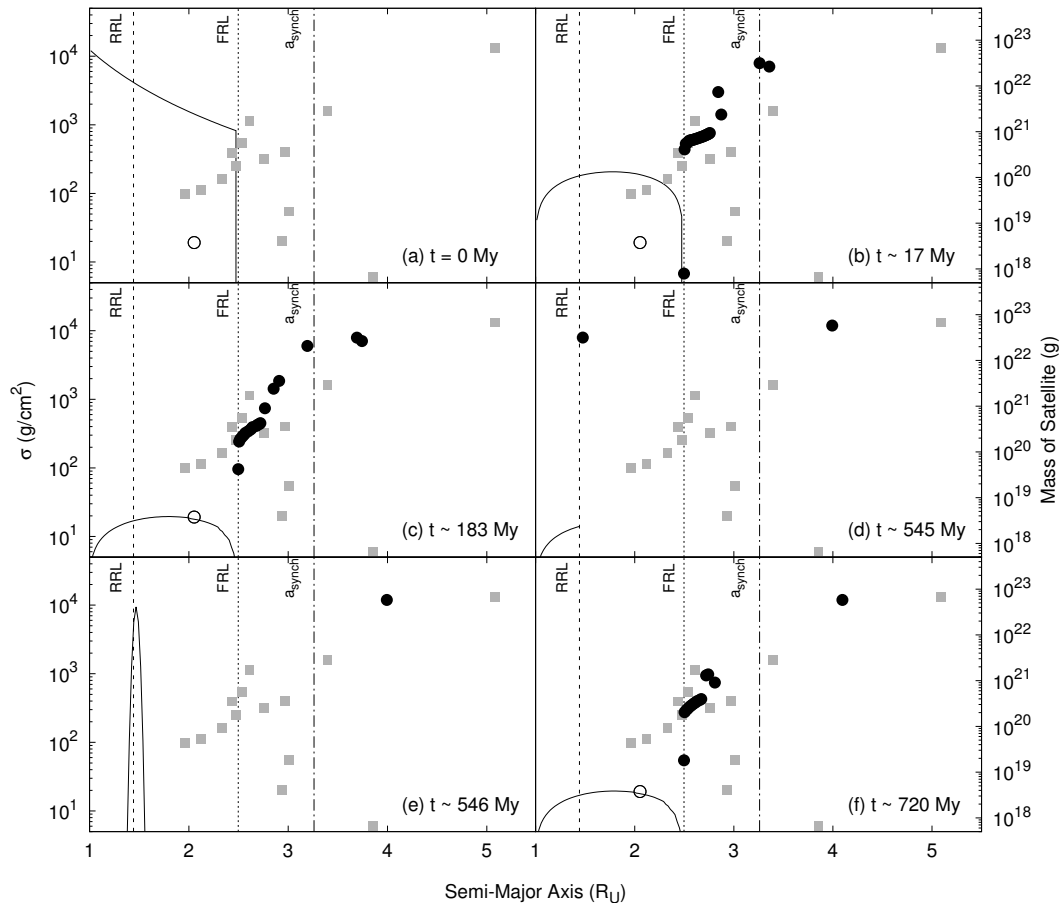


Figure 5.2. Evolution of the surface mass density of a Uranian ring with an initial mass of 3.0×10^{23} g. The horizontal axis marks the distance from Uranus, the left vertical axis marks the surface-mass density of the ring (black line), and the right vertical axis marks the mass of the satellites. Solid black circles represent RING-MOONS satellites while the current satellite population is shown as gray squares. The locations of the RRL, FRL, and the synchronous orbit are marked with vertical lines. The open circle marks the required surface-mass density at the $\mathcal{M} = 2$ mode for Equation 2.15 to be true for a satellite at a_{synch} , ignoring all other modes. (a) Initial conditions. (b) Two satellites have evolved beyond a_{synch} and the surface-mass density is above the threshold value. (c) The surface-mass density of the ring has fallen such that Equation 2.15 is no longer true. (d) The surface-mass density of the ring has declined. The two satellites orbiting beyond a_{synch} have merged into a Miranda-mass satellite. The 18 satellites interior to a_{synch} have merged into one massive satellite that has migrated to the RRL. (e) The massive satellite has been disrupted at the RRL, generating a new ring which has begun to viscously spread. (f) The ring generated by the destruction of the massive satellite has accreted a new generation of 14 satellites. However, the surface-mass density of the ring has fallen below the threshold value. Overtime these satellites may gravitationally scatter to produce a system similar to the one observed today.

the two satellites to migrate away from the primary. After ~ 183 My the ring has generated a total of 20 satellites. However, at this point the surface-mass density of the ring at the $\mathcal{M} = 2$ mode has fallen such that Equation 5.4 is no longer valid for a satellite located at a_{synch} . We see that the surface-mass density of the ring has fallen such that Lindblad torques are unable to cause any other satellites to migrate beyond a_{synch} . As the ring loses mass overtime, tidal torques cause the remaining 18 satellites orbiting inside a_{synch} to migrate inwards.

At ~ 215 My these two satellites merge to form a single Miranda-mass satellite. The Miranda mass satellite continues to be migrated away from the primary, and reaches Miranda's current semi-major axis at $\sim 4.2 \times 10^9$ years. As the simulation continues, the most massive satellite interior to a_{synch} migrates inwards. The tidal torque exerted on the massive satellite causes its semi-major axis to decrease more rapidly than any other satellites interior to a_{synch} . Thus, as the massive satellite migrates inwards it accretes all the satellites interior to a_{synch} . After ~ 675 My all satellites interior to a_{synch} have merged into one massive body that has migrated to the RRL (see Figure 5.2d).

Upon reaching the RRL, the massive satellite has rapidly disrupted, with its material generating a new ring of material, in agreement with Leinhardt et al. [2012]. The ring begins to viscously spread as displayed in Figure 5.2e. This ring deposits much of its mass onto Uranus, however it does spread material towards the FRL. After ~ 720 My, the ring has spread material beyond the FRL forming a new generation of 14 satellites interior to a_{synch} , which I show in Figure 5.2f. The most massive satellite generated by the new ring is roughly half the mass of the satellite Puck. However, as the mass of the ring decreases over time, the surface mass density of the new ring is insufficient to evolve any of these satellites beyond a_{synch} .

It is important to note that the value of k_2/Q has a strong effect on the results of the simulation. In Equation 5.4, Q and $\sigma(r)$ are inversely related. If $Q \sim 10,000$, in contrast to the value I derived, the magnitude of the tidal torques is reduced. In such a scenario, the surface-mass density of the ring for the Lindblad torques to

overcome the tidal torques would be substantially less. Thus, for the same mass ring, satellites would be more easily evolved to orbits beyond a_{synch} . However, once the satellite has been migrated beyond a_{Lind} tidal torques alone drive the migration of the satellite. In this scenario, a Miranda-mass satellite would be unlikely to reach its current orbit within 4 Gy due to the reduced tidal torque. Conversely, if $Q \sim 500$, the necessary surface-mass density for Equation 5.4 to be true would be substantially greater. Although such a ring would be able to evolve a satellite to the orbit of Miranda, the greater mass of the ring would result in a satellite much more massive than Miranda.

5.4 Discussion

While the results displayed in Figure 5.2 show that it is possible to evolve a Miranda-mass satellite to its current orbit from a Roche-interior ring, these results do not fully reproduce the system as we see it today. There are 13 Uranian satellites interior to a_{Lind} , and the RING-MOONS results do not reproduce all of the inner Uranian satellites. The most difficult satellites to model with RING-MOONS are the satellites Mab and Puck. I find that rings that are massive enough to perturb two bodies beyond a_{synch} typically produce satellites much more massive than Miranda and/or Puck.

There are several dynamical processes that are not modeled in RING-MOONS, but which may be important for reproducing the architecture of the inner Uranian satellite system. RING-MOONS treats all satellite-satellite interactions as direct mergers, whereas in reality close encounters could also cause satellites to disrupt, or scatter [Hesselbrock and Minton, 2017, Leinhardt and Stewart, 2012, Salmon and Canup, 2017]. This causes RING-MOONS to produce systems where satellite mass generally increases with semi-major axis, and prevents the model from producing small satellites that could be scattered into distant orbits. This may explain why the architecture of the inner satellite system in Figure 5.2f does not match the observed

system, especially for the satellites Perdita and Cupid (Figure 5.1). Furthermore, satellites accreting from a Roche-interior ring are often in near resonance with each other. A satellite orbiting beyond a_{Lind} will no longer directly exchange angular momentum with the ring. However, if an interior satellite that is still in resonance with the ring enters into resonance with the exterior satellite, the Lindblad torque exerted onto the interior satellite will be passed on to the exterior satellite. Thus, Lindblad torques may evolve a satellite to an orbit beyond a_{Lind} through a Laplace resonance chain [Salmon and Canup, 2017].

The limitations to satellite-satellite dynamics as modeled in RING-MOONS presents an additional difficulty when considering the major Uranian satellites, Ariel, Umbriel, Titania, and Oberon. The orbital migration of these bodies can have strong effects on each other, and also potentially an inner satellite system as well. In this work, I assume the major Uranian satellites formed soon after Uranus itself and are primordial. Thus, the orbital migration of the inner satellites which form in the Torque-Dependent regime differs from the orbital migration of the major satellites. However, the gravitational influence of the major satellites on the architecture of the inner satellite system as displayed in Figure 5.2 needs to be investigated further. I find that Miranda, in its outward migration, would encounter several mean-motion resonances with Ariel and Umbriel. Indeed these interactions may have left Miranda with the inclination observed today [Moons and Henrard, 1994, Tittlemore and Wisdom, 1990].

Reproducing the Uranian system as it is observed today is a significant challenge due to a number of factors. The inner Uranian satellites are currently tightly packed, leading to a highly dynamic, chaotic system [French and Showalter, 2012]. Many of these satellites experience a combination of mean-motion eccentricity and inclination resonances, making long term orbital integrations of the system difficult [French et al., 2015]. Furthermore, the satellites themselves are expected to have experienced multiple disruptive impacts with heliocentric material. Many of these collisions would likely be catastrophic to the inner satellites. It is thought that the system observed today has been collisionally evolved on a timescale of 10^8 years [Colwell and Esposito,

1992]. Colwell and Esposito [1992] argue that the ring-satellite system we observe today are leftover collision fragments from some older population of satellites. This makes it extremely challenging to even hypothesize which satellites existed millions to billions of years ago.

Lastly, the assumption that any satellite that has been migrated to the RRL would be tidally disrupted may be an oversimplification. The RRL marks the location where a cohesionless, strengthless object would be tidally disrupted, and is dependent upon the satellite bulk density. As discussed in Section 5.1, the bulk density of the inner Uranian satellites is indirectly constrained from the rings [Tiscareno et al., 2013], but my estimate to the location of the RRL may not be correct for every inner satellite. Furthermore, the inner Uranian satellites likely have some form of internal cohesion, which would prevent them from being tidally disrupted at the RRL [Black and Mittal, 2015]. The uncertainty in the location of tidal breakup does not affect my result for the formation of Miranda, but it does affect any results for satellites which accrete from rings created by tidally disrupted satellites (Figure 5.2f). If the location of tidal breakup is inward of the RRL, the subsequently formed ring would transport a smaller mass of material beyond the FRL to form satellites [Hesselbrock and Minton, 2017]. Thus, the mass of the satellite system shown in Figure 5.2f serves as an upper bound on the mass of the inner satellite system.

Due to these complications, connecting the results of RING-MOONS depicted in Figure 5.2 to the system observed today is not straightforward. The population of satellites interior to Miranda as produced by RING-MOONS and depicted in Figure 5.2f has a total mass of $\sim 6.6 \times 10^{21}$ g. This agrees with the current population of satellites interior to Miranda, which are estimated to have a total mass of $\sim 6.5 \times 10^{21}$ g. I expect that heliocentric impacts with the inner satellites generated by RING-MOONS would collisionally evolve the system to produce the ring-satellite system of Uranus observed today [Colwell and Esposito, 1992, 1993]. Nevertheless, my results do give some constraints on the origin of Miranda, and are in broad agreement

with the total mass of satellites interior to Miranda, even if they do not reproduce the details of their orbital architecture.

6. THE TIDAL EVOLUTION OF BINARY SYSTEMS

6.1 Motivation

Binary systems are common throughout the solar system and are typically comprised of two similar mass bodies orbiting their mutual barycenter. Binary systems are so numerous that it is possible that even all Trans Neptunian Objects (TNOs) formed as binary systems [Nesvorný et al., 2010]. Binary systems can form in a variety of ways, including the mutual capture of two bodies during a close encounter, or the catastrophic disruption of a single body into two. Additionally, rapidly spinning objects may experience rotational disruption as the centrifugal force overcomes the cohesive forces of the object, dividing the object to create a binary system.

Once a binary system has formed, the two objects exchange angular momentum via tidal torques. The total angular momentum of a binary system includes the spin angular momentum of each body, and the orbital angular momentum of the system. Tidal interactions allow spin angular momentum to be transferred to the mutual orbital angular momentum, or vice-versa. How angular momentum is transferred between bodies is dependent upon the location of the synchronous orbit relative to the semi-major axis of the system. The synchronous orbit is the location where the orbital period of the system is equal to the rotation period of the most massive body. I refer to the most massive body of the system as the “primary” and the less massive body as the “satellite.” If the semi-major axis of the system is inside the synchronous orbit, tidal interactions will transfer the orbital angular momentum of the system into the spin angular momentum of the bodies. This causes the two bodies to spin more rapidly and decreases the semi-major axis. If the semi-major axis of the system is outside the synchronous orbit, tidal interactions will transfer the spin

angular momentum of the bodies into the orbital angular momentum of the system. This causes the two bodies to spin more slowly and increases the semi-major axis.

There are two possible end states for the tidal evolution of binary systems. The first possibility is that angular momentum is transferred until the system reaches a fully synchronous state. A fully synchronous system is where the orbital period and the rotation periods of each body are all equal. If a binary system evolves to be fully synchronous, the tidal torque reduces to zero and angular momentum is no longer exchanged.

The second possibility is that the system experiences a runaway depletion of orbital angular momentum. The semi-major axis of the system will decrease until the satellite is either tidally disrupted, or the two bodies come into contact to form a contact binary. At the end stage of the tidal collapse of a binary orbit, material may potentially be shed from the surface of either body, either due to the tidal disruption of the satellite or during the impact of the two bodies as they make contact. If material is shed from the bodies' surface and is placed into orbit, a ring system could result. Recent observations indicate that several TNOs (Chariklo, Chiron, and Eris) are orbited by ring systems. While Binary TNOs (BTNOs) may potentially be common, it is not known how often ring systems orbit these objects. Examining the dynamics of the tidal collapse of a binary system, as well as the population of BTNOs that are likely to undergo such a collapse may indicate how often rings are produced in the outer solar system. Additionally, as contact binaries may have formed via a tidal collapse, they too may serve as good candidates for future ring studies.

Many TNOs may actually be contact binaries. These objects indicate that two separate similar mass bodies became attached after coming into contact with one another. It has been shown that 10 – 30% of TNOs in the solar system are actually contact binaries [Lacerda, 2011, Sheppard and Jewitt, 2004]. Some of these objects may have formed via low-velocity impacts during close encounters. However, I hypothesize that some contact binaries may have initially been a binary system that

subsequently experienced a mutual decay of the body orbits. The tidal decay of binary bodies is the focus of this work.

For binary systems that undergo a runaway depletion of orbital angular momentum the semi-major axis is continuously decreased. In planetary systems where the primary is significantly more massive than the satellite, the semi-major axis may decrease until the satellite reaches the Rigid Roche Limit (RRL). For cohesionless bodies, at this location the satellite begins to shed mass from its equator as material is rapidly removed from the surface of the satellite and placed into orbit. Much of the orbiting material impacts the satellite, creating a collisional cascade that quickly disrupts the satellite, forming a ring around the primary body.

In planetary systems where the bodies are of similar mass the semi-major axis may decrease until the two bodies come into contact. Depending upon the angular momentum of the system, the relative velocity between the two body surfaces at the moment of contact may be non-zero. During the moment of contact, friction between the two body surfaces will transfer spin momentum from the primary to the satellite until the relative velocity between the surfaces is reduced to zero. An increase to the satellite's rotation rate may reduce the acceleration of a particle on the equator until it is no longer bound to the body. The shedding of mass during the formation of a contact binary may evolve to form a ring around the contact binary as well.

Given the expected population of BTNOs and contact TNOs, as well as the discovery of ring systems in orbit around TNOs, the ability of a binary tidal collapse to produce rings is of particular interest. In this work I will examine the dynamics of binary systems to determine which systems undergo a complete tidal decay of their mutual orbit. After determining which types of systems undergo collapse, I will produce statistics that show the likelihood of tidal decay. Finally, I will examine the recently discovered ring systems around the centaurs Chariklo and Chiron. Chariklo and Chiron are both rapidly rotating bodies orbited by rings. I will investigate whether the existence of rings and their rapid rotation rates are both explained by a binary tidal collapse.

6.2 Methods

In this section I describe the tidal dynamics of binary systems, the conditions for tidal collapse, and review the possible end stages of collapse. In Section 6.2.1 I review the tidal dynamics of a binary system and determine the conditions necessary for a binary system to collapse. In section 6.2.2 I examine the likelihood that the satellite remains intact during the tidal collapse. As the mutual orbit decays, the gravitational force exerted on each body by the other increases, as does the rotation rate of each body. I will examine the possible end stages of a binary collapse and how the collapse dynamics may cause material to be removed from the satellite's surface. Finally, in Section 6.2.3, I will demonstrate how observations of a collapsed contact TNO binary can reveal the initial orbit of the binary system before the collapse occurred.

6.2.1 Tidal Evolution of Binary Systems

The dynamics of a binary system in which a primary with mass M_p , and a satellite with mass M_s , share a mutual orbit about their center of mass may be simplified into an equivalent system. The simplified system is described as a body of mass $M_p M_s / (M_p + M_s)$ which orbits a stationary body of mass $M_p + M_s$ [Taylor and Margot, 2010]. The mass ratio of the system is defined as $q = M_s / M_p$.

The total angular momentum of the binary system is the sum of the orbital angular momentum, and the spin angular momentum of the primary and the satellite. The total orbital angular momentum is given as [Taylor and Margot, 2011]:

$$L = \frac{q}{1+q} M_p a^2 n (1 - e^2)^{1/2}. \quad (6.1)$$

Here $n = \sqrt{G(M_p + M_s)/a^3}$ is the mean motion of the system and a and e are the semi-major axis and eccentricity of the mutual orbit. The total spin angular momentum of a binary system is given as [Taylor and Margot, 2011]:

$$S = \alpha_p M_p R_p^2 \omega_p \left[1 + \frac{\alpha_s}{\alpha_p} \left(\frac{\rho_p}{\rho_s} q^{5/3} \right) \frac{\omega_s}{\omega_p} \right]. \quad (6.2)$$

Here R_p is the radius of the primary, $\rho_{p,s}$, $\omega_{p,s}$, and $\alpha_{p,s}$ are the bulk densities, rotation rates, and moment of inertia coefficients for the primary and the satellite, respectively. For spherical bodies, $\alpha_p = \alpha_s = 2/5$.

The satellite exerts an acceleration on the surface of the primary [Murray and Dermott, 1999]. The acceleration from the orbiting satellite varies in magnitude across the primary's surface and is greatest for the surface closest to the satellite. The gradient tidal potential across the primary's surface distorts the primary's shape, creating a tidal bulge. The internal structure of the primary determines the response of the surface to the tidal potential. Internal friction dissipates the tidal acceleration and results in a lag between the tidal disturbance and the tidal response. The effect of tidal dissipation can lead to dramatic physical and orbital consequences for the primary and the satellite.

Although the satellite creates the tidal bulge on the primary, the acceleration of the bulge on the satellite exerts a torque on the satellite. The consequence of the tidal torque is dependent upon the semi-major axis of the satellite relative to the synchronous orbit. For a satellite in a Keplerian orbit, the synchronous orbit can be calculated via Equation 2.9. If the satellite is in a synchronous orbit with the primary, it completes one orbit for every full revolution of the primary, and therefore is always aligned with the tidal bulge. The gravitational attraction between the tidal bulge and the satellite is perpendicular to the satellite's motion, and no torque results.

However, if the satellite orbits interior to the synchronous orbit, its orbital period is shorter than the rotational period of the primary. As the satellite orbits, it passes over the surface of the primary. Due to the lag in the formation of the tidal bulge, the satellite is always "ahead" of the tidal bulge on the primary surface. The gravitational attraction between the tidal bulge and the satellite is no longer strictly perpendicular to the satellite's motion, and the tidal bulge exerts a torque on the satellite. For satellites orbiting interior to the synchronous orbit this torque transfers angular momentum from the satellite's orbit to the spin angular momentum of the primary, causing the satellite to migrate towards the primary.

Alternatively, if the satellite orbits exterior to the synchronous orbit, its orbital period is longer than the rotational period of the primary. As the satellite orbits, the surface of the primary rotates past the satellite. Due to the lag in the formation of the tidal bulge, the satellite is always “behind” the tidal bulge on the primary surface. The bulge again exerts a torque on the satellite. However, for satellites orbiting exterior to the synchronous orbit the tidal torque transfers spin angular momentum from the primary to the satellite’s orbital angular momentum, causing the satellite to migrate away from the primary. Thus, satellites which lie interior to the synchronous orbit migrate inwards by tides, whereas satellites which orbit exterior migrate outwards.

Similarly, the primary exerts an acceleration on the satellite’s surface. Just as the satellite creates a tidal bulge on the primary that subsequently leads to the tidal torque, so too does the primary create a tidal bulge on the satellite. The tidal bulge on the satellite surfaces perturbs the primary, exerting a tidal torque. Thus, tidal torques enable angular momentum to be exchanged between both a primary and its satellite.

Angular momentum is exchanged between the two bodies by changing the rotational speeds of each body, and the semi-major axis of the mutual orbit. The change in the rotational speed of the primary due to tidal torques is given as [Taylor and Margot, 2010]:

$$\begin{aligned} \dot{\omega}_p = & -\frac{8\rho_p^3(\pi GR_p q)^2}{19\alpha_p\mu_p Q_p} \left(\frac{R_p}{a}\right)^6 \text{sign}(\omega_p - n) \\ & \times \left[1 + \frac{19}{22} \left(\frac{R_p}{a}\right)^2 + \frac{380}{459} \left(\frac{R_p}{a}\right)^4 + \frac{475}{584} \left(\frac{R_p}{a}\right)^6 + \frac{133}{165} \left(\frac{R_p}{a}\right)^8\right]. \end{aligned} \quad (6.3)$$

Here μ_p and Q_p are the rigidity and the tidal dissipation factor of the primary, respectively. Similarly, the change in the rotational speed of the satellite due to tidal torques is given as [Taylor and Margot, 2010]:

$$\begin{aligned} \dot{\omega}_s = & -\frac{8\pi^2 G^2 \rho_p^3 R_p^3 q}{19\alpha_s\mu_s Q_s R_s} \left(\frac{R_p}{a}\right)^6 \text{sign}(\omega_s - n) \\ & \times \left[1 + \frac{19}{22} \left(\frac{R_s}{a}\right)^2 + \frac{380}{459} \left(\frac{R_s}{a}\right)^4 + \frac{475}{584} \left(\frac{R_s}{a}\right)^6 + \frac{133}{165} \left(\frac{R_s}{a}\right)^8\right]. \end{aligned} \quad (6.4)$$

μ_s and Q_s are the rigidity and the tidal dissipation factor of the satellite.

As ω_p and ω_s change, the spin momentum of the system changes. To conserve the angular momentum of the system the torque causes the semi-major axis to change, transferring momentum between the spin and orbital momenta. Thus, the change in the semi-major axis is [Taylor and Margot, 2010]:

$$\begin{aligned} \dot{a} = & \frac{8R_p^3 \sqrt{3\pi^3 G^3 \rho_p^5}}{19\mu_p Q_p} \left(\frac{R_p}{a} \right)^{11/2} \\ & \times \left[\text{sign}(\omega_p - n) + \left(\frac{R_s}{R_p} \right) \frac{\mu_p Q_p}{\mu_s Q_s} \text{sign}(\omega_s - n) \right. \\ & + \frac{19}{22} \left(\frac{R_p}{a} \right)^2 \left(\text{sign}(\omega_p - n) + \left(\frac{R_s}{R_p} \right)^3 \frac{\mu_p Q_p}{\mu_s Q_s} \text{sign}(\omega_s - n) \right) \\ & + \frac{380}{459} \left(\frac{R_p}{a} \right)^4 \left(\text{sign}(\omega_p - n) + \left(\frac{R_s}{R_p} \right)^5 \frac{\mu_p Q_p}{\mu_s Q_s} \text{sign}(\omega_s - n) \right) \\ & + \frac{475}{584} \left(\frac{R_p}{a} \right)^6 \left(\text{sign}(\omega_p - n) + \left(\frac{R_s}{R_p} \right)^7 \frac{\mu_p Q_p}{\mu_s Q_s} \text{sign}(\omega_s - n) \right) \\ & \left. + \frac{133}{165} \left(\frac{R_p}{a} \right)^8 \left(\text{sign}(\omega_p - n) + \left(\frac{R_s}{R_p} \right)^9 \frac{\mu_p Q_p}{\mu_s Q_s} \text{sign}(\omega_s - n) \right) \right]. \end{aligned} \quad (6.5)$$

Equation 6.5 is an expansion that includes higher order terms, and is more appropriate than Equation 2.10 for similar mass bodies with a semi-major axis $\leq 5R_p$.

Given enough time and left undisturbed, the tidal interaction between the satellite and the primary will result in one of two possible outcomes: a fully synchronous system, or a collapsed system [Taylor and Margot, 2011]. A fully synchronous system will result if $\dot{a} > 0$ (generally if $a > a_{synch}$). The semi-major axis of the system will increase while the rotation rate of both bodies changes, until $n = \omega_p = \omega_s$. At this point the system has become fully synchronous and $\dot{a} = 0$.

However, even systems where $\dot{a} < 0$ can become fully synchronous. As the semi-major axis of the system decreases, the rotation rate of both bodies increases as momentum is transferred from the orbit into the rotation rates of both bodies. a_{synch} is a function of ω_p and therefore changes as the rotation rate of the primary changes. As the primary speeds up, a_{synch} decreases. Depending on the angular momentum of the system, it is possible for the location of the semi-major axis to change more quickly

than the semi-major axis of the system [Taylor and Margot, 2011]. In these systems the synchronous orbit “catches up” to the satellite’s semi-major axis. Eventually, $a = a_{synch}$ and the system has become fully synchronous.

The second possible outcome can only occur for systems where $\dot{a} < 0$. For a specific population of binary systems, the semi-major axis changes more quickly than the location of the synchronous orbit. In these systems the semi-major axis continues to decrease until the semi-major axis of the system has completely collapsed. The tidal interaction collapses the orbit until the two bodies come into contact, or the satellite reaches the RRL and is tidally disrupted.

In this work I examine the tidal interaction of binary systems in order to determine the dynamics which cause specific binary systems to collapse. I assume that tidal interactions have caused all binary systems to evolve such that they have relaxed into fully synchronous states. If a system is disturbed from a fully synchronous state (whether from an impact or a close encounter), I define which systems will evolve to a collapsed state.

For any binary system, there are either one, or two possible fully synchronous states [Taylor and Margot, 2011]. Binary systems with two possible synchronous states have a solution with fast rotation rates and a small semi-major axis, and a solution with a greater semi-major axis and slower rotation rates. Given the mass-ratio of a system, there exists a fully synchronous “critical orbit.” A disturbance from this orbit can result in the system collapsing. The critical orbit is calculated as [Taylor and Margot, 2011]:

$$a_{crit} = \left[\frac{6}{5} \left(\frac{1+q}{q} \right) \left(1 + \left(\frac{\rho_p}{\rho_s} \right)^{2/3} q^{5/3} \right) \right]^{1/2}. \quad (6.6)$$

If a system is fully synchronous at this orbit and the system is disturbed such that $\dot{a} < 0$, the semi-major axis will decrease until the bodies come into contact or the satellite is tidally disrupted.

6.2.2 Mass Shedding

Whether a collapsing system results in contact between the two bodies or the tidal disruption of the satellite depends upon the location of the contact point as compared to the RRL. The contact location is simply when the semi-major axis is equal to the mutual radii of the two bodies:

$$a_C = R_p + R_s = R_p \left[1 + \left(\frac{q}{\mathcal{R}} \right)^{1/3} \right]. \quad (6.7)$$

Here $\mathcal{R} \equiv \rho_s/\rho_p$ is the ratio between the bulk densities of the satellite and the primary.

The RRL is the semi-major axis where the acceleration of material on the equator of a strengthless body is perpendicular to the body's surface. A satellite located at the RRL will shed material from its equator, which can set up a collisional cascade that rapidly disrupts the satellite [Black and Mittal, 2015, Hesselbrock and Minton, 2017]. The net force acting on a particle with mass δ located on the equator of the satellite is the sum of gravitational and centrifugal forces:

$$F_{net} = -\frac{G\delta M_p}{(a - R_s)^2} + n^2\delta(a - R_s) + \frac{GM_s\delta}{R_s^2} \quad (6.8)$$

The RRL is the semi-major axis where $F_{net} = 0$. Performing a Taylor expansion and solving for a we retrieve Equation 2.1.

By setting Equation 6.7 equal to Equation 2.1, I may determine q_{shed} , the mass ratio for which mass shedding will occur at the point of contact.

$$q_{shed} = \mathcal{R} \left[\left(\frac{3}{\mathcal{R}} \right)^{1/3} - 1 \right]^3. \quad (6.9)$$

I plot q_{shed} in Figure 6.1. The solid line shows the necessary mass ratio for when a_C is equal to a_{RRL} . If $q \leq q_{shed}$, during a tidal collapse the satellite will begin to shed mass from its equator at or before the moment of contact. For bodies of uniform density ($\mathcal{R} = 1$), the contact point is outside the RRL for all $q \gtrsim 0.1$. However, for bodies with different densities, for example $\mathcal{R} = 0.5$, the contact point is outside the RRL for $q \gtrsim 0.25$. Figure 6.1 shows that cohesionless bodies in any collapsing binary system with $q \lesssim 0.1$ will begin to shed mass before the two bodies come into contact.

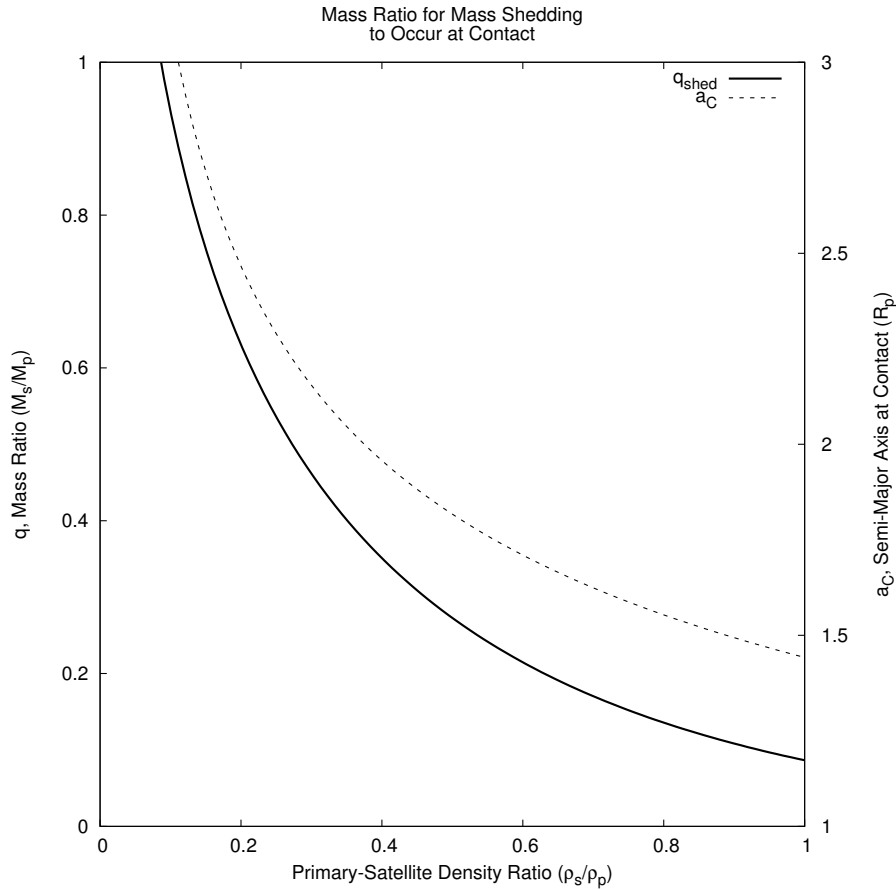


Figure 6.1. If the RRL is located at the point of contact between two objects, the satellite will begin to shed mass at its equator during contact. Given the ratio between the satellite and primary bulk densities, I show the required mass ratio for this to occur. The solid line marks the mass ratio where $a_{RRL} = a_C$ and the dashed line represents the semi-major axis of the contact point/RRL. If the mass ratio of the system is greater than q_{shed} , the system will not shed mass during contact. For systems with $q \leq q_{shed}$ the satellite will shed material from its equator during contact.

While q_{shed} is the maximum mass ratio a collapsing binary system may have for mass shedding to occur just as the two bodies reach the contact point, as the two bodies come into contact systems with $q > q_{shed}$ may still shed mass. In general, during the collapse the lower mass satellite is tidally locked and has a greater rotation

rate than the primary ($n = \omega_s > \omega_p$). As the two bodies approach one another, the surface of the primary spins parallel to the approaching satellite surface. While the two surfaces come into contact, friction will cause the slower rotating primary to transfer spin momentum to the satellite in the direction of the satellite's rotation until the surfaces rotate with the same velocity. Assuming no slippage occurs, the spin rate of the two bodies after contact is:

$$\omega'_s = \omega_p \left[\frac{(\rho_s/q\rho_p)^{2/3} + q\omega_s/\omega_p}{(\rho_s/q\rho_p)^{1/3} + q} \right], \quad (6.10a)$$

$$\omega'_p = \omega_p \left(\frac{q\rho_p}{\rho_s} \right)^{1/3} \left[\frac{(\rho_s/q\rho_p)^{2/3} + q\omega_s/\omega_p}{(\rho_s/q\rho_p)^{1/3} + q} \right]. \quad (6.10b)$$

The end result is the satellite “rolling along” the surface of the primary.

While Equation 6.10 depends upon the mass and density ratios, as well as the rotation rate of each body, $\omega'_s > \omega_s$ and $\omega'_p < \omega_p$. During contact, the transfer of spin momentum from the primary to the satellite increases the satellite's rotation rate. As the satellite spins faster, a particle on the surface of the satellite will experience a greater centrifugal force. Similar to the derivation of the rigid Roche limit from Equation 6.8, I may determine the net force exerted on a particle at the surface of the satellite after contact has been made:

$$F_{net} = -\frac{G\delta M_p}{R_p^2} + n^2\delta R_p + \frac{GM_s\delta}{R_s^2} - \omega_s'^2\delta R_p \quad (6.11)$$

If $F_{net} \leq 0$, the particle will be removed from the satellite's surface. Therefore, friction between the two bodies during contact may cause systems with $q > q_{shed}$ to shed mass. For example, a collapsing BTNO system with $R_p = 50$ km, $\rho_p = 1$ g/cm³ orbited by a satellite with $\mathcal{R} = 1$ and $q = 0.08$ will shed mass just as the two bodies come into contact, but friction will cause a similar collapsing system with $q = 0.431$ to shed mass after contact. Friction between the two bodies during contact can cause systems with mass ratios greater than q_{shed} to shed mass after contact.

6.2.3 Formation of Contact Binaries from Collapse

While contact binaries likely comprise 10 – 30% of the TNO population, resolving these bodies is exceptionally difficult [Lacerda, 2011, Sheppard and Jewitt, 2004]. For a particular hypothesized contact TNO, occultations may reveal the overall size of the object, and lightcurve analyses may indicate the object’s rotation period, but direct imaging of each hypothesized lobe remains difficult. Here I provide a general description of contact TNOs, provided their overall size and rotation rate. This description will permit me to hypothesize how an observed TNO may actually be a contact binary that experienced a tidal collapse. Furthermore, I will use the dynamics outlined in Section 6.2.1 to determine the conditions of the system before collapse, and whether any mass may have been shed from the satellite surface.

For a given TNO contact binary, I assume the total observed body radius R to be half the total body diameter. I assume a contact binary is composed of two spheres in contact with radius R_p and R_s . The mass ratio and the total body radius of the system today, $R = R_p + R_s$, are used to determine the radius of the primary and the satellite spheres:

$$\begin{aligned} R_p &= \frac{R}{1 + (q\rho_p/\rho_s)^{1/3}} \\ R_s &= \frac{R}{1 + (q\rho_p/\rho_s)^{1/3}} \left(\frac{q\rho_p}{\rho_s} \right)^{1/3} \end{aligned} \quad (6.12)$$

I assume that these objects were once binary systems with each sphere orbiting the other. Therefore $\alpha_p = 2/5$ and $\alpha_p/\alpha_s = 1$. From Equation 6.2, the spin momentum of the system at any point is then given by:

$$S = \frac{8\pi\rho_p}{15} \left[\frac{R}{1 + \left(\frac{q\rho_p}{\rho_s} \right)^{1/3}} \right]^5 \omega_p \left[1 + \left(\frac{\rho_p}{\rho_s} \right)^{2/3} q^{5/3} \frac{\omega_s}{\omega_p} \right]. \quad (6.13)$$

Assuming the bodies are on Keplerian orbits, from Equation 6.1 the orbital momentum of the two spheres at any point can be calculated as:

$$L = \frac{q}{(1+q)^{1/2}} \left(\frac{4\pi\rho_p}{3} \right)^{3/2} \left[\frac{R}{1 + \left(\frac{q\rho_p}{\rho_s} \right)^{1/3}} \right]^{9/2} [Ga]^{1/2}. \quad (6.14)$$

The total momentum of the system at any moment is the sum of Equations 6.13 and 6.14; $J = L + S$. For a given isolated system, J is a constant as momentum is conserved throughout the tidal interaction.

If I assume that these spheres experienced a complete collapse of their mutual orbit to form the system observed today, I may use the angular momentum of the system today as a constraint. The momentum of the system today is equal to the momentum of the two spheres in contact. In my simplified description, this corresponds to a semi-major axis equal to the total body radius, $a = R$. While the two bodies do not have any orbital momentum while in contact, in the reference frame of the reduced mass of the system there remains an “orbital momentum” component even at contact. This is calculated as:

$$L_C = \frac{qG^{1/2}R^5}{(1+q)^{1/2}} \left(\frac{4\pi\rho_p}{3} \right)^{3/2} \left[\frac{1}{1 + \left(\frac{q\rho_p}{\rho_s} \right)^{1/3}} \right]^{9/2}. \quad (6.15)$$

During contact the rotation rate of the primary is equal to the rotation rate of the satellite. Thus, the total momentum of a system at contact is given by Equations 6.13 and 6.15, with $\omega_s/\omega_p = 1$. Provided the radius of the object observed today, its rotation rate, and estimates for the densities of each sphere I can estimate J_t , the total momentum in the hypothesized contact binary today, as a function of q .

With the hypothesis that a contact binary with total radius R was once two separate bodies with radii R_p and R_s , I can calculate the total momentum of the system before contact. Assuming the system was initially fully synchronous ($n = \omega_p = \omega_s$) with semi-major axis $a = a_{crit}$, I may calculate J_{crit} , the total momentum of the system at the critical orbit. If the system was disturbed in such a way that the satellite lost spin momentum, the primary gained spin momentum, or the orbital momentum decreased, the system will collapse. Having calculated J_t and J_{crit} , I may determine the “critical mass ratio” q_C for which $J_t = J_{crit}$.

6.3 Results

I hypothesize that binary systems are common in the solar system, and that over time the tidal interaction between the two bodies drives the system into a fully synchronous state. I expect close encounters and impacts to disturb these systems from their fully synchronous state. Many systems may return to a fully synchronous state, but for systems with $a < a_{crit}$, tidal interactions between the two bodies will cause their mutual semi-major axis to decrease. I propose this as a possible formation mechanism for contact binaries. Furthermore, during the collapse process, the satellite may shed mass from its equator, which could serve as a possible source for ring material.

In Section 6.3.1 I compare the conditions for collapse derived in Section 6.2.1 with the currently known population of Binary Trans Neptunian Objects. This comparison will reveal any BTNO systems that are likely to experience a tidal collapse, as well as which systems may shed mass during the collapse process.

In Section 6.3.2 I apply my analysis in Section 6.2.3 to examine whether the centaurs Chariklo and Chiron were binary systems that underwent a tidal collapse, and whether this process could explain the existence of their ring systems.

6.3.1 Binary Trans-Neptunian Objects

There are currently 2810 known TNOs. Of this population, there are 59 observed BTNOs, with an additional 28 likely [Johnston, 2018]. While BTNOs currently make up $\sim 3\%$ of observed TNOs, it is possible that the entire TNO population formed as binary systems [Nesvorný et al., 2010]. Furthermore, 10 – 30% of the current TNO population may be contact binaries [Lacerda, 2011, Sheppard and Jewitt, 2004].

In Figure 6.2 I display the current known and likely population of BTNOs as a function of their mass ratio and the semi-major axis of their mutual orbit. From Figure 6.2 I observe that the majority of BTNOs have $q > 0.1$ and $a < 10^3 R_p$. Due to observational constraints, widely separated binary systems are more likely to be

discovered than systems in close tight orbits. Numerical models of TNOs have found that the majority of binary systems may be in tight orbits [Porter and Grundy, 2012].

I assume that all BTNOs are in fully synchronous orbits. In addition to the observed population of BTNOs, Figure 6.2 displays the location of a_{crit} . For BTNO systems with $a < a_{crit}$ in fully synchronous orbits, any disturbance that removes momentum from the primary, or adds momentum to the satellite, will cause the BTNO system to collapse. In Figure 6.2 I find that there are three systems with orbits and mass ratios in which a fully synchronous system could collapse if disturbed, or $\sim 3.5\%$ of the known BTNO population. From Figure 6.1 I find that a satellite in a system with $q \lesssim 0.08$ will begin to shed mass during the collapse process, or $\sim 17\%$ of the known BTNO population.

In addition to comparing the required semi-major axis and mass ratio for a fully synchronous system to collapse against the known BTNO population, I may examine how long such an evolution may take. I define a tidal timescale, τ_{tide} , as the ratio of a system's semi-major axis to the rate of change of the semi-major axis as calculated in Equation 6.5:

$$\tau_{tide} = \dot{a}/a \tag{6.16}$$

While a fully synchronous system with $a < a_{crit}$ would collapse, only those with $q \gtrsim 0.001$ do so within the age of the solar system.

6.3.2 Chariklo and Chiron

Planetary rings have recently been discovered around the centaurs Chariklo and Chiron and the TNO Haumea. Before these discoveries rings had only been observed in orbit around the outer giant planets, raising the question of how common these features may be in our solar system. Hypotheses for their origin have included tidal disruption during close planetary encounters, debris ejected into orbit by impact events, or three-body interactions between the primary object and two smaller ones.

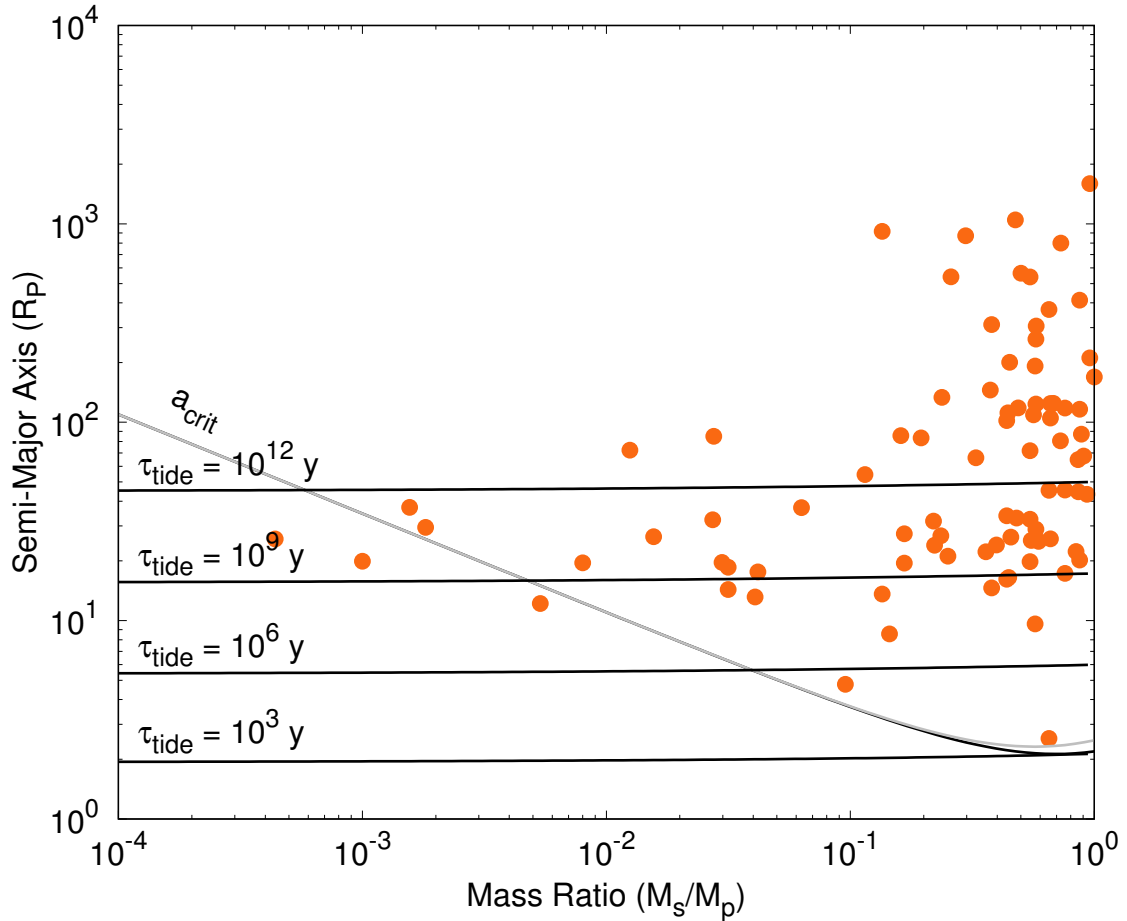


Figure 6.2. Here I plot the current population of observed known and likely Binary Trans-Neptunian Objects (BTNOs) as a function of their mass ratio (q), and the semi-major axis of their mutual orbit (a). The grey line marks the location of the critical orbit. BTNOs below the curve in fully synchronous orbits will likely experience a complete tidal collapse of their mutual orbit if they are disturbed. The nearly horizontal lines mark the evolution timescale, τ_{tide} , in years as a function of q and a for a system with $R_p = 50$ km and $\rho_p = 1$ g/cm³.

Unfortunately, none of these mechanisms has a high likelihood of producing a ring system.

The radius of Chariklo and Chiron is not well known, but they appear to be $\sim 200 - 300$ km in size. They are vary rapid rotators with Chariklo having a rotation period of ~ 7 hours and Chiron having a rotation period of ~ 5.9 hours. Their masses are poorly constrained, and they are estimated to have a bulk density of $0.5 - 1.5$ g/cm³. Haumea is much larger and is orbited by two small satellites which constrains its mass to be $\sim 4 \times 10^{24}$ g. Haumea rotates more rapidly with a period of ~ 3.9 hours and is expected be in hydrostatic equilibrium.

Of the three, Haumea is the only object to have a collisional family, which strongly indicates its rings may have formed during this collision. Chariklo and Chiron are not expected to have experienced collisions significant enough to produce rings, indicating a different mechanism for ring formation occurred. I propose that Chariklo and Chiron were fully synchronous binary systems that were disturbed from their relaxed state. This may have occurred via a close-encounter with Neptune [Wood et al., 2018], or via an impact. I hypothesize the system experienced a complete collapse of the mutual orbit. As the semi-major axis decreased, the satellite was either tidally disrupted to form a ring, or the two objects came into contact with the satellite spun up to the point that some mass was shed from its equator. The tidal collapse of the mutual orbit naturally produces the high spin rate of the objects observed today, and provides a ring formation hypothesis.

I hypothesize Chariklo and Chiron are both contact binaries consisting of two spheres in contact. I estimate Chariklo to have a total body radius of 1.6×10^7 cm and Chiron to have a total body radius of 1.35×10^7 cm [Groussin et al., 2004, Leiva et al., 2017]. In Figures 6.3 and 6.4 I plot J_t and J_{crit} as a function of q for Chariklo and Chiron, respectively. In both figures I have varied the density of the primary and the satellite.

Figures 6.3 and 6.4 show how the momenta of a binary system at the critical and a contact binary vary as a function of q . As momentum is conserved for an isolated system during the collapse process, there is only one mass ratio where the momentum of a fully synchronous binary system at the critical orbit is equal to the momentum

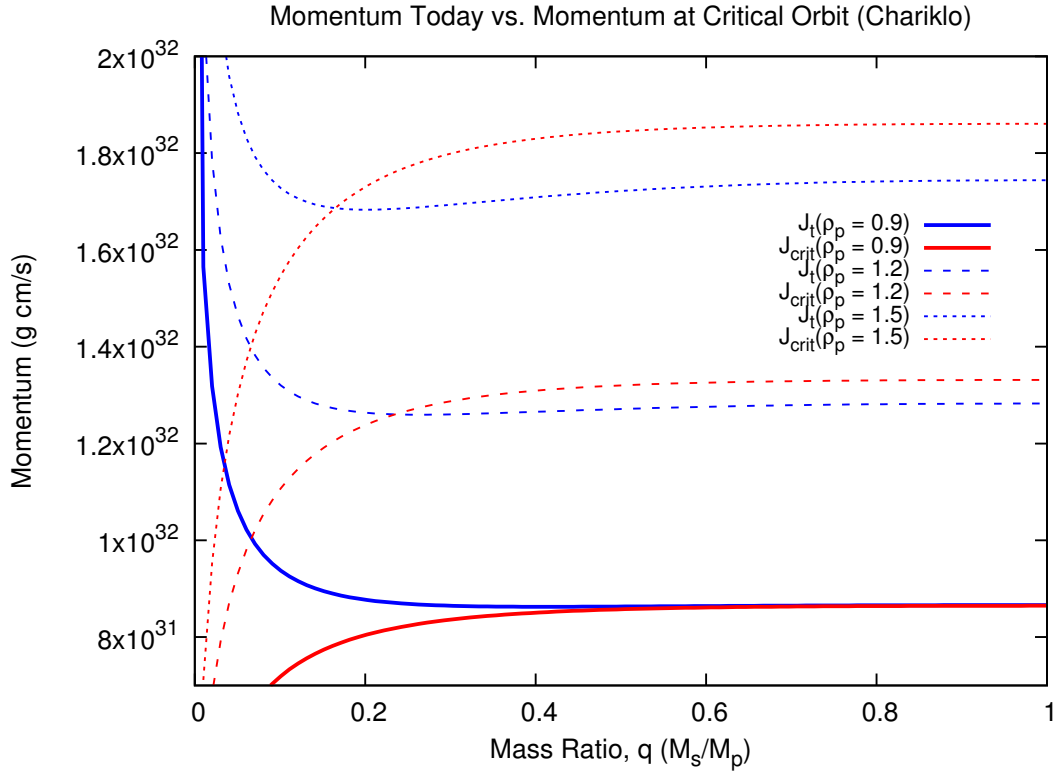


Figure 6.3. Here I display the total momentum of a Chariklo system as a function of the mass ratio q with $\rho_p = \rho_s$. Blue lines designate the momentum of the Chariklo system today (J_t) assuming it is two spheres in contact. Red lines designate the momentum of a fully synchronous system with semi-major axis a_{crit} (J_{crit}). The critical mass ratio q_c is the mass ratio at the intersection of the two curves. The line type corresponds to varying the density of the bodies from $0.9 - 1.5 \text{ g/cm}^3$. As the density of the bodies increases, the value of q_c decreases.

of the hypothesized contact binary observed today. As shown in Figures 6.3 and 6.4, q_{crit} is a function of the bodies' assumed bulk density. As the bulk density decreases, the critical mass ratio increases. It is important to note that if the bulk density of the bodies is too low, the curves do not intersect and there is no solution for q_{crit} , indicating that at least one of my assumptions is wrong.

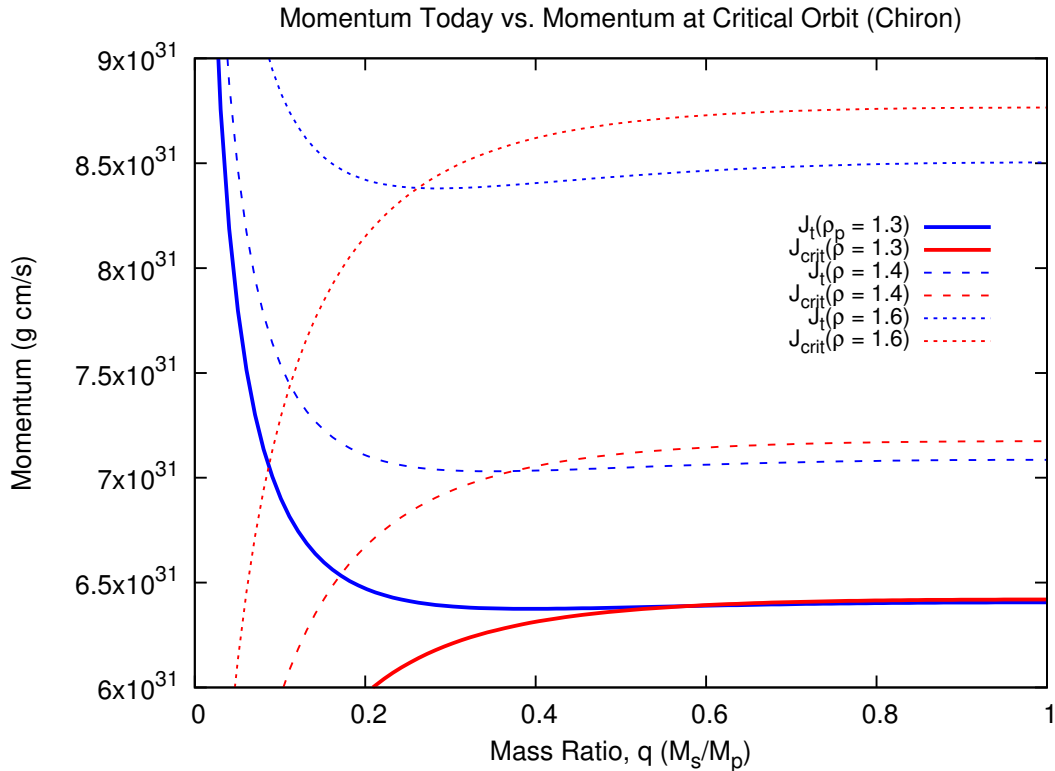


Figure 6.4. Here I display the total momentum of a binary system as a function of the mass ratio q . Blue lines designate the momentum of the Chiron system today (J_t) assuming it is two spheres in contact. Red lines designate the momentum of a fully synchronous system with semi-major axis a_{crit} (J_{crit}). The critical mass ratio q_c is the mass ratio at the intersection of the two curves. The line type corresponds to varying the density of the bodies from 1.3 – 1.6 g/cm^3 .

To investigate the Chariklo system, I examine Figures 6.1 and 6.3. I am interested in solutions where a binary system will collapse to form a contact binary with the radius and spin rate of the system observed today. Additionally, solutions where the collapse results in the shedding of material from the bodies will indicate possible ring formation. From Figure 6.1 I find that binary systems with $\mathcal{R} = 0.5$ and $q_{crit} \sim 0.25$ that experience an orbital collapse will begin shedding mass just as the two bodies come into contact. Figure 6.3 indicates that if $q_{crit} \sim 0.25$, then ρ_p is likely greater

than 1 g/cm^3 . The intersection of J_{crit} and J_t is dependent upon ρ_s . I find that a system with $\rho_p = 1.4 \text{ g/cm}^3$, $\mathcal{R} = 0.5$ will have $q_{crit} = 0.25$.

I use a numerical integration to calculate \dot{a} , $\dot{\omega}_p$, and $\dot{\omega}_s$ for a given system to determine its forward evolution. Provided $R, T_p, \rho_p, \mathcal{R}$ and q_{crit} for Chariklo I am able to model the evolution of a binary system that is fully synchronous with $a = a_{crit}$. I assume $\mu_p Q_p = \mu_s Q_s \sim 10^{11} \text{ Nm}^{-2}$ [Taylor and Margot, 2011]. If the system is disturbed \dot{a} , $\dot{\omega}_p$, and $\dot{\omega}_s$ are non-zero. Typically, a disturbance such that $\omega'_p = 0.95\omega_p$ is enough to cause the system to fully collapse. In Figure 6.5 I show the change in the semi-major axis of a binary system with $q_{crit} \sim 0.25$ that is fully synchronous with a semi-major axis a_{crit} and a period of ~ 10 hours. The system is disturbed in a manner such that the primary's rotation rate is reduced by 5%, causing the tidal collapse of the mutual orbit. In less than 10^3 years the semi-major axis has been completely reduced, forming a contact binary with a total radius and spin period equal to the Chariklo system observed today.

As shown in Figure 6.5, the semi-major axis of the satellite decreases until the satellite reaches the RRL. Upon reaching the RRL, the satellite will begin to shed mass, however I can also calculate the relative velocity (v_{rel} of the two surfaces at this point.

$$v_{rel} = \omega_p R_p - \left(\frac{a - R_p}{n} \right) - \omega_s R_s + \left(\frac{a - R_s}{n} \right). \quad (6.17)$$

In my Chariklo analog results, as the satellite reaches the RRL, $v_{rel} \approx 580 \text{ cm/s}$.

To investigate the Chiron system, I follow the same procedure I implemented for Chariklo. Figure 6.3 indicates that if $q_{crit} \lesssim 0.25$, then ρ_p for Chiron is likely greater than 1.5 g/cm^3 . I find that a system with $\rho_p = 2.0 \text{ g/cm}^3$, $\mathcal{R} = 0.5$ will have $q_{crit} \sim 0.25$. Provided $R, T_p, \rho_p, \mathcal{R}, \mu Q$, and q_{crit} for Chiron I model the evolution of a binary system that is fully synchronous with $a = a_{crit}$. In Figure 6.5 I show the change in the semi-major axis of a binary system with $q_{crit} \sim 0.25$ that is fully synchronous with a semi-major axis a_{crit} and a period of ~ 8.5 hours. The system is disturbed in a manner such that the primary's rotation rate is reduced by 5%, causing the tidal collapse of the mutual orbit. In less than 10^3 years the semi-major axis has

been completely reduced, forming a contact binary with a total radius and spin period equal to the Chiron system observed today. Similarly to my analysis for Chariklo, I may calculate the relative velocity between the two body surfaces when the satellite reaches the RRL. Following Equation 6.17, for Chiron I find $v_{rel} \approx 580$ cm/s.

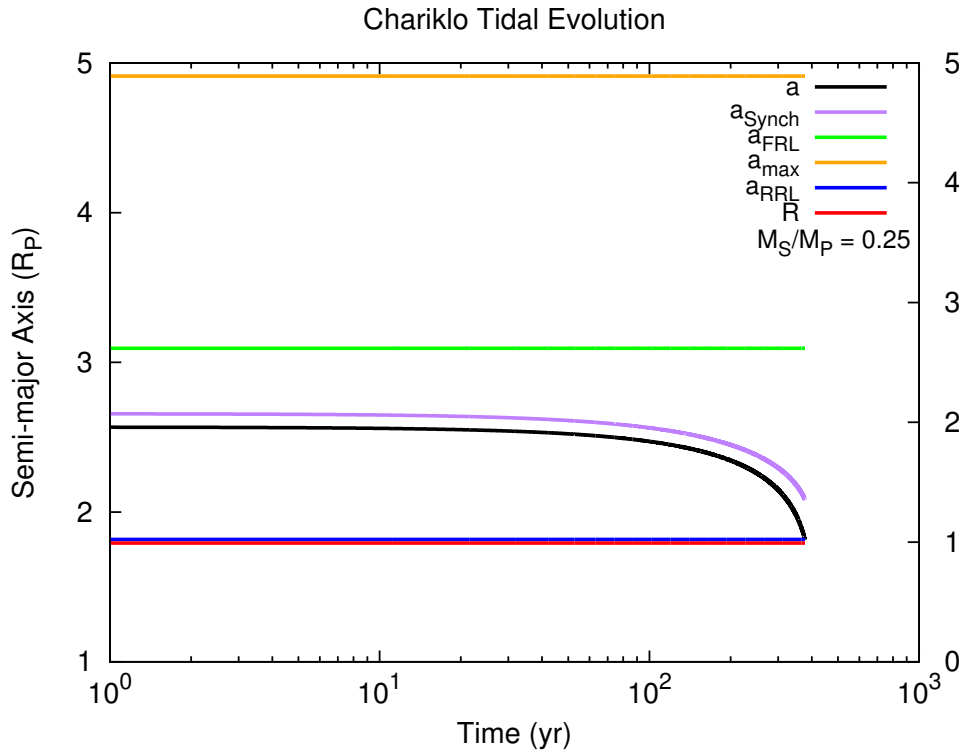


Figure 6.5. Here I display the collapse of the mutual orbit of a Chariklo analog binary system. The system has a critical mass ratio $q_c \sim 0.25$ and the initial semi-major axis is the critical orbit (a_{crit}) with a period of ~ 10 hours. $\rho_p = 1.4$ g/cm³ and $\rho_s = 0.5\rho_p$. In black I display the mutual orbit, in purple the location of the synchronous orbit, green the location of the FRL, blue the location of the RRL, orange the location of the maximum orbit allowed by the system's angular momentum, and in red the contact point. In $< 10^3$ years the mutual tidal interaction has caused the orbit to collapse until the bodies have come into contact. Assuming no slippage at contact, the final rotation period matches the currently observed 7 hours.

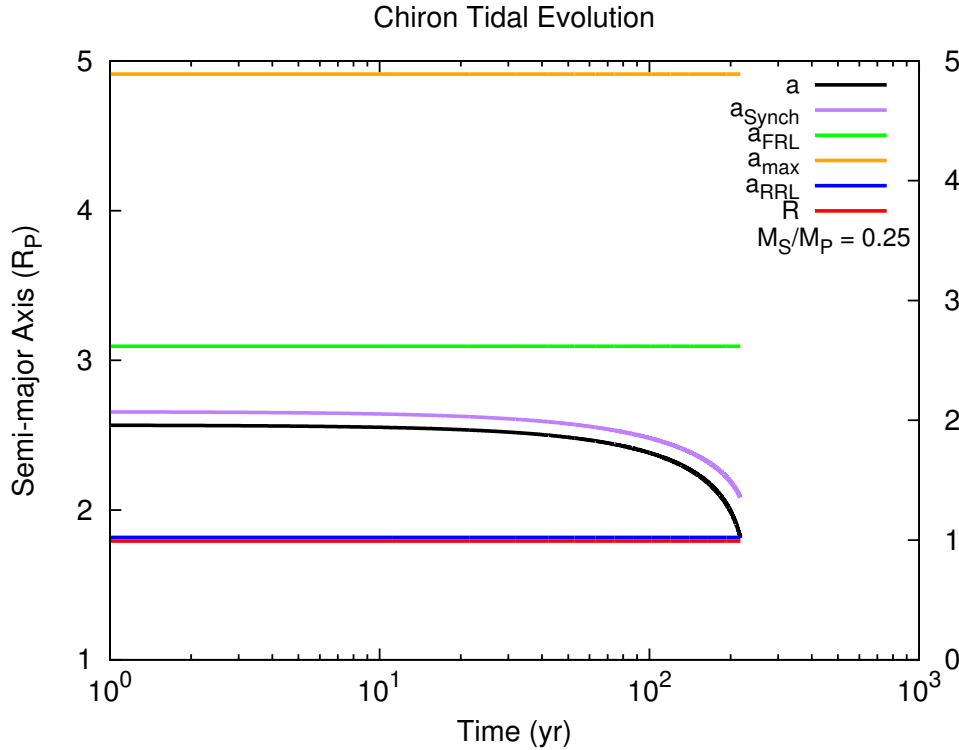


Figure 6.6. Here I display the collapse of the mutual orbit of a Chiron analog binary system. The system has a critical mass ratio $q_c \sim 0.25$ and the initial semi-major axis is the critical orbit (a_{crit}) with a period of ~ 8.5 hours. $\rho_p = 2 \text{ g/cm}^3$ and $\rho_s = 0.5\rho_p$. In black I display the mutual orbit, in purple the location of the synchronous orbit, green the location of the FRL, blue the location of the RRL, orange the location of the maximum orbit allowed by the system's angular momentum, and in red the contact point. In $< 10^3$ years the mutual tidal interaction has caused the orbit to collapse until the bodies have come into contact. Assuming no slippage at contact, the final rotation period matches the currently observed 5.9 hours.

6.4 Discussion

In this work I have analyzed how tidal interactions between bodies in a binary system may cause the mutual semi-major axis of the system to decrease. I have outlined the conditions for when this occurs, and have realized that some systems may undergo a complete decay of the mutual orbit. Fully synchronous systems with

a semi-major axis less than a “critical orbit” exist in an unstable configuration and may experience a “tidal collapse” if disturbed. As the semi-major axis of the system decreases, gravitational and rotational forces may remove material from the surface of the satellite. A cohesionless satellite in a collapsing binary system with a mass ratio $q \leq 0.1$ will begin to shed mass as it reaches the rigid Roche limit. The fact that a tidal collapse of a binary system may result in mass shedding serves as a possible formation hypothesis for ring systems in orbit around Trans-Neptunian Objects.

I have shown that as contact between the two bodies is made, mass shedding may occur for cohesionless satellites even when the mass ratio q is ≥ 0.1 . In deriving Equation 6.7 I assumed that the friction force between the two bodies coming into contact was sufficient to completely transfer momentum to the satellite such that no slippage occurs. This scenario demonstrates the most extreme possibility for the satellite to be spun up. At the point of contact, a small mass ratio system would have a large difference between the speeds of the two surfaces. But in this scenario, the inertia of the satellite is small and the necessary frictional force to spin up the satellite would be small. For a high mass ratio system, the satellite is larger and so is its inertia. However in this scenario, the difference in speed between the two surfaces just before contact is much smaller, causing only a small change to the spin of both bodies. Thus, while the derivation in Equation 6.7 is the most extreme scenario, I expect the change in rotation of the satellite during contact to be sufficient for systems with $q > q_{shed}$ to shed material.

I have compared the conditions for a binary tidal collapse to the known population of binary TNOs. This comparison has revealed that three known systems, or $\sim 3.5\%$ of the known BTNO population, have mass ratios and semi-major axes in which a fully synchronous system would likely experience a tidal collapse. Additionally, I find that $\sim 17\%$ of the known BTNO population have mass ratios such that if some mechanism drove the system to a collapsing orbit, the satellite would shed mass during the collapse.

A binary tidal collapse can result in a contact binary, which are expected to comprise 10–30% of the TNO population. I demonstrate how the angular momentum and known size of a hypothesized contact binary system can be used to resolve details of the system before a tidal collapse would have occurred. I apply this analysis to the centaurs Chariklo and Chiron. I assume both bodies are actually contact binaries, each composed of two spheres in contact. I use my analysis to show how a tidal collapse could and mass shedding could produce the systems we observe today. Additional work is needed to determine the likelihood that contact binaries are formed via a tidal collapse, or some other mechanism.

Due to observational constraints, it is challenging to resolve whether a TNO is a contact binary. For this reason, it is difficult to determine whether Chariklo and Chiron specifically are contact binaries that experience a tidal collapse. I have attempted to generalize my analysis of collapsing systems to include any hypothesized contact binary system. If a contact BTNO is resolved as a bilobate body, I may hypothesize an orbit that could produce the observed system.

Finally, I have drawn comparisons against my analysis with the population of BTNOs included in Figure 6.2. The typical member of this population has $q > 0.1$ and $10^1 < a/R_p < 10^3$, which is unlikely to result in a tidal collapse. It is important to note that multiple mechanisms exist to perturb a BTNO into a semi-major axis with a collapsing orbit, such as a close planetary encounter, or tidal-kozai cycles [Brunini, 2014, Porter and Grundy, 2012]. Perhaps of most importance, is that this is the known population of BTNOs. Observational constraints bias the known population to be systems with high mass ratios and wide separations. Therefore, while the known population may not indicate many binary systems today will undergo a tidal collapse, it is likely many systems have yet-to-be discovered and may have characteristics which favor a tidal collapse.

7. CONCLUSION

My dissertation work has examined the tightly coupled dynamics between primary bodies, rings, and satellites. In order to study these systems I found it necessary to develop my own numerical model. Included here is a short summary of my work, my conclusions, and any areas I find to be deserving of future study.

7.1 Boomerangs

Planetary rings are governed by a complex set of dynamics which may give rise to intricate structures. The state of a ring at any moment in time is a sum of perturbations from many sources. In my work, I have identified which factors dominate the long-term evolution of a planetary ring. These may be summed up as follows:

1. A ring in orbit around a primary will spread out through inter-particle collisions, which can be approximated as a “viscosity.”
2. The gravitational acceleration of the primary prevents ring particles interior to the fluid Roche limit from accreting into discrete satellites.
3. Ring particles may enter into resonance with an exterior orbiting satellite and exchange momentum via Lindblad torques.

Discrete satellites are also subject to many perturbing forces in their lifetimes. Satellite orbits may be unstable, or even chaotic. In my work, I have worked to identify the dominant factors in the formation and migration history of satellites in orbit near planetary rings. I summarize these factors to be:

1. Satellites orbiting near the edge of a planetary ring accrete mass from the ring.
2. The tidal interaction between the satellite and the primary.

3. The exchange of angular momentum between the satellite and ring material located at Lindblad resonances.
4. The rapid disruption of a satellite as it approaches the rigid Roche limit.

There are caveats to the dynamics of planetary rings and nearby satellites, which I have worked to elucidate throughout this work. I have found that the rotation rate of the primary body and the bulk density of orbiting ring material permit three satellite-ring evolution regimes. Slowly rotating primaries and high density ring particles fall within the “Boomerang” regime. In this regime, any satellites that accrete from ring material may initially migrate away from the ring, however eventually they will migrate inwards towards the primary as the surface mass density of the ring decreases over time. Fast rotating primaries with low density ring particles fall within the “Slingshot” regime. In this regime, Lindblad and tidal torques both work to migrate satellites accreting out of ring material away from the primary and the ring, in perpetuity. And finally, ring systems in the “Torque-Dependent” regime fall somewhere in the middle. Ring satellites in Torque-Dependent systems may initially exhibit Slingshot-like migration, but eventually all systems will transition to exhibit Boomerang-like migration as the ring mass decreases.

I derived Equation 2.13 to elucidate possible evolution histories for real and theoretical planetary ring systems. The three regimes defined by Equation 2.13 are plotted in Figure 2.2, which may be used to hypothesize about possible satellite-ring systems that may have existed in the solar system throughout its history. Planetary systems that exist in the Boomerang regime serve as strong candidates for possible ring systems. The dynamics of Boomerang systems allows orbiting material to cycle between ring material and discrete satellites for long time periods. Observations of boomerang systems serve as good candidates for the discovery of rings and interior satellites.

Examining Figure 2.2, we see that 50000 Quaoar, a TNO and possible dwarf planet, lies deep within the Boomerang regime. Quaoar, which is orbited by a

small satellite named “Weywot,” has a mass of 1.4×10^{21} g and a rotation period of ~ 17.7 hrs. With a bulk density of $2.7\text{--}5.0$ g/cm³ Quaoar is one of the densest known KBOs [Fraser et al., 2013]. Weywot has a semi-major axis $> 1.3 \times 10^4$ km $\geq 28R_p$ and orbits well beyond a_{synch} , but the slow rotation period of Quaoar indicates that a satellite-ring cycle may exist inside a_{synch} . Future observations of 50000 Quaoar may reveal a satellite-ring system.

In Figure 2.2 we see that the dwarf planet Eris lies on the boundary of the Boomerang and Torque-Dependent regimes. Ring-satellite systems in the Torque-Dependent regime may perturb a satellite to an orbit beyond a_{synch} , however eventually all of these systems transition to exhibit a Boomerang-like evolution. Eris is orbited by a small, distant satellite, named “Dysnomia.” Perhaps Eris was once orbited by a planetary ring with a sufficient surface mass density to perturb Dysnomia beyond a_{synch} . As the ring was depleted of mass, interior satellites would have followed a Boomerang-like evolution. Future observations may reveal that Eris is orbited by a ring-satellite system as well.

7.2 RING-MOONS

There are a number of simulation packages that model many of the dynamics of tightly coupled satellite-ring systems (e.g. HYDRORINGS), however none of these models are publicly available [Charnoz et al., 2010, 2011, Crida and Charnoz, 2012, Rosenblatt et al., 2016, Salmon and Canup, 2017]. While researching these models I found each of them either did not necessarily include all of the physics that I expected to be important, or made approximations that were not entirely robust. In Chapter 3 I outlined my own model in which I attempt to simulate the dynamical evolution of coupled ring-satellite systems. RING-MOONS is a numerical tool that models a planetary ring as a 1D series of Eulerian bins, with each bin representing a 2D annulus of the ring. Satellites form at the ring edge and are treated as Lagrangian particles.

RING-MOONS is robust compared to similar models in the literature, yet in light of the assertion that “all models are wrong, but some are useful,” RING-MOONS could perpetually be improved. In regards to the dynamics and evolution of a planetary ring, RING-MOONS is accurate and well founded. The viscosity model implemented into RING-MOONS is thorough, and includes several numerical techniques to avoid numerical instabilities. The model explicitly calculates the exchange of angular momentum with exterior satellites. RING-MOONS also tracks the transfer of mass through the interior boundary at the primary’s surface, something that had not been calculated in other models. Lastly, RING-MOONS can reveal gaps and buildups of ring material at Lindblad resonances, a feature often observed in real systems.

Yet, where RING-MOONS succeeds in modeling ring dynamics, it is lacking in its treatment of satellite dynamics. Satellites in RING-MOONS experience no direct gravitational perturbations against each other. The only influence one satellite exerts on another is when one satellite enters the Hill Sphere of another. At that point, the two satellites are merged together. Real satellites strongly influence the dynamics of others. Real satellite-satellite interactions can result in collisions, disruptions, ejections, migration, and resonance interactions. None of these dynamics are currently present in RING-MOONS. A vast improvement to the model would be to implement an N-body treatment for satellite-satellite interactions.

Rebound is an N-body integrator that has been well tested and contains a python wrapper. I have written RING-MOONS in Python and have examined the ability to implement the N-body dynamics of Rebound into RING-MOONS. While the implementation is straightforward, it is also thorough and would require extensive testing to ensure the ring-satellite dynamics are appropriately handled.

7.3 Mars

Phobos and Deimos were two objects long ignored. Their orbits and physical characteristics make them difficult objects to observe and complicates theories to their

origins. For decades the two satellites were thought to be captured asteroids, despite their orbits serving as evidence to the contrary [Szeto, 1983, Yoder, 1979]. Marinova et al. [2008] provided the first strong evidence that a giant impact may have placed a massive amount of debris into orbit around Mars. With evidence that a debris ring may have orbited Mars, Phobos and Deimos were studied in greater detail as scientists worked to test whether the satellites may have formed from a massive Martian debris disk [Citron et al., 2015, Craddock, 2011, Rosenblatt and Charnoz, 2012]. Rosenblatt et al. [2016] was the first work to successfully model the formation of both satellites, however issues remained in the tidal evolution of Phobos.

The formation hypothesis put forth in Rosenblatt et al. [2016] leaves little room for error. Planetary tides are causing Phobos to migrate inwards at a rapid rate. In < 70 My the satellite will no longer exist [Black and Mittal, 2015]. Not only are we extremely fortunate to observe the satellite today, but Phobos's current orbit presents only a small window for any formation hypothesis to place the satellite into its current orbit. This window is pervasive and must be addressed in any formation hypothesis. In Rosenblatt et al. [2016], and many other similar works, if any parameters are off by only a small fraction, the opportunity for Earthlings to observe Phobos would be missed.

In Chapter 4 I put forth the hypothesis that a giant impact ejected massive amounts of material into orbit around Mars. This material coalesced to form a massive ring interior to the FRL, and the smaller satellite Deimos near the synchronous orbit. Hesselbrock and Minton [2017] demonstrated that the massive ring would form massive satellites, however this system would have existed in the Boomerang regime. Any satellites that accreted from the roche-interior ring eventually were disrupted into ring material. I showed how this process would eventually produce Phobos in the orbit we observe today.

Hesselbrock and Minton [2017] presented a formation hypothesis for Phobos and Deimos that may explain the current system, but more importantly, the discovery of the Boomerang regime presented a new set of dynamics, making the hypothesis

that much more resilient. In Chapter 4 I showed how a very specific set of parameters would produce the Phobos and Deimos system observed today, but more importantly, I demonstrated how the dynamics of the Boomerang regime ensures that even if those parameters are not exact, a wide range of parameters could yield similar results to place Phobos in its current orbit.

Work continues on Phobos and Deimos, but a very exciting and unexpected result from Hesselbrock and Minton [2017] was the possibility of ring material being deposited onto the Martian surface. The amount of material placed into orbit following the impact described by Marinova et al. [2008] is significant. The subsequent ring-satellite cycle delays this material from falling back onto the Martian surface. Whenever a massive satellite reaches the RRL and is tidally disrupted, the majority of its mass rapidly enters the Martian atmosphere [Hesselbrock and Minton, 2017]. Further work should investigate what happens as this occurs. Do the ring particles impact the surface? Should we expect to see a disproportionate amount of craters near the Martian equator? Or rather, does the ring material disrupt in the atmosphere to slowly drift and deposit onto the Martian equator? The mass of these deposits would be significant. What should we expect to see in the Martian geologic record? Or lastly, are the ring particles disrupted into microscopic particles, becoming suspended in the atmosphere for long-periods of time? How would this affect the Martian climate?

These questions provide exciting possibilities for future studies. I would argue that the first step in answering these questions is to examine how the ring particles interact with the atmosphere. The ring particles modeled in RING-MOONS are uniform in size, whereas in reality there would be a size-distribution to these particles. Examining how a satellite is tidally disrupted upon reaching the RRL could yield information about the population of particles following this disruption, and therefore the characteristics of particles entering the martian atmosphere. From there one could examine how such particles would interact with the atmosphere as they fall towards the surface.

7.4 Miranda

In Chapter 4, I used RING-MOONS to study a satellite-ring system in the Boomerang regime. That work motivated me to then study a system in the Torque-Dependent regime. In Chapter 5, I discussed how examination of Figure 2.2 revealed that Uranus exists in the Torque-Dependent regime. In addition to numerous inner and “irregular” satellites, Uranus is orbited by five massive “regular” satellites. These regular satellites, Miranda, Ariel, Umbriel, Titania, and Oberon, were thought to have formed shortly after Uranus itself. Of these five satellites, Miranda is less massive by more than two orders of magnitude, and is the most interior. Realizing that Miranda’s semi-major axis was not too distant from the synchronous orbit of Uranus, I decided to investigate whether Miranda may have formed from a massive ring interior to the FRL and subsequently migrated to its current orbit.

Using RING-MOONS, I found that a ring mass of $\sim 3 \times 10^{23}$ g had a surface mass density sufficient to perturb satellites beyond a_{synch} , and would produce a Miranda-like satellite in a few hundred million years. This ring existed in the Torque-Dependent regime and as it was depleted of mass over time, tidal torques eventually dominated any Lindblad torques. Any satellites interior to a_{synch} during this transition began to migrate inwards. These satellites merged into a massive satellite that disrupted upon reaching the RRL. A new cycle began and produced a collection of 14 satellites.

The results in Figure 5.2f do not perfectly match the system observed today. I expect that the inclusion of an N-body integration for satellite dynamics would provide a much better match to the current Uranian system. Furthermore, the Uranian system is subject to impacts with heliocentric objects and it is thought that these impactors have heavily disrupted the current system [Colwell and Esposito, 1992]. In addition to including an N-body integration, a future numerical study should estimate the rate at which small satellites are disrupted by heliocentric impacts. These two factors, along with the parameters given in Chapter 5, may provide a strong match to the Uranian system observed today.

7.5 Small Bodies

The Boomerang, Torque-Dependent, and Slingshot regimes are each determined in part by the location of the synchronous orbit, which is dependent upon the rotational period of the primary. The rotation period of a primary body is not a fixed value. The problems I have been interested in have all dealt with tides, which cause an exchange between spin and orbital momenta for both the primary and the satellite. Examining Figure 2.2, I was motivated to investigate how a change in T_p would affect the evolution regime of a satellite-ring system as defined by Equation 2.13.

The satellites produced in the Mars and Uranus systems of which I had investigated were several orders of magnitude less massive than their primaries. The change to the rotation period, and thus the synchronous orbit, for Mars and Uranus was negligible. However, the tidal interaction between a satellite that was nearly as massive as its primary would have a significant change to the rotation period of both bodies. I found that this change could be enough for a system to transition from one evolution regime into another, and quickly began to investigate binary systems.

Binary systems are common throughout the solar system, and in fact the entirety of the TNO population may have formed as binary systems [Nesvorný et al., 2010]. The discovery of planetary rings in orbit around the TNOs Chariklo, Chiron, and Haumea motivated me to investigate not only how tidal interactions may affect the satellite-ring regime of a binary system, but whether tidal interactions could produce the systems observed today. I discovered a set of conditions that would determine whether a fully synchronous system may undergo a complete tidal collapse of the mutual orbit. Furthermore, I was able to determine whether the satellite would shed mass at any point during the collapse.

For systems where the satellite is not completely disrupted, a contact binary would result. It is estimated that as much as 30% of the current TNO population are contact binaries. In Chapter 6, I hypothesized that Chariklo and Chiron were both contact binary systems, which we are currently unable to resolve due to observational

constraints. Using the rotation rate of each body, as well as their physical size, I estimated the angular momentum of each system today to hypothesize the binary system that may have existed. In Figures 6.5 and 6.6 I show how these binary systems, if disturbed, would have experienced a complete tidal collapse and mass shedding to produce the systems we observe today.

While Chariklo and Chiron may not be contact binaries, the analysis I put forth in Chapter 6 is generalized such that it may be applied to any contact BTNO. The population of contact binaries is expected to be high, and some may have been observed [Lacerda, 2011, Sheppard and Jewitt, 2004]. Due to the dynamics of tidal collapse and possible mass shedding, I find that contact BTNOs are good candidates for future searches of planetary rings.

7.6 Denouement

This work was a story of origins and outcomes. The outcome of tidal stresses disrupting a satellite may be the origin of a planetary ring. The origin of a satellite may be the outcome of a viscously spreading ring. The outcome of a tidal collapse may be the origin of a contact binary. Through efforts both great and small, I have worked to explain the origins and outcomes of satellite-ring systems orbiting bodies both great and small.

I have constructed RING-MOONS, a numerical model to simulate the dynamics of tightly coupled satellite-ring systems. I have used this model to argue that Phobos is a natural result of an ongoing satellite-ring cycle. I have shown that Miranda may be the only long-term surviving satellite that formed from an ancient Uranian ring system. And finally, I have shown that the tidal interactions in a binary TNO system could result in the formation of a contact binary orbited by a planetary ring, which may explain the Chariklo and Chiron systems.

While developing RING-MOONS I have understood much of the physics that dominates these systems, and have worked to incorporate as many physical processes

into the model as is practical. Motivated by the utility of RING-MOONS to produce significant results for systems of interest across the solar system, I have placed the model into the public domain. Therefore, any future studies utilizing the RING-MOONS model are left as an exercise to the reader.

REFERENCES

REFERENCES

- J. D. J. Anderson. *Computational Fluid Dynamics*. McGraw-Hill, Inc., New York, 1995.
- J. C. Andrews-Hanna, M. T. Zuber, and W. B. Banerdt. The Borealis basin and the origin of the martian crustal dichotomy. *Nature*, 453(7):1212–1215, June 2008.
- G. T. Bath and J. E. Pringle. The evolution of viscous discs. I - Mass transfer variations. *Monthly Notices of the Royal Astronomical Society*, 194:967–986, Mar. 1981a.
- G. T. Bath and J. E. Pringle. The evolution of viscous discs. I - Mass transfer variations. *Annual Review of Astronomy and Astrophysics*, 194:967–986, Mar. 1981b.
- B. A. Black and T. Mittal. The Demise Of Phobos And Development Of A Martian Ring System. *NatGe*, 8(December):913–917, 2015. ISSN 1752-0894. doi: 10.1038/NNGEO2583. URL <http://www.nature.com/ngeo/journal/v8/n12/full/ngeo2583.html>.
- F. Braga-Ribas, B. Sicardy, J. L. Ortiz, C. Snodgrass, F. Roques, R. Vieira-Martins, J. I. B. Camargo, M. Assafin, R. Duffard, E. Jehin, J. Pollock, R. Leiva, M. Emilio, D. I. Machado, C. Colazo, E. Lellouch, J. Skottfelt, M. Gillon, N. Ligier, L. Maquet, G. Benedetti-Rossi, A. R. Gomes, P. Kervella, H. Monteiro, R. Sfair, M. El Moutamid, G. Tancredi, J. Spagnotto, A. Maury, N. Morales, R. Gil-Hutton, S. Roland, A. Ceretta, S.-H. Gu, X.-B. Wang, K. Harpsøe, M. Rabus, J. Manfroid, C. Opitom, L. Vanzi, L. Mehret, L. Lorenzini, E. M. Schneiter, R. Melia, J. Lecacheux, F. Colas, F. Vachier, T. Widemann, L. Almenares, R. G. Sandness, F. Char, V. Perez, P. Lemos, N. Martinez, U. G. Jørgensen, M. Dominik, F. Roig, D. E. Reichart, A. P. Lacluyze, J. B. Haislip, K. M. Ivarsen, J. P. Moore, N. R. Frank, and D. G. Lambas. A ring system detected around the Centaur (10199) Chariklo. *Nature*, 508:72–75, Apr. 2014. doi: 10.1038/nature13155.
- A. Brunini. On the dynamical evolution and end states of binary centaurs. *MNRAS*, 437(3):2297–2302, 2014. ISSN 00358711. doi: 10.1093/mnras/stt2045.
- J. A. Burns. *Contradictory clues as to the origin of the Martian moons*, pages 1283–1301. 1992.
- A. G. W. Cameron and W. R. Ward. The Origin of the Moon. *Abstracts of the Lunar and Planetary Science Conference*, 7:120, Mar. 1976.
- R. Canup and J. Salmon. Origin of phobos and deimos by the impact of a vesta-to-eres sized body with mars. *Science Advances*, 4(4), 2018. doi: 10.1126/sciadv.aar6887. URL <http://advances.sciencemag.org/content/4/4/eaar6887>.
- R. M. Canup. Origin of Saturn’s rings and inner moons by mass removal from a lost Titan-sized satellite. *Nature*, 468:943–946, Dec. 2010. doi: 10.1038/nature09661.

- R. M. Canup and L. W. Esposito. Accretion in the Roche zone: Coexistence of rings and ring moons. *Icarus*, 113:331–352, Feb. 1995. doi: 10.1006/icar.1995.1026.
- R. M. Canup and J. Salmon. On an Origin of Phobos-Deimos by Giant Impact. In *47th Lunar and Planetary Science Conference*, page 2598, Texas, 2016.
- B. W. Carroll and D. A. Ostlie. *An Introduction to Modern Astrophysics*. Pearson Addison-Wesley, Illinois, 2007.
- R. O. Chancia, M. M. Hedman, and R. G. French. Weighing Uranus Moon Cressida with the η Ring. , 154:153, Oct. 2017. doi: 10.3847/1538-3881/aa880e.
- S. Chandrasekhar. *Ellipsoidal Figures of Equilibrium*. Yale University Press, 1969.
- S. Charnoz, J. Salmon, and A. Crida. The recent formation of Saturn’s moonlets from viscous spreading of the main rings. *Nature*, 465(7299):752–754, 2010. ISSN 0028-0836. doi: 10.1038/nature09096.
- S. Charnoz, A. Crida, J. C. Castillo-Rogez, V. Lainey, L. Dones, Ö. Karatekin, G. Tobie, S. Mathis, C. Le Poncin-Lafitte, and J. Salmon. Accretion of Saturn’s mid-sized moons during the viscous spreading of young massive rings: Solving the paradox of silicate-poor rings versus silicate-rich moons. *Icarus*, 216(2):535–550, 2011. ISSN 00191035. doi: 10.1016/j.icarus.2011.09.017.
- S. Charnoz, R. M. Canup, A. Crida, and L. Dones. Rings in the solar system: a short review. In M. S. Tiscareno and C. D. Murray, editors, *Planetary Ring Systems*, chapter 18. Cambridge Planetary Science, Cambridge, 2018.
- R. I. Citron, H. Genda, and S. Ida. Formation of Phobos and Deimos via a giant impact. *Icarus*, 252 IS -:334–338, Feb. 2015.
- J. E. Colwell and L. W. Esposito. Origins of the rings of Uranus and Neptune. I - Statistics of satellite disruptions. *Journal of Geophysical Research*, 97:10, June 1992. doi: 10.1029/92JE00788.
- J. E. Colwell and L. W. Esposito. Origins of the rings of Uranus and Neptune. II - Initial conditions and ring moon populations. *Journal of Geophysical Research*, 98: 7387–7401, Apr. 1993. doi: 10.1029/93JE00329.
- R. A. Craddock. *Icarus*, 211:1150–1161, 2011.
- a. Crida and S. Charnoz. Formation of regular satellites from ancient massive rings in the solar system. *Science (New York, N.Y.)*, 338(6111):1196–9, Nov. 2012. ISSN 1095-9203. doi: 10.1126/science.1226477. URL <http://www.ncbi.nlm.nih.gov/pubmed/23197530>.
- M. J. Duncan, H. F. Levison, and M. H. Lee. A Multiple Time Step Symplectic Algorithm for Integrating Close Encounters. *The Astronomical Journal*, 116:2067–2077, Oct. 1998.
- J. L. Elliot, E. Dunham, and D. Mink. The rings of Uranus. *Nature*, 267:328–330, May 1977. doi: 10.1038/267328a0.
- L. W. Esposito. *Planetary Rings*. July 2006.

W. C. Fraser, K. Batygin, M. E. Brown, and A. Bouchez. The mass, orbit, and tidal evolution of the Quaoar-Weywot system. , 222:357–363, Jan. 2013. doi: 10.1016/j.icarus.2012.11.004.

R. G. French, R. I. Dawson, and M. R. Showalter. Resonances, Chaos, and Short-term Interactions Among the Inner Uranian Satellites. *The Astronomical Journal*, 149:142, Apr. 2015. doi: 10.1088/0004-6256/149/4/142.

R. S. French and M. R. Showalter. Cupid is doomed: An analysis of the stability of the inner uranian satellites. *Icarus*, 220:911–921, Aug. 2012. doi: 10.1016/j.icarus.2012.06.031.

P. Goldreich and S. Tremaine. The excitation of density waves at the Lindblad and corotation resonances by an external potential. *The Astrophysical Journal*, 233:857, Oct. 1979.

P. Goldreich and S. Tremaine. The Dynamics of Planetary Rings. *Annu. Rev. Astro. Astrophys.*, 20(1):249–283, Sept. 1982.

P. Goldreich and S. D. Tremaine. The velocity dispersion in Saturn’s rings. *Icarus*, 34:227–239, May 1978. doi: 10.1016/0019-1035(78)90164-1.

O. Groussin, P. Lamy, and L. Jorda. Properties of the nuclei of Centaurs Chiron and Chariklo. *Astronomy & Astrophysics*, 413:1163–1175, Jan. 2004. doi: 10.1051/0004-6361:20031564.

D. P. Hamilton and J. A. Burns. Origin of Saturn’s E Ring: Self-Sustained, Naturally. *Science*, 264:550–553, Apr. 1994. doi: 10.1126/science.264.5158.550.

A. J. Hesselbrock and D. A. Minton. An ongoing satellite-ring cycle of Mars and the origins of Phobos and Deimos. *Nature Geoscience*, 10:266–269, Mar. 2017. doi: 10.1038/ngeo2916.

W. B. Hubbard, A. Brahic, B. Sicardy, L.-R. Elicer, F. Roques, and F. Vilas. Occultation detection of a Neptunian ring-like arc. *Nature*, 319:636–640, Feb. 1986. doi: 10.1038/319636a0.

T. Hurford, E. Asphaug, J. Spitale, D. Hemingway, A. Rhoden, W. Henning, B. Bills, S. Kattenhorn, and M. Walker. Surface Evolution from Orbital Decay on Phobos. *American Astronomical Society*, 47, Nov. 2015.

C. Huygens. *Cristiani hugenii zulichemii, const. f. systema saturnium. Ex typographia Adriani Vlacq*, 1659.

R. Hyodo, H. Genda, S. Charnoz, and P. Rosenblatt. On the Impact Origin of Phobos and Deimos. I. Thermodynamic and Physical Aspects. *The Astrophysical Journal*, 845:125, Aug. 2017. doi: 10.3847/1538-4357/aa81c4.

R. A. Jacobson, J. K. Campbell, A. H. Taylor, and S. P. Synnott. The masses of Uranus and its major satellites from Voyager tracking data and earth-based Uranian satellite data. *The Astronomical Journal*, 103:2068–2078, June 1992. doi: 10.1086/116211.

W. Johnston. Binary minor planets compilation v2.0, 2018. URL `urn:nasa:pds:astbinaryparameterscompilation`.

E. S. Kite, I. Halevy, M. A. Kahre, M. J. Wolff, and M. Manga. Seasonal melting and the formation of sedimentary rocks on Mars, with predictions for the Gale Crater mound. *Icarus*, 223:181–210, Mar. 2013. doi: 10.1016/j.icarus.2012.11.034.

E. Kokubo, S. Ida, and J. Makino. *Icarus*, 148:419–436, 2000.

P. Lacerda. A Change in the Light Curve of Kuiper Belt Contact Binary (139775) 2001 QG₂₉₈. *AJ*, 142:90, Sept. 2011. doi: 10.1088/0004-6256/142/3/90.

V. Lainey. Quantification of tidal parameters from Solar System data. *Celestial Mechanics and Dynamical Astronomy*, 126:145–156, Nov. 2016. doi: 10.1007/s10569-016-9695-y.

Z. M. Leinhardt and S. T. Stewart. Collisions between Gravity-dominated Bodies. I. Outcome Regimes and Scaling Laws. *The Astrophysical Journal*, 745(1):79, 2012.

Z. M. Leinhardt, G. I. Ogilvie, H. N. Latter, and E. Kokubo. Tidal disruption of satellites and formation of narrow rings. *Monthly Notices of the Royal Astronomical Society*, 424:1419–1431, Aug. 2012. doi: 10.1111/j.1365-2966.2012.21328.x.

R. Leiva, B. Sicardy, J. I. B. Camargo, J.-L. Ortiz, J. Desmars, D. Bérard, E. Lelouch, E. Meza, P. Kervella, C. Snodgrass, R. Duffard, N. Morales, A. R. Gomes-Júnior, G. Benedetti-Rossi, R. Vieira-Martins, F. Braga-Ribas, M. Assafin, B. E. Morgado, F. Colas, C. De Witt, A. A. Sickafoose, H. Breytenbach, J.-L. Dauvergne, P. Schoenau, L. Maquet, K.-L. Bath, H.-J. Bode, A. Cool, B. Lade, S. Kerr, and D. Herald. Size and Shape of Chariklo from Multi-epoch Stellar Occultations. *The Astronomical Journal*, 154:159, Oct. 2017. doi: 10.3847/1538-3881/aa8956.

G. Leone, P. J. Tackley, T. V. Gerya, D. A. May, and G. Zhu. Three-dimensional simulations of the southern polar giant impact hypothesis for the origin of the Martian dichotomy. *Geophysical Research Letters*, 41(2):8736–8743, Dec. 2014.

D. Lynden-Bell and J. E. Pringle. The Evolution of Viscous Discs and the Origin of the Nebular Variables. *Monthly Notices of the Royal Astronomical Society*, 168:603–637, 1974.

M. M. Marinova, O. Aharonson, and E. Asphaug. Mega-impact formation of the Mars hemispheric dichotomy. *Nature*, 453(7199):1216–1219, June 2008.

M. M. Marinova, O. Aharonson, and E. Asphaug. Geophysical consequences of planetary-scale impacts into a Mars-like planet. *Icarus*, 211(2):960–985, Feb. 2011.

E. D. Miner, R. R. Wessen, and J. N. Cuzzi. *Planetary Ring Systems*. Praxis, New York, 2007.

M. Moons and J. Henrard. Surfaces of section in the Miranda-Umbriel 3:1 inclination problem. *Celestial Mechanics and Dynamical Astronomy*, 59:129–148, June 1994. doi: 10.1007/BF00692129.

A. Morbidelli, K. Tsiganis, K. Batygin, A. Crida, and R. Gomes. Explaining why the uranian satellites have equatorial prograde orbits despite the large planetary obliquity. *Icarus*, 219:737–740, June 2012. doi: 10.1016/j.icarus.2012.03.025.

C. D. Murray and S. F. Dermott. *Solar system dynamics*, volume New York, New York. book, 1999.

D. Nesvorný, A. N. Youdin, and D. C. Richardson. Formation of Kuiper Belt Binaries by Gravitational Collapse. *AJ*, 140:785–793, Sept. 2010. doi: 10.1088/0004-6256/140/3/785.

F. Nimmo, S. D. Hart, D. G. Korycansky, and C. B. Agnor. Implications of an impact origin for the martian hemispheric dichotomy. *Nature*, 453(7):1220–1223, June 2008.

J. L. Ortiz, R. Duffard, N. Pinilla-Alonso, A. Alvarez-Candal, P. Santos-Sanz, N. Morales, E. Fernández-Valenzuela, J. Licandro, A. Campo Bagatin, and A. Thirouin. Possible ring material around centaur (2060) Chiron. *Astronomy and Astrophysics*, 576:A18, Apr. 2015. doi: 10.1051/0004-6361/201424461.

J. L. Ortiz, P. Santos-Sanz, B. Sicardy, G. Benedetti-Rossi, D. Bérard, N. Morales, R. Duffard, F. Braga-Ribas, U. Hopp, C. Ries, V. Nascimbeni, F. Marzari, V. Granata, A. Pál, C. Kiss, T. Pribulla, R. Komžík, K. Hornoch, P. Pravec, P. Bacci, M. Maestripieri, L. Nerli, L. Mazzei, M. Bachini, F. Martinelli, G. Succi, F. Ciabattari, H. Mikuz, A. Carbognani, B. Gäehrken, S. Mottola, S. Hellmich, F. L. Rommel, E. Fernández-Valenzuela, A. C. Bagatin, S. Cikota, A. Cikota, J. Lecacheux, R. Vieira-Martins, J. I. B. Camargo, M. Assafin, F. Colas, R. Behrend, J. Desmars, E. Meza, A. Alvarez-Candal, W. Beisker, A. R. Gomes-Junior, B. E. Morgado, F. Roques, F. Vachier, J. Berthier, T. G. Mueller, J. M. Madiedo, O. Unsalan, E. Sonbas, N. Karaman, O. Erece, D. T. Koseoglu, T. Ozisik, S. Kalkan, Y. Guney, M. S. Niaei, O. Satir, C. Yesilyaprak, C. Puskullu, A. Kabas, O. Demircan, J. Alikakos, V. Charmandaris, G. Leto, J. Ohlert, J. M. Christille, R. Szakáts, A. T. Farkas, E. Varga-Verebélyi, G. Marton, A. Marciniak, P. Bartczak, T. Santanaros, M. Butkiewicz-Bąk, G. Dudziński, V. Alí-Lagoa, K. Gazeas, L. Tzouganatos, N. Paschalis, V. Tsamis, A. Sánchez-Lavega, S. Pérez-Hoyos, R. Hueso, J. C. Guirado, V. Peris, and R. Iglesias-Marzoa. The size, shape, density and ring of the dwarf planet Haumea from a stellar occultation. *Nature*, 550:219–223, Oct. 2017. doi: 10.1038/nature24051.

S. B. Porter and W. M. Grundy. KCTF evolution of trans-neptunian binaries: Connecting formation to observation. *Icarus*, 220(2):947–957, 2012. ISSN 00191035. doi: 10.1016/j.icarus.2012.06.034. URL <http://dx.doi.org/10.1016/j.icarus.2012.06.034>.

A. Rivkin, R. Brown, D. Trilling, J. Bell III, and J. Plassmann. *Icarus*, 156:64–75, 2002.

P. Rosenblatt and S. Charnoz. On the Formation of the Martian Moons from a Circum-Martian Accretion Disk. *Icarus*, 221(2):806–815, Nov. 2012.

P. Rosenblatt, S. Charnoz, K. M. Dunseath, M. Terao-Dunseath, A. Trinh, R. Hyodo, H. Genda, and S. Toupin. Accretion of Phobos and Deimos in an extended debris disc stirred by transient moons. *Nature Geoscience*, 9(August):4–8, 2016. ISSN 1752-0894. doi: 10.1038/ngeo2742. URL <http://www.nature.com/doifinder/10.1038/ngeo2742>.

J. Salmon and R. M. Canup. Accretion of Saturn’s Inner Mid-sized Moons from a Massive Primordial Ice Ring. *The Astrophysical Journal*, 836:109, Feb. 2017. doi: 10.3847/1538-4357/836/1/109.

J. Salmon, S. Charnoz, a. Crida, and a. Brahic. Long-term and Large-scale Viscous Evolution of Dense Planetary Rings. *Icarus*, 209(2):771–785, 2010a.

J. Salmon, S. Charnoz, A. Crida, and A. Brahic. Long-term and large-scale viscous evolution of dense planetary rings. *Icarus*, 209(2):771–785, Oct. 2010b.

S. S. Sheppard and D. Jewitt. Extreme Kuiper Belt Object 2001 QG₂₉₈ and the Fraction of Contact Binaries. *AJ*, 127:3023–3033, May 2004. doi: 10.1086/383558.

W. L. Slattery. Giant impacts on a primitive Uranus. *Icarus*, 99:167–174, Sept. 1992. doi: 10.1016/0019-1035(92)90180-F.

B. A. Smith, L. A. Soderblom, T. V. Johnson, A. P. Ingersoll, S. A. Collins, E. M. Shoemaker, G. E. Hunt, H. Masursky, M. H. Carr, M. E. Davies, A. F. Cook, J. M. Boyce, T. Owen, G. E. Danielson, C. Sagan, R. F. Beebe, J. Veverka, J. F. McCauley, R. G. Strom, D. Morrison, G. A. Briggs, and V. E. Suomi. The Jupiter system through the eyes of Voyager 1. *Science*, 204:951–957, June 1979. doi: 10.1126/science.204.4396.951.

A. M. K. Szeto. Orbital evolution and origin of the Martian satellites. *Icarus*, 55:133–168, July 1983. doi: 10.1016/0019-1035(83)90056-8.

R. Tajeddine, P. D. Nicholson, P.-Y. Longaretti, M. E. Moutamid, and J. A. Burns. What Confines the Rings of Saturn? *The Astrophysical Journal Supplement Series*, 232(2):28, 2017. ISSN 1538-4365. doi: 10.3847/1538-4365/aa8c09. URL <http://stacks.iop.org/0067-0049/232/i=2/a=28?key=crossref.61846fc3632be3fbcd1e186>

T. Takeuchi, S. M. Miyama, and D. N. C. Lin. Gap Formation in Protoplanetary Disks. *The Astrophysical Journal*, 460:832, Apr. 1996. doi: 10.1086/177013.

P. A. Taylor and J. L. Margot. Tidal evolution of close binary asteroid systems. *Celestial Mechanics and Dynamical Astronomy*, 108(4):315–338, 2010. ISSN 09232958. doi: 10.1007/s10569-010-9308-0.

P. A. Taylor and J.-L. Margot. Binary asteroid systems: Tidal end states and estimates of material properties. *Icarus*, 212(2):661–676, 2011. ISSN 00191035. doi: 10.1016/j.icarus.2011.01.030. URL <http://linkinghub.elsevier.com/retrieve/pii/S0019103511000418>.

M. S. Tiscareno, M. M. Hedman, J. A. Burns, and J. Castillo-Rogez. Compositions and Origins of Outer Planet Systems: Insights from the Roche Critical Density. , 765:L28, Mar. 2013. doi: 10.1088/2041-8205/765/2/L28.

W. C. Tittlemore and J. Wisdom. Tidal evolution of the Uranian satellites. III - Evolution through the Miranda-Umbriel 3:1, Miranda-Ariel 5:3, and Ariel-Umbriel 2:1 mean-motion commensurabilities. , 85:394–443, June 1990. doi: 10.1016/0019-1035(90)90125-S.

A. Toomre. On the gravitational stability of a disk of stars. *The Astrophysical Journal*, 139:1217–1238, 1964.

S. C. Werner and K. L. Tanaka. Redefinition of the crater-density and absolute-age boundaries for the chronostratigraphic system of Mars. *Icarus*, 215:603–607, Oct. 2011. doi: 10.1016/j.icarus.2011.07.024.

J. Wood, J. Horner, T. C. Hinse, and S. C. Marsden. Measuring the severity of close encounters between ringed small bodies and planets. *MNRAS*, 480:4183–4198, Nov. 2018. doi: 10.1093/mnras/sty2047.

C. F. Yoder. Notes on the origin of the Trojan asteroids. *Icarus*, 40:341–344, Dec. 1979.

APPENDICES

A. TABLES

Table A.1.
Masses and Timescales for Mars Ring/Satellite Cycles

Cycle no.	Initial Ring Mass (g)	Final Satellite Mass (g)	1 km particles (Myr)	Cycle Time:	Estimated Cycle Time:
				0.18 m Particles (Myr)	0.18 m Particles (Myr)
6	1.2×10^{23}	2.6×10^{22}	0.46		190
5	2.6×10^{22}	5.4×10^{21}	1.1		290
4	5.4×10^{21}	1.1×10^{21}	2.8		270
3	1.1×10^{21}	2.4×10^{20}	5.3		350
2	2.4×10^{20}	5.0×10^{19}	22		750
1	5.0×10^{19}	1.0×10^{19}	61		2500

Here I show the initial mass for each cycle, the mass of the satellite produced at the end of the cycle, and how long the cycle takes to complete for the nominal 6-cycle case. Also included are estimated completion times for a ring composed of 0.18 m radius particles. The relatively long completion time for the first two cycles of a ring composed of 0.18 m particles is due to both the longer spreading time for rings with smaller particles, and the fact that the masses of the first cycles are sufficient for Lindblad torques to drive satellites far from the FRL, increasing the orbital evolution time. The time shown for Cycle 1 is when the satellite reaches the current orbit of Phobos, and not the RRL (as it is for the previous cycles).

Table A.2.
Global and Equatorial Depths of Estimated Ring Deposits Onto Mars

Cycle no.	Total Volume of Deposit (km^3)	Depth of Deposit (global) (m)	Depth of Deposit (20° Band at Equator) (m)	Estimated Time to Deposit (Myr)	Estimated Time in Geologic Record (Gyr)	Geologic Era
6	5.3×10^7	370	2120	0.3	(4.4 – 4.5)	Noachian
5	1.1×10^7	77	440	0.4	(4.2 – 4.5)	Noachian
4	2.3×10^6	16	93	0.4	(3.8 – 4.5)	Noachian
3	4.9×10^5	3.4	19	0.5	3.6	Hesperian
2	1.0×10^5	0.71	4.1	1.1	3.3	Hesperian
1	2.2×10^4	0.15	0.88	3.8	2.5	Amazonian

Here I report the estimated volume of deposits for each cycle, global depths and equatorial depths, the time to deposit 80% of the material, and what time I would expect the deposit to occur in Martian geologic history for the nominal 6-cycle case [Werner and Tanaka, 2011]. All deposit depths are calculated using results for rings composed of particles with a 1 km radius. Uncertainties in the exact time at which the

dichotomy-forming impact occurred, as well as which cycle best represents the initial ring, and the dynamics of satellites in the early cycles (see Figure 4.3) prevent us from precisely dating the deposits for the first few cycles in the Martian geologic record.

Table A.3.
Maximum Semi-Major Axis of Satellites

Cycle no.	Maximum Satellite Orbit R_M
6	4.9
5	3.9
4	3.5
3	3.3
2	3.1
1	3.1

Here I report the maximum semi-major axis for the “nominal” case (where satellite breakup occurs at the RRL) that Lindblad torques could possibly evolve any accreted satellites for each cycle. In cycles 6 and 5 the mass of the ring is massive enough for Lindblad torques to overcome tidal torques and drive the satellites far away from the ring. However, by cycle 4 the mass of the ring has been depleted enough that satellites are not driven far from the ring. In the most recent cycles the Lindblad torques are not sufficient to drive the satellite away from the ring, with their maximum semi-major axis existing near the ring edge.

VITA

VITA

Andrew J. Hesselbrock**Education**

Purdue University Physics and Astronomy Ph.D. 2018

Advisor: Prof. David A. Minton

Miami University Physics M.S. 2012

Advisor: Prof. Stephen G. Alexander

Miami University Physics B.S. 2010

Publications

- **Hesselbrock, A.J.**; Minton, D.A., “An Ongoing Satellite-Ring Cycle of Mars and the Origins of Phobos and Deimos.” *Nature Geoscience*, 10:266-269, 2016.
- **Hesselbrock, A.J.**; Alexander, S.G.; Harp, T.W.; Abel, N.P., “An Investigation of the Relationship Between Shape and Rotation to Explain the Light Curve of Nereid.” *The Astronomical Journal*, 145:144, 2013.
- Alexander, S.G.; **Hesselbrock, A.J.**; Wu, T.; Abel, N.P., “On the Rotational Behavior of Nereid.” *The Astronomical Journal*, 142:1, 2011.

Publications Under Review

Hesselbrock, A.J.; Minton, D.A., “Three Dynamical Evolution Regimes for Coupled Ring-Satellite Systems and Implications for the Formation of the Uranian Satellite Miranda.” Submitted to *The Astronomical Journal*.

Conference Proceedings

- Hesselbrock, A.J.; Minton, D. “Boomerang Satellites.” 49th AAS Meeting for the Division of Planetary Sciences, Provo, UT. October 2017.
- Hesselbrock, A.J. “Planetary Rings that Crash onto Planets, and Crash Your Computer.” Numerical Integration Methods in Planetary Science, Toronto, CA. August 2017.
- Hesselbrock, A.J.; Minton, D. “The Cyclic Nature of Martian Satellites.” 48th AAS Meeting for the Division of Planetary Sciences, Pasadena, CA. October 2016.
- Hesselbrock, A.J.; Larson, J.; Minton, D. “Development of a Circum-Embryo Disk Model Subject to Collisions from the Heliocentric Swarm.” 46th AAS Meeting for the Division of Planetary Sciences, Tucson, AZ. November 2014.
- Hesselbrock, A.J.; Larson, J.; Minton, D. “Development of a Circum-Embryo Disk Model Subject to Collisions from the Heliocentric Swarm.” Michigan Institute for Research in Astrophysics Conference, Ann Arbor, MI. October 2014.
- Hesselbrock, A.J.; Alexander, S.G. “The Effects of a Variable Torque on Neptunes Satellite Nereid.” Ohio Section APS Meeting, Marietta, OH. October 2010.

Honors and Awards

NASA Earth and Space Sciences Fellowship to pursue Ph.D., 2016.

Graduate Teaching Award, Purdue University Teaching Academy, 2016.

Summer Grant, Purdue Research Foundation, 2014.

Outstanding Graduate Researcher, Miami University, 2012.

Induction into Sigma Pi Sigma National Honors Society, 2011.

George and Carolyn Arfken Scholarship, Miami University, 2009.

Raymond M. Hughes Scholarship, Miami University, 2008.

R.L. Edwards Scholarship, Miami University, 2007.

Professional Service & Outreach

- Science on Tap, *Emcee/Promoter*, Lafayette, IN (2015-2017).
- Physics Graduate Student Association, *President, Vice President, Social Chair*, Purdue University (2013-2017).
- Strategic Planning Committee, *Graduate Representative*, Purdue University (2016).
- Imagination Station, *Summer Camp Presenter, Planetary Science Day Chair*, Lafayette, IN (2016).
- Department of Physics and Astronomy, *Graduate Student Mentor*, Purdue University (2014-2016).
- STEM Day - INDY Women in Tech, *Demonstration Participant*, Purdue University (2015).
- Cumberland Elementary School Fair, *Presenter*, West Lafayette, IN (2014).
- Lafayette Central Catholic Junior/Senior High School Science Fair *Judge*, Lafayette, IN (2013).
- Nano Days - Cincinnati Museum Center, *Demonstration Participant*, Miami University (2012).
- Science and Engineering Expo - Southwest Ohio District, *Judge*, Cincinnati, OH (2011).
- Department of Physics Chair Search, *Graduate Representative*, Miami University (2011).
- Department of Physics, *Graduate Representative*, Miami University (2011).